UPC CTTC

Numerical study and experimental optimization of air curtains

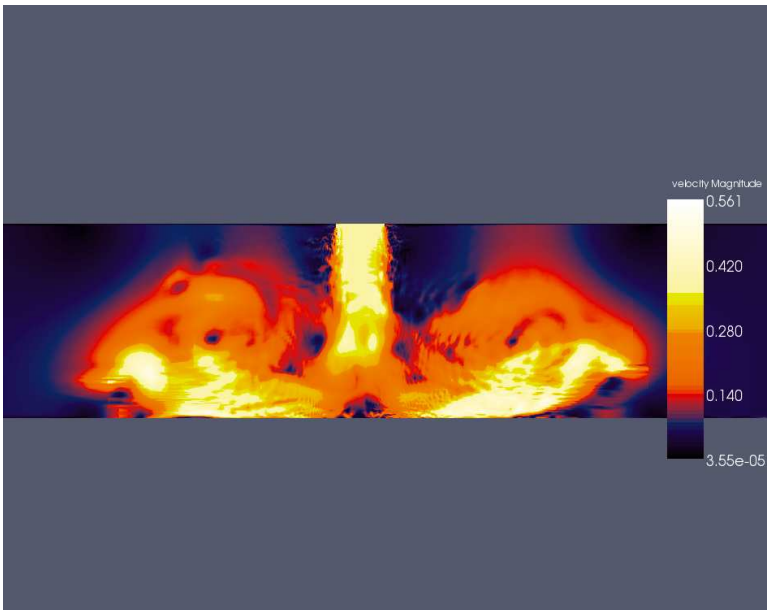

Centre Tecnològic de Transferència de Calor
Departament de Màquines i Motors Tèrmics
Universitat Politècnica de Catalunya
Héctor Giráldez García
Doctoral Thesis

Numerical study and experimental optimization of air curtains

Héctor Giráldez García

TESI DOCTORAL

presentada al

Departament de Màquines i Motors Tèrmics
E.T.S.E.I.A.T.
Universitat Politècnica de Catalunya

per a l'obtenció del grau de

Doctor Enginyer Industrial

Terrassa, March 2015

Numerical study and experimental optimization of air curtains

Héctor Giráldez García

Directors de la Tesi

Dr. Carlos David Pérez Segarra

Dr. Assensi Oliva Llena

Tribunal Qualificador

Dr. Carles Oliet Casasayas
Universitat Politècnica de Catalunya

Dr. Francisco Javier Rey Martinez
Universidad de Valladolid

Dr. Joaquim Rigola Serrano
Universitat Politècnica de Catalunya

Dr. Jose Manuel Pinazo Ojer
Universidad Politécnica de Valencia

Dr. Maria Manuela Prieto Gonzalez
Universidad de Oviedo

Agradecimientos

Agradezco la colaboración en la realización de esta tesis a todos los compañeros del CTTC.

En primer lugar, a David Pérez-Segarra y a Assensi Oliva, por dirigir y corregir este trabajo.

A Dani Fernández, Gabriel, Octavi y Ramiro por toda la ayuda en informática y su gran amistad.

A Julián, por explicarme los modelos RANS y por sus numerosas indicaciones en mis comienzos en el tema de cortinas de aire. También por su apoyo personal.

A Xavi Trias, por ayudarme con sus indicaciones y corrección de errores, y por las charlas durante los cafés en pleno agosto.

A Carles, por su apoyo en diferentes aspectos de esta tesis. Por su ayuda en el tema de aire húmedo y por ser un gran compañero de sala.

A Manolo y Victor, por su colaboración e indicaciones sobre materiales y procedimientos en el montaje experimental.

A Joan Farnós, por su valiosa compañia y consejos, amistad y ayuda en la sala experimental.

A Fei, Joan Calafell, Lluís, Jordi Ventosa, Jordi Chiva, Jesús, Roser, Quim y Guillem, por atenderme en mil consultas sobre CFD u otros temas.

A Ivette, por leer y corregir meticulosamente el artículo sobre método semianalítico hasta dejarlo listo para enviar.

A Nico, Santiago y Alex por las conversaciones y ayuda en temas diversos.

A Kike, por editar una de las figuras, acompañarme a salir a correr (aunque es un poco lento) y por perdonar este agradecimiento.

A Ali, por su amistad y apoyo. Por los consejos.

Y a mi familia.

A mi padre, por el interés que ha mostrado en que realizase este Doctorado.

Mari Carmen, por su alegría y por sus dibujos.

Germán, por su paciencia y por las risas cuando se cayó de la litera.

Minerva, por su cercanía mientras se encuentra tan lejos de casa.

Y Lorena, por su energía y por recordar siempre nuestro cumpleaños.

A Alejandra y Aiko, por su cariño.

A mi madre, por cuidarnos.

Contents

Abstract

The main objective of the present thesis is to study and optimize the sealing efficiency of air curtains. Therefore, the phenomenology of the breakthrough and the parameters which affect it has been studied. Considering the level of turbulence in the studied flowfields, this work employs numerical methods which will allow us to take all the transport phenomena into account, for both laminar and turbulent regimes. This is not the first effort within the CTTC ("Centre Tecnològic de Transferència de Calor") research group on this subject, but the continuation of a research activity carried out in the past years.

For this purpose, chapter 1 contains an introduction to air curtains, and the basic phenomenology is discussed. The different stages of an air jet are detailed. It is also given a discussion on when the installation of these devices should be considered as a good solution for air flow sealing. In this chapter are also defined the basic concepts used throughout this work. It ends with a brief description of the three main approaches employed in this thesis to analyse air curtains: computational fluid dynamics, semianalytical methods and experimental measurements.

The semianalytycal methods, which are suitable only for steady regime calculations, are introduced in chapter 2. The main results obtained in different situations are also presented. The semiananlytycal approach allows to characterize the air curtains with a much less time consuming method than higher level calculations.

In chapter 3, the Computational Fluid Dynamics methodology is described, with Large Eddy Simulation as approach. The models employed to solve the Navier Stokes equations are Smagorinsky and Wale. A simmetry preserving discretization is employed. The solvers employed are also outlined.

If we wish to solve real problems, we face the fact that the performance of the air curtains depend strongly on the boundary conditions. There are situations where the usually assumed steady behavior of the media involved is far from being true. Because of this reason, in chapter 4, special emphasis has been placed on the experimental measurements of actual air curtains. This interest resulted on a detailed study about the standard on the characterization of air curtains, and the construction of an experimental set up according to the standard requirements. The more significant results are presented.

In chapter 5 a plenum optimization procedure is carried out. Both experimental and numerical approaches are employed.

In chapter 6 the application of air curtains to refrigerating chambers is studied in detail. The capability of the air curtain to avoid thermal and moisture entrainment is quantified.

The results obtained from CFD simulation, semianalytical calculations and exper-

imental measurements have been compared. According to the results obtained and presented in the chapter 5, the objective of optimizing air curtains proposed in this thesis has been satisfied.

Chapter 7 contains some final general remarks as well as ideas on how the present work could be continued.

Finally the appendice include some material which would disturb the normal reading flow of the thesis. The experimental setup, the calibration procedure and some examples of results obtained with the developed software are presented in the appendice. In the appendice it is also described the interface developed at CTTC to evaluate the thermal efficiency and other relevant aspects for of air curtains.

All this material follows from the five-year period on which this thesis has been developed.

List of Figures

Nomenclature

A	area $[m^2]$
A_o	air curtain discharge nozzle area $[m^2]$
A_{lat}	lateral unprotected area $[m^2]$
ACU	air curtain unit
b_0	air curtain discharge nozzle width $[m]$
$C_{1,2,3,4}$	analytical jet distribution constants[-]
CS	control surface $[m^2]$
C_w	pressure coefficient of wind [-]
C_{wale}	turbulent model constant [-]
c_p	specific heat at constant pressure
D	PLenum inner curve diameter [m]
D_v	diffusivity of water vapour in air $[m^2/s]$
def	deflection $[m]$
E_{ff}	air curtain sealing efficiency
Fp	Pressure-induced forces [N]
f	Frequency of vortex shedding $[s^{-1}]$
$\dot{G}$	mass flux rate $[kg/m^2/s]$
g	gravity acceleration $[m/s^2]$
g_{ij}	velocity gradient tensor ij component $[s^{-1}]$
H_{ent}	enthalpy flow of indoor air [J]
H_{jet}	enthalpy flow carried by the jet into the space [J]
H_{env}	enthalpy flow through the envelope [J]
H_{lat}	enthalpy flow blown into the space through the lateral area [J]
h	height of the door $[m]$
I_o	turbulence intensity[-]
M_0	jet discharge momentum flux per length [N/m]
L_v	latent heat of vaporisation $[J/kg]$
L_c	Length of the potential core region $[m]$
l_o	nozzle length $[m]$
Pr	Prandtl number $Pr = \rho\nu c_p/\lambda$ [-]
p_o	pressure at the outside of the building [Pa]
p_i	pressure at the inside of the building [Pa]
Q_{ac}	thermal loss with the air curtain [J]
Q_d	thermal loss through the entrance without the air curtain [J]
Q_{ta}	total thermal loss [J]
r	position vector $[m]$

r_n	normal distance $[m]$
S	rate of stress tensor $m/s]$
Sc	Schmidt number $Sc = \nu/D_v$ [-]
St	Strouhal Number [-]
$\boldsymbol{\mathcal{S}}$	traceless symmetric part of square of $\boldsymbol{\gamma}$ $[s^{-2}]$
$\mathbf{u}$	velocity vector with components (u,v,w) $[m/s]$
v	air jet velocity [m/s]
v_c	core velocity [m/s]
v_0	discharge velocity [m/s]
v_w	wind velocity [m/s]
W_{door}	door width $[m]$
Y_v	mass fraction of water vapor[-]
z	vertical coordinate $[m]$
z_{ns}	neutral level of pressure $[m]$

Greek symbols

α	air jet angle [°]
α_o	air curtain discharge nozzle angle [°]
$\boldsymbol{\gamma}$	velocity gradient tensor $[s^{-1}]$
Δ	length scale of the filter $[m]$
$\boldsymbol{\delta}$	unit tensor [-]
η	dimensionless transverse coordinate [-]
η_e	point at which there is zero net flow through the doorway [-]
η_1	impact point of the jet [-]
λ	thermal conductivity [W/m/K]
ν	kinematic viscosity $[m^2/s]$
ν_e	kinematic eddy viscosity $[m^2/s]$
ρ	density $[kg/m^3]$
σ	constant of the developed region velocity profile [-]
$\boldsymbol{\tau}$	Reynolds stress tensor $[m^2/s^2]$
$\overline{\phi}$	volume average (ϕ=$\mathbf{u}$,p,...)

Subscripts

da	dry air
δ	liquid-gas interface
e	effective
g	gas phase
t	turbulent

v	water vapor
ω	water

1

Introduction

1.1 Introduction to air curtains

The function of an air curtain is to supply a plane jet over the whole opening, with momentum enough to act as ambient separator. If the produced air jet has not a velocity high enough to seal the whole door it will deflect under the effect of the wind, pressure, or temperature differences.

The installation of the air curtain presents different configurations depending on the type of door; the air curtain can be placed vertically blowing (upwards or downwards) or horizontal blowing. There are two main types of suction (it can be a recirculating or non-recirculating system).

The application affects directly on the air curtain design and installation. The most typical applications are:

Public Buildings : where the velocity must be low and downward blowing configuration is the usual choice because it does not disturb the normal pedestrians access.

Industrial Application : as in refrigeration storages, for example, where the velocity must be higher and the jet thicker. The configuration depends on the door width: if the door is very high the air curtain is placed blowing horizontally, if it is very wide it is place as a vertical blowing device.

In the technical dimensioning of an air curtain both a fluid mechanical approach and a thermal approach is needed. An air curtain with a correct design can be an efficient saving energy solution, but if the design is flawed, the device could produce more losses than the sole opening door configuration.

The important parameters that must be taken into account to get an optimum design of an air curtain can be classified in fluid mechanical parameters and thermal parameters:

Fluid mechanical parameters : suction location, pressure difference across the opening, ventilation imbalance, angle discharge, nozzle width, jet velocity exit, opening height, overall plenum geometry.

Thermal parameters : temperature difference, temperature discharge.

The natural approach to design an air curtain is to reduce the number of possible parameters and configurations defining a priori some parameters based on the experience and finding out the optimum values for the other non defined parameters.

This is the simplest way to take the effect of the modifications into account, and it comes, in general, at a low experimental cost. The design optimization is detailed in chapter 5.

1.2 Jet Physics Understanding

In order to be able to characterize an air curtain, first we need to understand the physics of the air jet, since an air curtain is simply a device which produces a plane air jet strong enough to act as an ambient separator against external temperature, pollution, humidity, insects or other non desirable particles to enter the protected air space. As has been said, the study of plane impinging jets is fundamental for the correct understanding of air curtains behaviour. For a detailed study of the physics of plane impinging jets see the study of Jaramillo et al. [1].

According Soliec [2], a plane air jet is divided en three main stages, which will be four in the case of an impinging jet.

We can distinguish the potential core region, the transition zone and the developed zone. In the case of the impinging jet it will appear the recompression or impinging zone. A sketch of the distribution of the principal cinematic variables is represented in figure 1.1.

1.2.1 Potential core zone

The potential core region extends from the air curtain dicharge to a maximum of $6b_o$, being b_o the width of the nozzle. In cases where the air jet includes a high level of turbulence (a non desirable feature) the length of the potential core region will be shorter. The main characteristic of the potential core region is that in this region the centerline velocity remains constant and equal to the velocity at the air curtain discharge. Van and Howell [3] give an empirical relation between the length of the potential core and the turbulence intensity:

$$L_c = 5.39 - 0.266 I_o \tag{1.1}$$

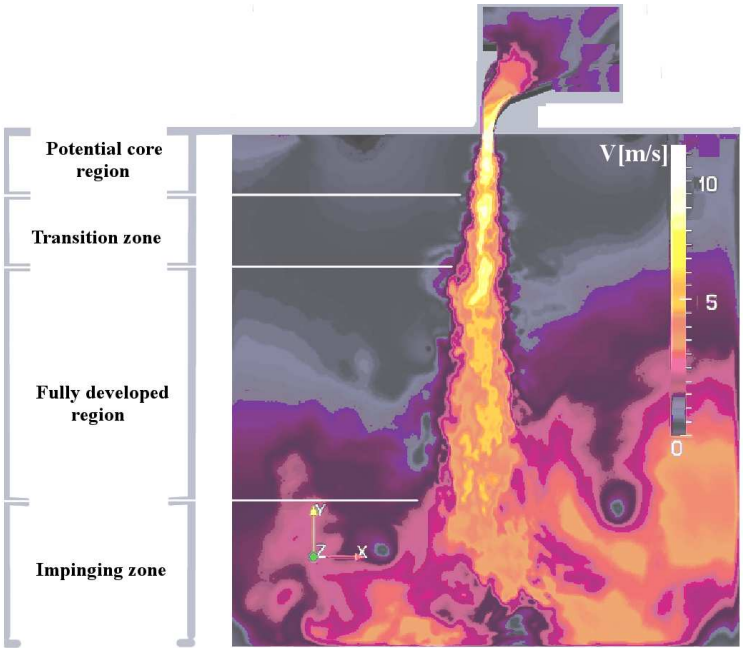

Figure 1.1: Regions observed along an impinging air jet

1.2.2 Transition zone

When the potential core region has been consumed, (progressively the transversal area which has the velocity equal to the dicharge velocity is narrower) it appears the so called transition zone, which, if the jet has a low level of turbulence, and accordingly Schlichting [4] follows the analytical distribution

$$\frac{U(x,y)}{U_o} = \frac{1}{2}\left(1 - erf\left(C_1 \frac{y - \frac{e}{2}}{x}\right)\right) \; where \; C_1 = 13.5 \tag{1.2}$$

1.2.3 Affinity or developed zone

A general expression for the developed zone is not present in the literature, however, in the case of the free plane jet all authors agree to express the evolution of the centerline in the following form:

$$\frac{U_c(x)}{U_o} = C_2(\frac{x}{e} - C_3)^{-\frac{1}{2}} \tag{1.3}$$

The value of the constants C_2 and C_3 differs between the studies, due to the

different operating conditions with, of course, different levels of turbulence as a consequence.

According Schlichting [4], the velocity field U(x,y) can be calculated by:

$$\frac{U(x,y)}{U_o} = \frac{\sqrt{3}}{2}\sqrt{\frac{7.67e}{x}}(1 - tanh^2(7.67\frac{y}{x})) \tag{1.4}$$

There is no agreement about which is the distance when the jet becomes self-similar. Some author (Antonia et al. [5]) point out a distance of 20e ,while other (Jenkins et al. [6]) say 25e, and 40e(Bashir et al. [7]).

Beltaos [8] inserted additional factor that takes into account the relative height H/e.

$$\frac{Uc(x)}{U_o}\sqrt{\frac{H}{e}} = C_4(\frac{x}{H})^{-\frac{1}{2}} \; where \; C_4 = 2.5 \tag{1.5}$$

This expression is available from the potential core region and for x/H $<$ 0.65. All the authors determine empirically the coefficient C_4 obtaining a value close to 2.5.

In this thesis these constants will be adjusted once again to fit our own experimental measurements.

1.2.4 Impinging zone

In the last region of the air jet, just before it arrives to the opposite extrem of the opening, the centerline velocity decrease sharply. It decrease is called the ground effect. According Soliec [2], we can consider that the height of the impinging zone is close to a value equal to 0.13H +- 0.02. This results shows that the height of the impinging zone is independent of both the ratio H/e and the nozzle width.

1.3 State of the art

The evaluation and improvement of the air curtain sealing efficiency is the major goal of the air curtain studies. Air curtains have been principally studied by means of experimentation or designed with simple mathematical models. Only some numerical works have been carried out, and most of them assuming oversimplifying geometries. The study of an air curtain isolating an inner space from outside air entrainment requires also an specific review of the literature concerning the moisture transport.

In this section a scientific literature review concerning air curtains is done.

The three main approaches to the problem of determining the air jet behaviour are experimental measurements, semi-analytical methods ans CFD calculations. All the papers found in the literature rely on one or more of these approaches. If turbulent impinging jets have been the subject of a lot of experimental research works, they have been less studied by numerical simulations like DNS or LES. Classical statistical

model like $k - \epsilon$ have shown their limits for this problem: overestimation of the potential core, underprediction of the jet expansion and/or impinging zone poorly described.

The past research in those topics used formulations that simplify so much that a distorted impression of the air curtain it is given. Even as the calculations carried out by means of those method are not accurate enough, they identify most of the parameters that affect any air curtain sealing efficiency.

For instance, some of those parameters are the turbulence intensity, the discharge nozzle width and the discharge velocity.

Turbulence intensity at the jet discharge as a boundary condition is a measure of mixing enhancement. The more distance that the air curtain travels provides more opportunities for the air curtain to widen. This widen is directly proportional to the turbulence intensity.

Discharge nozzle width of an air curtain provides the initial length for the flow to move laterally, which also can enhance the widening of the jet.

Discharge velocity specifies how much kinetic energy is available.This kinetic energy amplifies the turbulence kinetic energy within the air curtain.

These three parameters are some of the most important factors to a correct understanding of air curtain performance.

An experimental study was carried out by Hetsroni and Hall [9]. They study the air entrainment-spill mechanism across air curtains and introduced analytical expressions to quantify the heat transfer through the air curtain and the obtained sealing efficiency.

The stack effect and other pressure differences which affect the curvature of an air jet are presented by Hayes and Stoecker [10]. These pressures must be taken into account in the air curtain dimensioning. They assume that the bulding has a tighly sealed envelope. The only one opening is the door wher the air curtain is installed. They propose analytical expressions based on the observations and one example of air curtain design procedure is described. In this study it is pointed out that if the outlet velocity is very high, it is possible that an air curtain could increase the rate of heat transfer.

Howell and Shibata [11] looks at the relationship between the heat transfer through a recirculated air curtain and the deflection of the air curtain. They stated that the heat transfer through the air curtain decrease as the Reynolds increases. They revealed also that the ratio of the opening height to the discharge width (H/w) affect the efficiency of air curtains. They stated that there is a value of deflection for each air curtain configuration which minimizes the rate of heat transfer across the air

curtain. Howell and Shibata [11] pointed out that the initial turbulence intensity has a moderate effect on the rate of heat transfer through an air curtain,accelerating the widening of the jet, hence causing a higher heat transfer across the air curtain. It is found that 75% of the refrigeration load in an open vertical display case is a result of the warm air entrainment across the air curtain.

Partyka [12] applied the laminar and turbulent jet equations [4] to determine a mathematical model for an air curtain comprising two air jets. He did an analytical study of flow impact region of two jets to develop the mathematical model that yields data for the air curtain performance. The theory permitted him to establish the quantitative influence of the jet properties and duct geometry on the pressure difference and to predict flow conditions. He also presented experimental measurements.

Experimental studies of display cabinets were presented by Faramarzi [13]. He presented a discussion about the cooling load composition in an open display cabinet. He concludes that the most important loss is due to infiltration.

Stribling et al. [14] presented a two-dimensional computational study with a commercial code of a vertical display, finding that this model could be used in the design and optimisation of such equipment but it needs further validation to be accepted as quantitatively accurate. It should be noticed that in this study Stribling employs Reynolds Average Navier-Stokes models (RANS). He found a good agreement between the numerical simulations and the experimental measurements for their centerline velocity. It is pointed out that the velocity in the edges of the air curtain curtain is less accurate. In the opinion of the author a finer grid with higher order discretisation scheme should have remedied this lack of accuracy. So he carried out calculations with finer grids and higher order schemes but he does not reach conclusive results.

Guyonnaud et al. [15] worked experimentally to find correlations for air curtains efficiency and to establish the validity of scaled models in designing air curtains, they found that the turbulence intensity does not affect the air curtain performance and only the mean flow is required to ensure the sealing (in contrast with previous studies). They do not produce a general correlation, but an extrapolation correlation was determined for an opening from 0.2 to 1.44 m height.

Solliec et al. [2] carried out a parametric analysis of a turbulent plane jet by means of laser Doppler velocimetry (LDV) and particle image velocimetry (PIV). In contrast with other studies, they focus their attention in the impinging zone and quantify its length as 12% of the total length of the jet independently of the Reynolds numbers. Between other industrial applications, they indicate that air curtains can be employed for the sealing of contaminants and they explain how the mass transfer happens.

Pavageau et al. [16] also carried out experimental measurements by means of LDV and PIV. They indicate some recommendations for the dimensioning and installation

of air curtains.

Most of the recent works intend to use modern techniques such as CFD and advanced experimental methods to increase the details and obtain a better quantification of the behaviour of air curtains. The best methodology seems to depend on an effective and careful combination of both technologies.

Ge and Tassou [17] studied display cabinets by means of finite differences technique and based on their results developed correlations for the heat transfer across these devices. They validate the model against experimental results and obtain a good agreement.

Also, in this year Kim et al. [18] carried out a computational fluid dynamics (CFD) 3D simulation, using the standard $k-\epsilon$ model, with the purpose of analysing indoor cooling/heating. The CFD study is coupled with a radiative analysis. In this, the view factor and the radiation heat transfer between the walls were calculated by the Monte Carlo method. Heating, ventilating and air-conditioning (HVAC) controlling system in a room is also coupled to the CFD simulation. The loop feed backs the outputs of the HVAC system control to the input boundary conditions of the CFD, and this method included a human model to evaluate the thermal comfort environment. This is maybe one of the first papers that simulates air curtains using CFD placed as ambient separator in an building. To examine the performance of the model, a thermal environment within a semi-enclosed space, which opens into an atrium bigger space, is analysed during summer season.

Navaz et al. [19] have demonstrated that a combination between the digital particle image velocimetry (PIV) experimental technique and CFD simulation can be quite effective to study the flow field characteristics and performance of the air curtain of an open vertical display case. The PIV can calibrate the numerical technique after which the CFD code can be used for parametric studies with the object of air curtain design optimisation. They have shown that this hybrid approach effectively produce curve fits similar to previous works that can be useful for engineering calculations for entrainment rate and heat transfer. Also, they concluded that changes that lead to a better performance of the air curtain must primarily affect the momentum of the flow field. Finally, they demonstrated that the validation of a CFD model with reliable and comprehensive experimental data is a prerequisite for generating reasonable results.

Other example of the combination of CFD and experimental techniques was presented by Foster et al. [20]. Who used a CFD model of air movement through a doorway, which was verified against conventional and LDA measurements. Boussinesq hypothesis and the standard k-epsilon model were used. The predicted velocity out of the room at the bottom was 0.3 to 0.5 m/s lower than measured. The highest velocity out of the room was near the floor and the highest velocity in was close to

top. The shape of the profile was well predicted by CFD. However, it under-predicted the velocity of the air leaving the chamber at the bottom of the opening.

The analytical model which is modified in the present thesis was developed by Siren [21, 22], who provided valuable information for the design of vertically upwards-blowing air curtains. He presented a technical dimensioning of an air curtain considering effects of building envelope and ventilation system, then presented practical mathematical formulations for the dimensioning of air curtains. The method was based on the momentum-of-momentum principle, which enables the considerations of the jet impact point. A new equation was proposed for the jet discharge angle, which is one of the important factors for the jet's ability to resist the breakthrough. The second part was addressed to the thermal behaviour of the air curtain. Finally, a procedure that summarises the technical dimensioning of vertically upwards-blowing air curtains was proposed.

Havet et al. [23] made a experimental work to determine the sensitivity of air curtains to external perturbations in the form of sharp changes of pressure on the flow field of a device designed to avoid air-borne contamination, highlighting that the control of air curtains used in openings should be further investigated. Experimental techniques used indicated that the air curtain is strongly sensitive to perturbations such as draughts.

Bhattacharjee and Loth [24] studied the entrainment through a refrigerated air curtain, but the shelf structure of a display case was idealised to that of a plane, adiabatic wall subjected to refrigerated wall jets at laminar and transitional regimes. In general, the results yielded a significant variation in entrainment as a function of Reynolds number, with a minimum occurring at flow speeds immediately prior to transition. The entrainment rates were also sensitive to the initial velocity distribution, whereby a constant gradient profile (where any local velocity gradient peaks were minimised) provided the least entrainment. Entrainment was also found to decrease with increasing Richardson number. They imposed different inlet profiles to test its influence downstream and found that a ramp profile consistently gave the lowest entrainment for both laminar and transitional flow conditions, while an uniform profile gave the consistently highest entrainment. The results indicated that avoiding a local peak of the velocity gradient in the inflow profile yields a reduction in entrainment.

A similar work was carried out by Field and Loth [25]. They found that the mass entrainment rate was proportional to the curtain speed, so by reducing speed the rate of entrainment of the ambient air can be linearly decreased. Therefore, one way to minimise the thermal entrainment and the associated energy losses, is to reduce the jet velocity, but only in the regime where attachment can be ensured.

Cui and Wang [26] used CFD method to evaluate the energy performance of the air curtain for horizontal refrigerated display cabinets and to optimise its design.

The CFD model was validated with experimental results. With CFD technique, the factors that influence the cooling load of the air curtain were studied and some new designs were proposed to make the air curtain more energy efficient. A commercial code was used.

Chen and Yuan [27] studied experimentally the effects of several factors on the performance of a refrigerated display cabinet, including ambient air temperature, indoor relative humidity, ambient air flow, air supply velocity, air flow from perforated back panels and night covers. All the tests were conducted in a controlled environment room, which can be utilised to simulate various indoor conditions. T-type thermocouples were used for temperature measurement, and aluminium oxide capacitive sensors were used for measuring relative humidity, and hot-wire anemometers were employed to measure air velocities. The results showed that ambient temperature and relative humidity increase causes temperatures and heat gain to raise. While the effect of air flow parallel to the cabinet is very limited.

Rouad et al. [28] studied the effect of fluctuating pressures acting against the air jet. Other researchers have not focus their attention in transient external conditions, so this paper presents a very interesting reference. The influence of this fluctuations on the behaviour of the air curtain are evaluated by means of experimental and numerical studies. Only a qualitative agreement is obtained between both techniques. The observations indicate that the air curtain is very sensitive to rapid pressure variations. They indicate that the model fails in the prediction of the amount of contamination measured at sampling points.

The effect of the Richardson and Reynolds numbers on the shape of the streamlines representing the entrained air at the discharge grill has been studied by Chen and Yuan [29] by means of CFD simulations. This work was quite valuable because it quantified the effects of the Richardson number, $Ri = \frac{Gr}{Re^2}$ (ratio of Grashoff to the square of Reynolds number), on the entrainment of ambient air into the cold air jet. The results showed that for a given Grashof number, the Richardson number must be less than a critical value to assure thermal insulation. They also found that the ratio of the opening height to the width of the initial air jet (height/width ratio) was also an important factor that would influence the performance of air curtains.

Navaz et al. [30] employed experimental (DPIV) as well as computational (CFD) methods to evaluate those parameters that have significant effects on the amount of entrained air in an open refrigerated display cabinet. They identified, quantified and the rate of entrainment is expressed as a function of these parameters. They found that the turbulence intensity, the shape of the mean velocity profile at the discharge air grill, and the Reynolds number are mainly responsible for the amount of entrained air in a display case. Also, from LDA measurements it was possible to assume the display case to be essentially two-dimensional. They showed that the turbulence

intensity and kinetic energy are indicators for the amount of mixing and responsible for creation of eddies in the flow. Therefore, they postulated that the 'shape' of the vertical velocity profile and the turbulence intensity present at the discharge control the entrainment rate. Finally they recommended to run the discharge at a Reynolds number of about 3200-3400 to minimise ambient air entrainment without violating the stability of the air curtain structure.

Recently Navaz et al. [31] published a comprehensive discussion about the past, present and future research toward air curtain performance characterisation and optimisation focused in open display cases. Some of the works previously mentioned have been taken into account in their review. They concluded that there have been a misconception regarding the entrainment rate in the sense that it has always been associated with the infiltration rate. They also indicated that one should always make a distinction between the two. Increased entrainment does not necessarily mean increased infiltration because only a portion of the entrained air is infiltrated into the display case, depending on the extent of mixing. A 100% ideal air curtain may entrain air but will not allow any entrained air to infiltrate into the display case.

This year Navaz et al. [32] have presented a work to address the effects of velocity profile at the discharge air grill on the amount of entrained air into an open refrigerated display case. The study was carried out using experimental techniques (DPIV and LDV) and also by means of CFD simulations. They found that a skewed parabolic profile with the peak shifted towards the inner section of the case generates the minimum entrainment and demonstrates that with simple changes to the geometry of the discharge grill, a significant reduction in the entrainment rate could be achieved.

Finally, a couple of works dealing with air curtains placed in door openings to separate two different ambients have been published this year. The first, presented by Foster et al. [33] studied the effectiveness of a commercially available air curtain at different jet velocities and found the optimum jet velocity to give the maximum effectiveness. Then, compared the experimental results with predictions from an analytical model and CFD simulations.

Experimental studies were carried out on a cold storage room used in previous studies by Foster et al. [20]. The air curtain was fitted and set up by a contractor and had controls to enable adjustment of the jet velocity and angle. Air exchange was calculated by the measured decay of an elevated CO_2 concentration in the room over time. CO_2 was released into the room and mixed using the evaporator fans. All CO_2 concentrations were measured with a CO_2 infra-red analyser. The jet from the air curtain was modelled as a constant velocity inlet into the domain. An opening boundary condition was set at the top side of the air curtain, this opening removed an identical mass of air that entered from the inlet. All other boundaries were adiabatic walls. The total number of grid nodes for the problem was 42000. They found some discrepancies between measured and predicted values of effectiveness and optimum

velocity and these were attributed to differences in geometry and boundary conditions used.

Costa et al. [34] studied numerically the influence of the different dynamic and geometrical parameters on the sealing efficiency of a down ward-blowing air curtain device, which is installed between two contiguous room with distinct ambient temperatures. Therefore, only stack effect was considered. The CFD was based on a 2D simulation using the standard $k-\epsilon$ model with two-layer wall functions approach. The performance of the air curtain was expressed by two parameters, the sealing efficiency and effectiveness, which provide the assessment of the energy savings predicted. The geometry of the calculation domain corresponded to the vertical plane of symmetry at half-width of the rooms, together with the relevant boundary conditions and dimensions. It was assumed that the air curtain device was mounted on the dividing wall at the height of the doorway. Ceiling, floor, concrete beam and separating wall were all assumed to be adiabatic. On the other hand, the extreme (nominal) temperature levels in the rooms were specified by imposing such values (T_i and T_o) along the columns of nodes that were adjacent to the lateral walls. They concluded that a vertical air curtain working close to the optimum conditions could provide energy savings up to $75 - 80\%$.

As far, it was not possible to find a paper that study the air curtain with the environment influence together by means of steady state fully 3D simulations. Furthermore, most of the works that carried out numerical simulations used commercial codes and it seems that the influence of important things such as the turbulence model and the grid used in the computations have not been studied in detail. Then, future works should include these parameters and the combination of CFD 3D simulations with advanced experimental techniques (PIV, LDA, hot-wire anemometry, etc.) to validate the numerical results.

One of the most recent papers in the scientific literature is due to Jaramillo et al. "Analysis of the dynamic behavior of refrigerated spaces using air curtains" [36]. In this publication the effects of the curtain in a quickly opened door are presented. The efficiency of the device is characterized comparing the losses produced with and without the curtain in the door.

In another recent paper, "Detailed Analysis of turbulent flows in air curtains" [37] Jaramillo et al. carried out a detailed numerical study of the turbulence in the plenum of an air curtain and the influence of the blades in the orientation of the jet.

The study of air curtains acting as ambient separator is also attempted by E.Nino et al. in their study about the rate of infiltration of little droplets through an air jet [38].They conclude the infiltration rate is dependent of the Reynolds.

The infiltration rate and the parameters that affect it in the case of Open refrigerated cavities has been studied by Mazyar Amin et al. [39].They use the tracer gas

method to quantify the rate of infiltration. The also concluded that the infiltration rate is proportional to the Reynolds number. They also concluded that the interaction of the different geometrical variables affects the infiltration more so than the Reynolds.

The simulation of air curtains employing 3D calculations is indicated in the study by Foster et al. [40], in which, the discrepancies between 3D simulations and 2D predictions are exposed and the 3D flow structures produced by a conventional commercial air curtain working on usual conditions are described.They conclude that the 3D simulations are necessary in order to fully understand the behaviour of those devices.

Other studies regarding the efficiency of air curtains can be found in the recent literature. Costa et al. [41] found that the efficiency of a downward blowing ACU is roughly 75% in optimum conditions, while the studies of Gonçalves et al. [42] [43], shown that the maximum sealing efficiency was observed for the down-blowing configuration, and that this sealing efficiency can reach values slightly above 75%.

The process of characterization, design and modification by means of CFD simulations and experimental measurements has been carried out in a study by the authors [45]. In this study CFD, semi-analytical and experimental approaches has been employed. An initial air curtain prototype is characterized by means of experimental measurements employing hot wire anemmometers (HWA). The measurements give insight about some not desirable characteristics of the produced air jet. Some of these characterictics are excessive turbulence, excessive turbulence, lack of homogeneity or a too low mean velocity. By means of a re-design , different plenums are proposed and tested by means of CFD simulations. The optimum design is constructed and tested experimentally. A remarkable improvement is obtained in the different charcteristics of the air jet. All the measurements are carried out according to the AMCA standard [44], with unidimensional probe sensor. This type of technology ensures the precision required by the standard. This paper has been included as one of the chapters in this thesis.

In a very recent study, the already mentioned classical semi-analytical method proposed by Siren [21,22] has been modified according to experimental and numerical onbservations by the authors [46]. The proposed modification takes into account the effect of the lateral unprotected area. This area appears when the air jet suffers a progressive deflection by the effect of the different forces acting against it. This paper has been also included as one of the chapters in this thesis.

1.4 Antecedents at the CTTC

The present thesis is mainly the continuation of the previous research activity carried out in the past years at the CTTC ("Centre Tecnològic de Transferència de Calor"). The Julian Jaramillo thesis [35] describes the previous research work carried out by the group in this subject.

1.5 Objectives and structure of this thesis

The main objective of this thesis is the study and optimization of air curtains. For this purpose, numerical, semianalytical and experimental methods will be used, covering each one of them different aspects of the process.

This thesis follows an intuitive procedure: in the first stage of the thesis different approaches are employed and the devices will be characterized and, taken into account the flaws observed, the ACU will be optimized adding the required modifications. In the last stage it will be presented some comparatives. The effect of the wind, moisture, difference of temperature and other factors will be studied.

The three chapters 2, 3, 4 are divided according to the different methodologies of study and all three chapters complete the characterization stage by means of semianalytical methods, numerical simulations and experimental measurements respectively.

In the chapter 2, the semianalytical method is presented. Based on the previous model developed by Siren [21, 22], an improved method is presented, taking into account the three dimensional behaviour of the air curtains intallations. The improved method is probed to be a reliable method in the determination of the efficiency of air curtains.

In the chapter 3, a brief overview of the Large Eddy Simulation models is presented. The numerical methodology, the employed meshes and the data treatment is explained.

In the chapter 4 the experimental characterization of a commercial air curtain is carried out. By means of hot wire anemometry technique, the different air jets produced with different plenum geometries are evaluated.

If we compare the three approaches, the semianalytical methods are faster than the numerical simulations with CFD, but the solutions are less detailed and much less accurate. The CFD are for sure the best way to characterize the air curtains, but they are very time consuming. And, at last, the experimental measurements by means of Hot Wire Anemometry allow us to assess the physical reliability of the previous calculations, but these measurements require an experimental setup which is more expensive than the other characterization methods.

In the chapter 5 the air curtain plenum is optimized according to the possible flaws in the initial design of the air curtain. It will be observed that an overall new design is needed, being not single modifications the answer to the innecesary pressure losses

inside the device. The initial design presents a sudden expansion of the discharge channel, as well as sharp angles in the path followed by the air from the fans to the discharge nozzle. As a result, the produced air jet is weaker than expected, and also has a lack of homogeneity and a high level of turbulence. The proposed design avoids that undesired bahaviour of the air jet by means of a smoother plenum. Both, the measuremnts and the numerical simulations indicate a remarkable improvement of the quality of the air jet.

In the chapter 6 the application of recirculating and non-recirculating air curtain units in the refrigeration and climatization field is studied. The air curtains behaviour in a refrigerating room is evaluated by means of advanced CFD models. The water vapour condensation produced in the different walls is quantified. The efficiency of the air curtain is evaluated for thermal and moisture entrainment. Recirculating and non-recirculating air curtains efficiencies are compared.

In the chapter 7 the final conclusions of the work and possible future lines of research are presented.

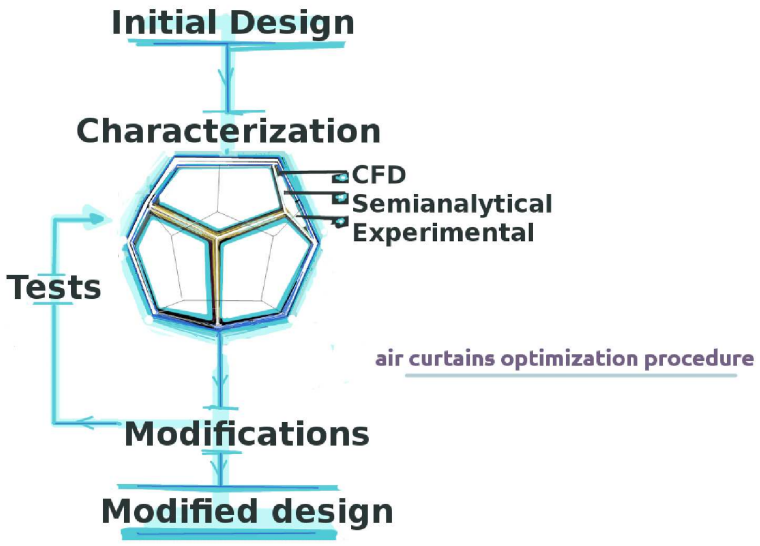

Figure 1.2: The ACU optimization methodology employed in the present thesis.

1.6 Conclusions

In this chapter, an overview of air curtains is given. The fundamental parameters used to study them are explained, and it is defined how to obtain better designs in these devices.

Also, a brief description of the typical air curtain geometry is performed. The state of the art has also been explained.

The fundamental approaches of this thesis for the study of air curtains have being indicated. In order to carry out swift calculations, the semianalytical methods of the SACS application will allow to determine the performance of the devices. For higher level calculations we will use the CFD code TermoFluids, which is much more time consuming but gives more accurate results. In order to assess wether the calculations describe properly the physical phenomena, we will carry out experimental measurements according to the international standards and employing hot wire anemometry technology.

References

[1] JE. Jaramillo, FX. Trias, A. Gorobets, CD. Pérez-Segarra, and A. Oliva. DNS and RANS modelling of a turbulent plane impinging jet. *International Journal of Heat and Mass Transfer*, 55(1):789–801, 2012.

[2] C. Solliec, S. Maurel, M. Pavageau, and P. Le Cloirec. Isolation of Contaminated Areas and Control of Fugitive Emissions Using Air Curtains. *Pollution Atmosphérique*, 169:127–137, 2001.

[3] Nguyen Q. Van and Ronald H. Howell. Influence of initial turbulence intensity on the development of plane air-curtain jets. *ASHRAE Transactions*, 82(pt 1):208–228, 1976.

[4] H. Schlichting. *Teoría de la capa límite*. Ediciones Urmo, 1972.

[5] Antonia RA, Browne LW, Rajagopalan S, Chambers AJ. On the organised motion of a turbulent plane jet. *J Fluid Mech*, 134: 49–66, 1983.

[6] Jenkins PE, Goldschmidt VW. Mean temperature and velocity in a plane turbulent jet. *J Fluid Eng*, 95: 581–584, 1973.

[7] Bashir J, Uberoi MS. Experiments on turbulent structure and heat transfer in a two-dimensional jet. *Phys FLuids*, 18: 405–410, 1975.

[8] Beltaos S, Rajaratnam N. Plane turbulent impinging jets. *J Hydraulic Res*, 1: 29–60, 1973.

[9] G. Hetsroni, C. W. Hall, and A. M. Dhanak. Heat Transfer Properties of an Air Curtain. *ASAE Transactions*, 1:328–334, 1963.

[10] F. C. Hayes and W. F. Stoecker. Design Data for Air Curtains. *ASHRAE Transactions*, 2121:168–179, 1969.

[11] R. H. Howell and M. Shiabata. Optimum Heat Transfer Through Turbulent Recirculated Plane Air Curtains. *ASHRAE Transactions*, 86(1):188–200, 1980.

[12] T. S. Park and H. J. Sung. A Nonlinear low-Reynolds-number $k - \epsilon$ model for Turbulent Separated and Reattaching Flows–I. Flow Field Computations. *International Journal of Heat and Mass Transfer*, 38:2657–2666, 1995.

[13] R. Faramarzi. Efficient Display Case Refrigeration. *ASHRAE Journal*, Nov.:46–54, 1999.

[14] D. Stribling, S.A. Tassou, and D. Marriott. A Two Dimensional CFD Model of a Refrigerated Display Case. *ASHRAE Transactions*, 103(1):88–94, 1999.

[15] L. Guyonnaud, C. Solliec, M. Dufresne de Virel, and C. Rey. Design of air curtains used for area confinement in tunnels. *Experiments in Fluids*, 28:377–384, 2000.

[16] M. Pavageau, E. M. Nieto, and C. Rey. Odor and VOC confining in Large Enclosure. *Water, Science and Technology*, 4(9):165–171, 2001.

[17] Y.T. Ge and S.A. Tassou. Simulation of the Performance of Single Jet Air Curtains for Vertical Refrigerated Display Cabinets. *Applied Thermal Engineering*, 21:201–219, 2001.

[18] T. Kim, S. Kato, and S. Murakami. Indoor cooling/heating load analysis based on coupled simulation of convection, radiation and HVAC control. *Building and Environment*, 36:901–908, 2001.

[19] H.K. Navaz, R. Faramarzi, M. Gharib, D. Dabiri, and D. Modarress. The Application of Advanced Methods in Analyzing the Performance ot the Air Curtain in a Refrigerated Display Case. *Journal of Fluids Engineering*, 124(1):756–764, 2002.

[20] A. M. Foster, R. Barrett, S. J. James, and M. J. Swain. Measurement and prediction of air movement through doorways in refrigerated rooms. *International Journal of Refrigeration*, 25(8):1102–1109, 2002.

[21] K. Sirén. Technical Dimensioning of a Vertically Upwards Blowing Air Curtain. Part I. *Energy and Buildings*, 35:681–695, 2003.

[22] K. Sirén. Thechnical Dimensioning of a Vertically Upwards Blowing Air Curtain-part II. *Energy and Buildings*, 35:697–705, 2003.

[23] M. Havet, O. Rouaud, and C. Solliec. Experimental Investigations of an Air Curtain device Subjected to External Perturbations. *International Journal of Heat and Fluid Flow*, 24:928–930, 2003.

[24] P. Battacharjee and E. Loth. Entrainment by a Refrigerated Air Curtain Down a Wall. *Journal of Fluids Engineering*, 126(5):871–879, 2004.

[25] B. S. Field and E. Loth. An air Curtain Along a Wall With High Inlet Turbulence. *Journal of Fluids Engineering*, 126:391–398, 2004.

[26] J. Cui and S. Wang. Application of CFD in evaluation and energy-efficient design of air curtains for horizontal refrigerated display cases. *International Journal of Thermal Sciences*, 43:993–1002, 2004.

[27] Y. G. Chen and X. L. Yuan. Experimental study of the performance of single-band air curtains for multi-deck refrigerated display cabinet. *Journal of Food Engineering*, 69:261–267, 2005.

[28] Olivier Rouaud and Michel Havet Behavior of an Air Curtain Subjected to Transversal Pressure Variations *J. Envir. Engrg.*,132(2), 263–270, 2006.

[29] Y. G. Chen and X. L. Yuan. Simulation of a cavity insulated by a vertical single band cold air curtain. *Energy Conversion Management*, 46:1745–1756, 2005.

[30] H. K. Navaz, B. S. Henderson, R. Faramarzi, A. Pourmovahed, and F. Taugwalder. Jet entrainment rate in air curtain of open refrigerated display cases. *International Journal of Refrigeration*, 28:267–275, 2005.

[31] H. K. Navaz, D. Dabiri, M. Amin, and R. Faramarzi. Past, Present, and Future Research Toward Air Curtain Performance Optimization. *ASHRAE Transactions*, 111:1083–1088, 2005.

[32] H. K. Navaz, M. Amin, S. C. Rasipuram, and R. Faramarzi. Jet entrainment minimization in an air curtain of open refrigerated display case. *International Journal for Numerical Methods for Heat and Fluid Flow*, 16(4):417–430, 2006.

[33] A. M. Foster, M. J. Swain, R. Barrett, P. D'Agaro, and S. J. James. Effectiveness and optimum jet velocity for a plane jet air curtain used to restrict cold room infiltration. *International Journal of Refrigeration*, 29(5):692–699, 2006.

[34] J. J. Costa, L. A. Oliveira, and M. C. G. Silva. Energy savings by aerodynamic sealing with a downward-blowing plane air curtain-A numerical approach. *Energy and Buildings*, 38:1182–1193, 2006.

[35] J. E. Jaramillo. *Suitability of Different RANS Models in the Description of Turbulent Forced Convection Flows. Application to Air Curtains.* PhD thesis, Universitat Politècnica de Catalunya, 2008.

[36] J. E. Jaramillo, C. D. Pérez-Segarra, A. Oliva, and C. Oliet. Analysis of the Dynamic Behaviour of Refrigerated Space Using Air Curtains. *Numerical Heat Transfer, Part A*, 55(6):553–573, 2009.

[37] J. E. Jaramillo, C. D. Pérez-Segarra, O. Lehmkuhl, and J. Castro. Detailed Analysis of Turbulent Flows in Air Curtains. *Progress in Computational Fluid Dynamics*, 11(6):350–362, 2011.

[38] Nino, E., Fasanella, R., Di Tommaso, R.M. Submerged rectangular air jets as a particulate barrier *Building and Environment*, 46(11):2375–2386, 2011.

[39] Amin, M., Dabiri, D., Navaz, H.K. Comprehensive study on the effects of fluid dynamics of air curtain and geometry, on infiltration rate of open refrigerated cavities *Applied Thermal Engineering*, 31 (14-15), 3055–3065, 2011.

[40] A. M. Foster, M. J. Swain, R. Barrett, P. DAgaro, L. Ketteringham, and S. J. James. Three-Dimensional Effects of an Air Curtain Used to Restrict Cold Room Infiltration. *Applied Mathematical Modelling*, 31(6):1109–1123, 2007.

[41] J.J. Costa, L.A. Oliveira, and M.C.G. Silva. Energy Savings by Aerodynamic Sealing with a Downward-blowing Plane Air Curtain, A Numerical Approach. *Energy and Buildings*, 38(10):1182 – 1193, 2006.

[42] J.C. Gonçalves, J.J. Costa, A.R. Figueiredo, and A.M.G. Lopes. CFD Modelling of Aerodynamic Sealing by Vertical and Horizontal Air Curtains. *Energy and Buildings*, 52:153 – 160, 2012.

[43] J.C. Gonçalves, J.J. Costa, A.R. Figueiredo, and A.M.G. Lopes. Study of the Aerodynamic Sealing of a Cold Store, Experimental and Numerical Approaches. *Energy and Buildings*, 2012.

[44] Air Movement and Control Association International. *ANSI/AMCA Standard 220-05. Laboratory Methods of Testing Air Curtain Units for Aerodynamic Performance Rating.*, 2005.

[45] H. Giráldez, C. D. Pérez-Segarra, I. Rodríguez, and A. Oliva. Optimization of the Thermal and Fluid Dynamic Behaviour of Air Curtains. Analysis of the Plenum by Means of LES. In *Proceedings of the 15th International Conference on Fluid Flow Technologies,Budapest,Hungary*, 2012.

[46] H. Giráldez, C. D. Pérez-Segarra, I. Rodríguez, and A. Oliva. Improved semi-analytical method for air curtains prediction. *Energy and Buildings*, 60:256–266, 2013.

2

Semianalytical mathematical models

Main contents of this chapter have been published in:
H. Giráldez, C.D. Pérez Segarra, I. Rodríguez, A. Oliva, Improved semi-analytical method for air curtains prediction, Energy and Buildings, Volume 66, 258-266, November 2013.

2.1 Abstract

The present chapter is devoted to the analysis and prediction of the efficiency of air curtains. The attention is focused on improving existing semi-analytical methods with the information from CFD simulations and experimental measurements. The goal is to obtain an accurate simplified model which describes the three-dimensional behaviour of the air jet without requiring large time consuming calculations. The interaction of the air curtain with other agents, e.g. pedestrians and flying insects, is also revised. The model is validated against both experimental data and advanced LES calculations carried out by the authors. Furthermore, a parametric study shows the air curtain behaviour for different configurations.

2.2 Introduction

An air curtain unit (ACU) is basically a device which produces a plane impinging jet acting as an ambient separator. The simplest case of heat and mass transfer through the opening protected by an ACU appears when the phenomenon reaches its steady state. It is worth noting that the capability of any ACU to protect the inner space depends on the conditions and on the application, which determine the minimum sealing required. For instance, an ACU working under the most demanding

conditions protecting a door in a commercial store application does not require as much momentum as an ACU under the same conditions for the refrigeration field.

One of the first studies about air curtains was carried out by Hetsroni and Hall [1]. They studied experimentally the air entrainment-spill mechanism across air curtains. They introduced analytical expressions to quantify the heat transfer through the ACU. Later, Hayes and Stoecker [2] presented a comprehensive explanation of the different kind of pressure differences, which must be taken into account in air curtains design.

Different semi-analytical models can be found in the literature [3,4]. These models established the quantitative influence of the jet properties on the ACU performance. One of the last analytical models was developed by Siren [5, 6]. This model enabled the consideration of the jet impact point and provided information for the design of vertically upwards-blowing air curtains.

Air curtains have also been studied by means of detailed numerical techniques. These techniques allow the resolution of the velocity, pressure and temperature field, but their main drawback is that they are very expensive in terms of computational resources and CPU time. Navaz et al. [7] demonstrated that the combination of digital particle image velocimetry (PIV) and computational fluid dynamics (CFD) can be effective to study the flow field characteristics and performance of the air curtains of an open vertical display case.

A combination of CFD and experimental techniques was also presented by Foster et al. [8]. In a different study, Foster et al. [9], studied the effect of the discharge jet velocity on the efficiency and the three-dimensional behaviour of the air jet. They concluded that jets produced by air curtains can not be considered bi-dimensional.

In the study of Carlson et al. [10], the capacity of three commercial air curtains placed in the doorway of a simulated aircraft was evaluated. The measurements showed that, when the units are working, more than the 97% of mosquitoes and 98% of flies are prevented from entering the aircraft. They stated that air curtains which provide air jets with velocities lower than 2m/s do not provide a good protection against flying insects. ¿From the industrial point of view, it is not necessary to provide a 100% protection against flying insects, therefore a 70% is considered enough for many applications. A velocity higher than 4 m/s may be sufficient for industrial purposes. Additional entrainment of flying insects is produced when pedestrians cross the door. This circumstance is, in the opinion of Carlson et al. [10], unavoidable.

Lu et al. [11] evaluated experimentally the interaction between air curtains and pedestrians. The flow of an ACU mounted above a doorway in which was placed a mannequin was studied using stereo particle image velocimetry. According to this study, the interaction is confined to a region nearby the pedestrian, without affecting

the far regions from the person and does not cause a large reduction in the ACU efficiency.

Lu et al. [11] evaluated experimentally the interaction between air curtains and pedestrians. The flow of an ACU mounted above a doorway in which was placed a mannequin was studied using stereo particle image velocimetry. According to this study, the interaction is confined to a region nearby the pedestrian, without affecting the far regions from the person and does not cause a large reduction in the ACU efficiency.

Jaramillo et al. [12] carried out a detailed study of the plenum of an ACU by means of Reynolds Average Navier Stokes equations (RANS) techniques. Later, Jaramillo et al. [13] studied in detail the turbulent plane jet produced by an ACU and conclude that the quality of the produced air jet is strongly affected by the geometry of the plenum and the turbulence at the discharge nozzle.

The effects of air curtains for reducing the heat gains in refrigerated chambers was analysed by Jaramillo et al. [14], by means of RANS models. Their studies showed satisfactory results when compared with experimental measurements. Furthermore, they showed that an ACU working near its ideal conditions can achieve sealing efficiencies up to approximately 75%. These results are also in agreement with the semi-analytical predictions.

The study of plane impinging jets is fundamental for the correct understanding of air curtains behaviour. For a detailed study of the physics of plane impinging jets see the study of Jaramillo et al. [15].

Other studies regarding the efficiency of air curtains can be found in the recent literature. Costa et al. [16] found that the efficiency of a downward blowing ACU is roughly 75% in optimum conditions, while the studies of Gonçalves et al. [17] [18], shown that the maximum sealing efficiency was observed for the down-blowing configuration, and that this sealing efficiency can reach values slightly above 75%. The

main objective of the present study is to propose an improved semi-analytical methods which is based on the model proposed by Siren [5, 6]. The approach presented is based on the flow distribution which allow a semi-analytical integration [5, 6] and it is complemented by the use of different expressions for each region of the jet.

One of the advantages of these semi-analytical models is the reduction obtained in the resolution of the average flow field produced by the ACU when compared with detailed calculations such as those used in [19, 20].

With the semi-analytical method, the problem of finding the downstream jet evolution is diverted to calculate a set of expressions that only depend on the initial jet velocity and orientation of the discharge. In the present study the main agents which affect the efficiency of the ACU as a barrier are considered. In the following sections,

the expressions for the characterization of an ACU are presented together with the equations for defining the velocity and temperature profiles. The basic dimensioning of the ACU is also defined. The jet deflection is expressed as a function of the external forces acting against the air jet. The method extracted from the literature [5] is modified adding a new term corresponding to the lateral entrainment. The modified semi-analytical method is validated by comparison with experimental measurements and with the flow obtained by means of CFD simulations. After the validation of the method, a parametric study of the effect of the door geometry is carried out. The effect of the lateral entrainment and the importance of the ACU geometry in order to minimize this effect, specially in applications where the energy gains are critical, are also pointed out.

2.3 Semi-analytical Mathematical Models

In this section the basic equations which describe the velocity, temperature and deflection of the air jet are presented. The expression for the basic dimensioning of an ACU is also described. The energy balance of the space protected by an ACU is presented. The modification of the energy balance proposed in the present study consists in the addition of the lateral entrainment.

2.3.1 Jet velocity and temperature profiles

Semi-analytical models usually predict the downstream evolution of the air jet produced by an ACU assuming that the jet behaviour is bi-dimensional [5, 6]. These methods assume that the deflection is low and, hence, the jet curvature is negligible.

In the first zone, the so called potential core region, the axis velocity is equal to the discharge velocity. After the potential core region is consumed, the transition zone and the developed zone decrease progressively the axis velocity. The last zone is the impinging region, where the velocity quickly decays to zero. In the developed zone there are two assumptions: the momentum in the stream-wise direction is conserved and the velocity distribution in the transversal direction is described by the following expression [6]:

$$\frac{v}{v_c} = \frac{1}{\cosh^2 \eta} \tag{2.1}$$

where v_c is the velocity at the jet centreline and $\eta = \dfrac{\sigma x}{s}$, being σ a constant of value 7.67 and s the longitudinal distance from the nozzle along the jet axis. Here, this distance is replaced by the vertical distance, $s = z$. These assumptions are employed in the developed zone.

Based on the conservation of momentum flux in the jet and the velocity profile (eq. 2.1), it can be written the expression for the downstream evolution of the jet:

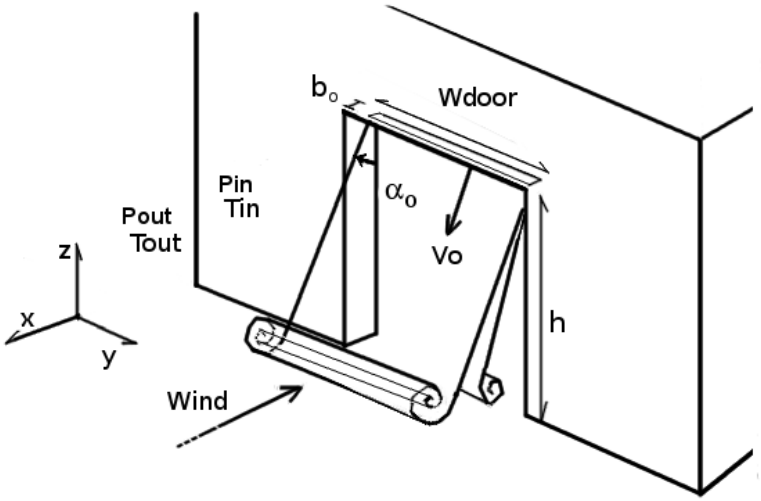

Figure 2.1: Geometry of the problem.

$$\frac{v_c}{v_0} = \frac{1}{2}\sqrt{\frac{3\sigma b_0}{z}} \tag{2.2}$$

here v_0 is the velocity at the discharge.

In the case of zero mass flow through the door, the impact point can be determined as [6]:

$$\eta_e = \pm\sqrt{\frac{\sigma b_0}{3h}} \tag{2.3}$$

The following is an expression for the jet temperature profile, which showed a fairly good consistency with measurements [21]. For a case where the warm space is on the left side in the coordinate system (see Fig.2.1) takes the form [6]:

$$\frac{T - T_0}{T_i - T_0} = 1 + \frac{4}{\pi}\sqrt{\frac{\sigma}{3}\frac{b_0}{z}}\frac{T_0 - (T_i + T_0)/2}{T_i - T_0}\frac{1}{\cos h\eta} - \frac{2}{\pi}\arctan e^{\eta} \tag{2.4}$$

The temperature profile is not symmetrical. With the two previous expressions for the velocity and the thermal distribution the air jet can be described.

2.3.2 Dimensioning of the air curtain jet

The dimensioning of the ACU consist in determining the momentum flux of the jet required to counteract the external forces [2]. The approach presented was proposed by Sirén [5], and takes moment-of momentum balance in the doorway, assuming conservation of angular momentum. The general moment-of momentum is the cross product of the forces F acting on a control volume and the vectors of position r from a given point of rotation.

$$\sum \mathbf{r} \times \mathbf{F_P} = \int_{CS} \rho \mathbf{r} \times \mathbf{vv} \cdot d\mathbf{A} \tag{2.5}$$

Applying the above expression to a two-dimensional case:

$$\sum r_n F = \int_{CS} \rho r_n v^2 dA \tag{2.6}$$

The force acting against the ACU is due to the total pressure and the point of impact is chosen as the point of rotation

$$W_{door} \int_0^h \left[p_0\left(z\right) - p_i\left(z\right)\right]\left(h - z\right) dz = \rho_0 A_0 v_0^2 \sin\alpha_0 h - \rho_0 A_0 v_0^2 \cos\alpha_0 x_1 \tag{2.7}$$

where x_1 is the distance of the point of impact from the door-plane (see Fig. 2.2) and α_0 is the nozzle discharge angle. The induced pressure difference is a consequence of the temperature difference, wind effect and mechanical pressure. It can be obtained from:

$$p_o(z) - p_i(z) = \left(\rho_i - \rho_o\right) g(z - z_{ns}) + \frac{1}{2} C_w \rho_o v_w^2 \tag{2.8}$$

here z_{ns} stands for neutral pressure level and C_w stands for pressure coefficient of the wind.

Substituting the pressure term of the Eq.2.7 with Eq.2.8, and integrating yields

$$\frac{1}{2} W h^2 \left[(\rho_o - \rho_i) g(z_{ns} - \frac{1}{3} h) + \frac{1}{2} C_w \rho_o v_w^2\right] = \rho_o b_o l_o v_o^2 (h \sin\alpha_0 - x_1 \cos\alpha_0) \tag{2.9}$$

Rearranging and solving the discharge momentum flux per unit length gives

$$M_0 = \rho_0 b_0 v_0^2 = \frac{h}{2(\sin\alpha_0 - (x_1/h)\cos\alpha_0} \left[\left(\rho_0 - \rho_1\right) g \left(z_{ns} - \frac{1}{3} h\right) + \frac{1}{2} C_p \rho_0 v_w^2\right] \tag{2.10}$$

This expression gives the required momentum to counteract the external forces.

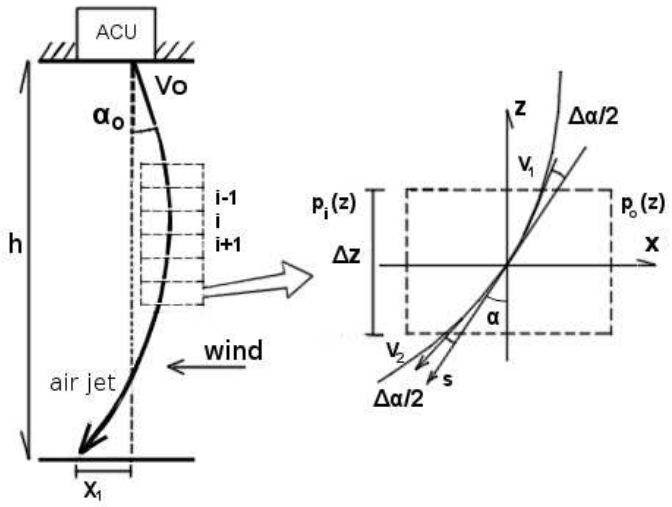

Figure 2.2: Control volume scheme in the jet trajectory.

2.3.3 Jet deflection

The jet deflection is calculated with a numerical approach. The path that the jet follows from the discharge to the impact point is described by means of a momentum balance in x-direction.

According to the coordinate system in Fig.2.2:

$$(p_o - p_i)\Delta z = \rho_1 b_1 v_1^2 sin(\alpha - \frac{1}{2}\Delta\alpha) - \rho_2 b_2 v_2^2 \sin(\alpha + \frac{1}{2}\Delta\alpha) \tag{2.11}$$

The numerical calculation advances assuming one way behaviour, being affected every position and angle only by the previous values:

$$\sin\alpha_1 = \sin\alpha_0 + \frac{(\rho_o - \rho_i)g(z/2 - z_{ns})z}{\rho_0 b_0 v_0^2} - \frac{\frac{1}{2}C_w\rho_o v_w^2 z}{\rho_0 b_0 v_0^2} \tag{2.12}$$

$$x_1 = x_0 + tan(\alpha_0)\Delta z; \tag{2.13}$$

It is worth noting that this deflection is produced by the superposition of the effect of the stack pressure difference and the wind effect.

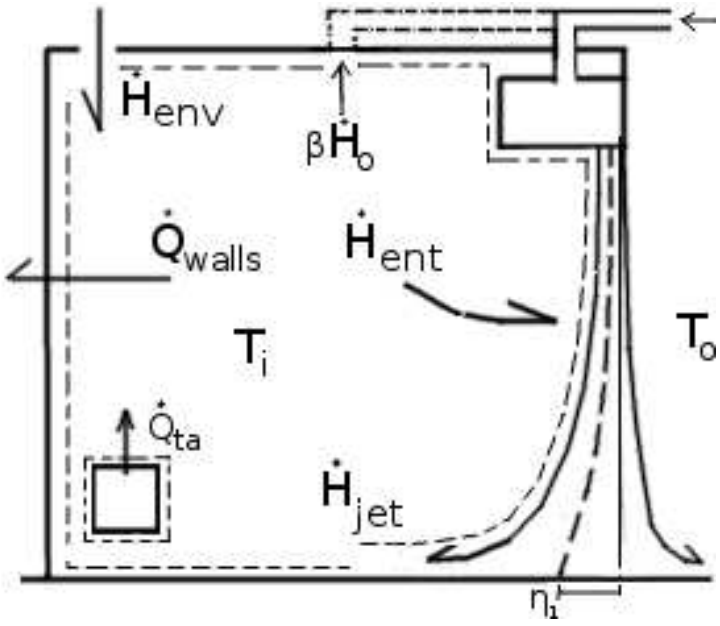

Figure 2.3: Energy balance of the protected space.

2.3.4 Total thermal losses

From an energy balance of the inner space (see Fig.2.3), the following energy equation can be obtained

$$\dot{Q}_{ta} - \dot{Q}_{walls} = \dot{H}_{ent} + \dot{H}_o - \dot{H}_{env} - \dot{H}_{jet} \tag{2.14}$$

where $\dot{Q}_{ta}$ represents the heat delivered to (or extracted from) the space to maintain the inner temperature T_i, $\dot{Q}_{walls}$ is the heat losses through the walls, $\dot{H}_{ent}$ is the enthalpy flow of indoor air entrained into the jet, $\dot{H}_o$ indicates the enthalpy flow when the suction is from inside, $\dot{H}_{env}$ is the enthalpy flow through the envelope which is generated to compensate the flow through the doorway and $\dot{H}_{jet}$ the enthalpy flow carried by the part of the jet which is blown in the space.

The total thermal loss due to the use of the ACU can be calculated by applying the velocity and temperature profiles and performing the integration across the jet.

$$\dot{H}_{ent} = \dot{m}_{ent} h_i \tag{2.15}$$

$$\dot{H}_o = \beta \dot{m}_o h_i \tag{2.16}$$

$$\beta = 1 \text{ suction from inside}$$

$$\beta = 0 \text{ suction from outside}$$

$$\dot{H}_{env} = \dot{m}_{env} h_{io} \tag{2.17}$$

$$h_{io} = h_o \text{ if } \dot{m}_{env} > 0$$

$$h_{io} = h_i \text{ if } \dot{m}_{env} < 0$$

$$\dot{H}_{jet} = \int_{-\infty}^{\eta_1} \rho h v d\eta \tag{2.18}$$

where η_1 represents the impact point of the jet (see Fig. 2.3). As was mentioned before, in case of zero mass flow through the door, the impact point is given by eq. 2.3. In this specific case, $\eta_1 = \eta_e$.

2.4 Validation of the semi-analytical model: comparison with CFD simulations

In order to validate the semi-analytical method, the ACU flow has been described by means of CFD simulations. The calculation domain,the mesh employed, the mathematical and numerical model and the code employed are described in the following sections.

2.4.1 Calculation domain

The geometry of the physical domain consists of two adjacent room with different dimensions, connected by a door featuring 1.0 m width and 2 m height (see Fig.2.4(a)), with an ACU installed on the top. One of the rooms represent the protected space to maintain sealed, and the other corresponds to the outdoor environment. The discharge nozzle, on the lower face of the ACU, has a width of 6 cm. A length of 1 m is considered for the discharge nozzle to ensure that the jet covers the whole door width.

2.4.2 Computational mesh

An unstructured mesh is employed, the mesh has 1,045,931 control volumes, most of them in the region which covers the air jet (see Fig.2.4(b)). It is employed a high stretching near the solid walls in order to correctly solve the boundary layer.

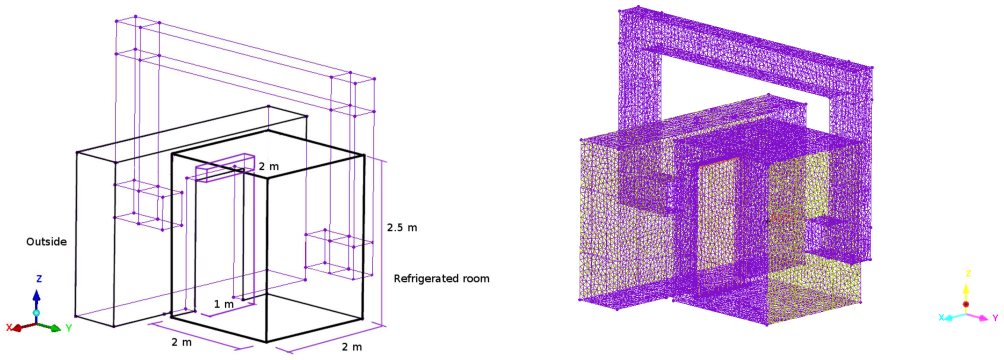

(a) (b)

Figure 2.4: (a) Geometry of the calculation domain and (b) sketch of the computational mesh.

2.4.3 Mathematical and numerical model

As the flow is highly unsteady and turbulent, a detailed study of the complex fluid dynamics in the ACU is carried out by means of large-eddy simulations (LES). Results are compared with the semi-analytical model in terms of the average statistics, obtained by the integration of the instantaneous results.

The spatially filtered Navier Stokes equations used in LES can be written as follows:

$$\nabla \cdot \overline{u} = 0 \tag{2.19}$$

$$\partial_t \overline{u} + (\overline{u} \cdot \nabla)\, \overline{u} + \nabla \overline{p} - 2\nu \nabla \cdot S(\overline{u}) = \nabla \cdot \left(\overline{u}\overline{u}^T - \overline{uu^T} \right) \tag{2.20}$$

Modelling the right-hand side in terms of $\overline{u}$ yields a simplified representation of the large eddies.

$$\nabla \cdot \left(\overline{u}\overline{u}^T - \overline{uu^T} \right) \approx 2\nabla \cdot (\nu_e S(\overline{u})) \tag{2.21}$$

To close the formulation, an appropriate definition of the subgrid-scale viscosity (ν_e) should be given. In the present work the Wall Adapting Local Eddy viscosity (WALE) model [22] is used. According to this model the expression for the eddy viscosity is given by

$$\nu_e = (C_{wale}\Delta)^2 \frac{\left(\&_{ij}^d \&_{ij}^d\right)^{3/2}}{\left(S_{ij}S_{ij}\right)^{5/2} + \left(\&_{ij}^d \&_{ij}^d\right)^{5/4}} \tag{2.22}$$

$$C_{wale} = 0.5 \tag{2.23}$$

where & is the traceless symmetric part of the square of the velocity gradient tensor:

$$\&_{ij}^d = \frac{1}{2}\left(\overline{g}_{ij}^2 + \overline{g}_{ji}^2\right) - \frac{1}{3}\delta_{ij}\overline{g}_{kk}^2 \tag{2.24}$$

$$\overline{g}_{ik}^2 = \overline{g}_{ik}\overline{g}_{kj} \tag{2.25}$$

$$\overline{g}_{ij} = \frac{\delta \overline{u}_i}{\delta x_j} \tag{2.26}$$

and δ_{ij} is the Kronecker delta operator.

2.4.4 Boundary and initial conditions

The envelope of the calculation domain has been taken as impervious, air changes being allowed only through the doorway between the two spaces. As initial conditions, the air has been assumed stagnant all over the whole domain. All surfaces has been considered adiabatic, smooth and no-slipping.

2.4.5 Numerical code

All the simulations are carried out using the CFD & HT code Termofluids [23], which is an unstructured and parallel object-oriented code for solving industrial flows. In Termofluids, the governing equations are discretized on a collocated unstructured grid arrangement, by means of second-order spectre-consistent schemes [24]. Such discretization preserves the symmetry properties of the continuous differential operators, and ensure both stability and conservation of the global kinetic-energy balance on any grid. For the temporal discretization a two-step linear explicit scheme on a fractional-step method has been used for the convective and diffusive terms [25], while for the pressure gradient term an implicit first-order scheme has been implemented. This methodology has been previously used with accurate results for solving the flow over bluff bodies with massive separation [26, 27].

2.5 Validation of the semi-analytical model

In this section a comparison between the semi-analytical model with both experimental data and LES calculations is presented.

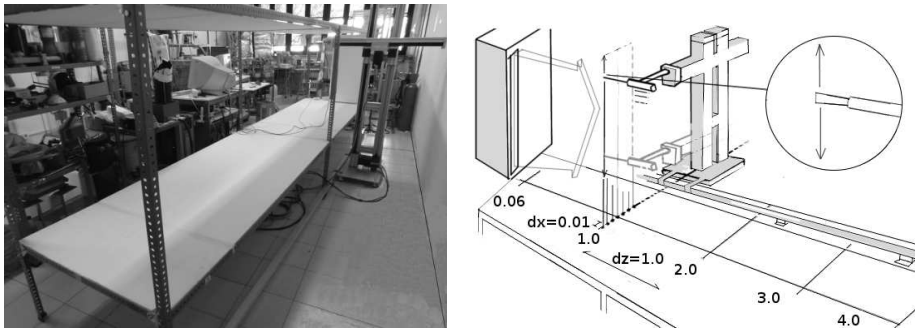

(a) (b)

Figure 2.5: (a) The experimental setup where the HWA measurements are carried out and (b) velocity measurement procedure scheme.

2.5.1 Validation based on experimental data

Predicted downstream evolution using the semi-analytical approach is compared with experimental measurements using hot wire anemometry
(HWA). An experimental set-up to evaluate the flow produced by the ACU is constructed (see Fig.2.5(a)). The dimensions of the channel are 5 x 1.1 x 1 m. The main parts of the experimental set-up are the channel itself, the probe positioning Cartesian robot and the HWA system. Obviously, the ACU is fixed at the beginning of the channel.

The experimental set-up allows the characterization of the flow in the range between the discharge (z=0) and the end of the channel itself (z=4 m), without external perturbations by the action of the baffles situated at each side of the ACU.

The Cartesian robot allows a positioning with resolution of 10^{-6}m. The measurements are taken in every transversal section programming the Cartesian robot to cover all the required domain in a time interval equal to the acquisition time. The relative movement of the robot does not affect the measurement of the velocity because the probe only captures the components of the velocity which acts in the plane normal to its wire (see Fig.2.5(b)). The measurements are carried out with unidimensional probes at a sample rate of 1000 Hz, during an acquisition time of 128 s in each test line. The test lines have a length of 1.0 m, covering all the span-wise direction of the ACU discharge and with a separation of 0.01 m between each test line. The separation between measurement planes is 1 m, being the first plane at a distance equal to the nozzle width.

Moreover, attached to the probe there is also a thermocouple, which allows to

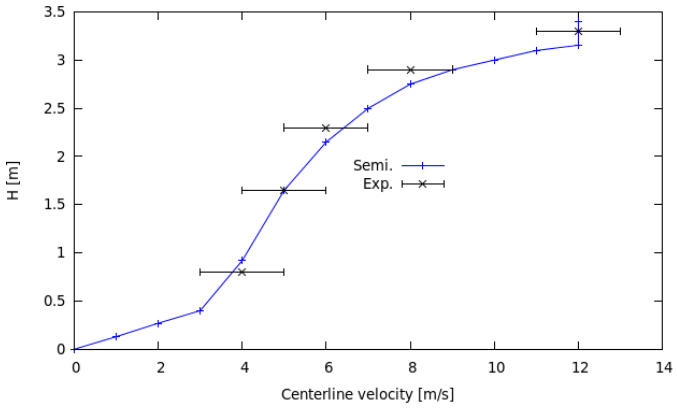

Figure 2.6: Experimental measurements of the downstream evolution of the jet compared to the semi-analytical expression (Eq.2.2). Note: dots indicate the mean velocity while the bars show the root mean square of the velocity.

correct the discrepancies produced by the possible deviations between the ambient temperature in the moment of calibration of the probe and the ambient temperature in the moment of data acquisition.

The measurements are carried out according to the AMCA standard [28], with unidimensional probe sensor. This type of technology ensures the precision required by the standard. The errors produced are due to the calibration, the temperature difference between the calibration and the data acquisition, the pressure fluctuations and other possible interferences due to the environment. For further details about the calibration or the measurement procedure refer to [29].

In Fig.2.6 a comparison between experimental measurements and the semi-analytical results is presented. The bars show the fluctuating part (root mean square) of the mean velocity. In this test the discharge velocity has been fixed at 12 m/s. It can be observed a reasonable agreement between the results and the experimental measurements.

Three different regions can be observed in the semi-analytical curve:

- The potential core region, where the core velocity remains equal to the discharge velocity. This region extends from the discharge to $5b_0$ in the downstream direction, being b_0 the nozzle discharge width.
- The developed zone, where the jet velocity decays progressively. This region extends from the end of the potential core to $0.1H$, being H the door height.

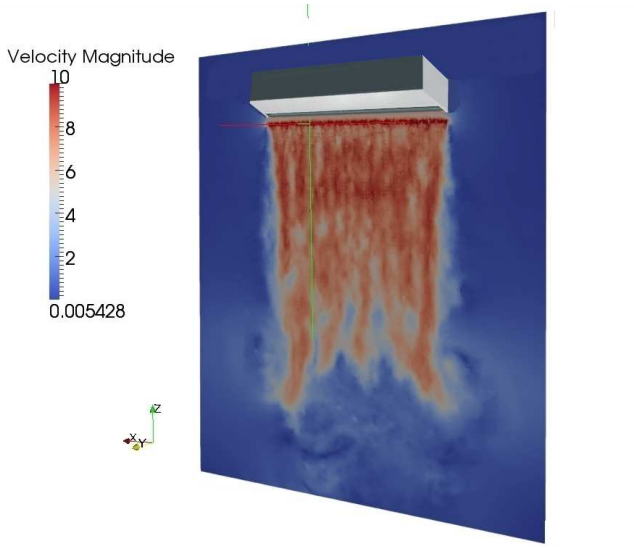

Figure 2.7: Overall view of an instantaneous velocity distribution according to the CFD simulation.

- The impinging region, where the decay rate is faster and nearly linear. This region extends from $0.1H$ to the floor.

2.5.2 Validation based on advanced CFD modelling

The results from CFD simulations are compared with the predictions of the semi-analytical approach, in order to determine the degree of agreement between the two approaches.

The simulations are carried out with the code TermoFluids [23].

In this test, the door height is 2 m, the door width is 1 m and the discharge velocity has been fixed at 10 m/s. In the Fig. 2.7 an overall view of the instantaneous velocity distribution is presented. The downstream evolution of the jet is presented in the Fig. 2.8. It can be seen the progressive spread produced in the jet, which modifies the initial flat profile and tends to acquire a Gaussian-like profile. The velocity is quite homogeneous in the discharge of the jet and the axial component is dominant.

The predicted downstream evolution according to the semi-analytical model and the one obtained from the CFD simulation are depicted in Fig. 2.9. In the CFD simulations it has been measured in the jet centreline. As can be observed, there is a reasonable agreement between the two approaches.

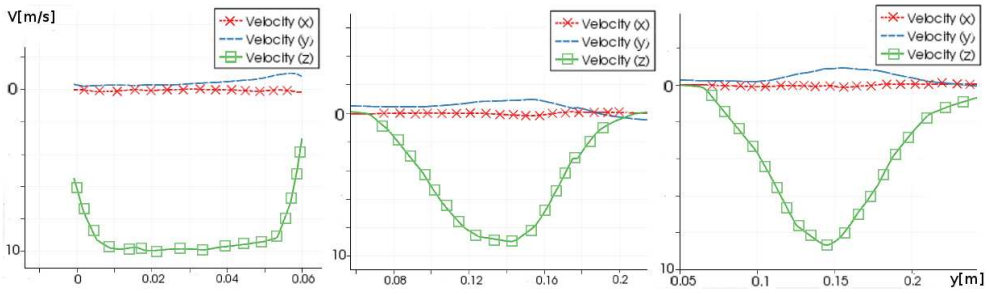

Figure 2.8: Downstream evolution of the jet. Average velocity profile at the discharge (left), at 10 cm (middle) and at 20 cm from the discharge (right).

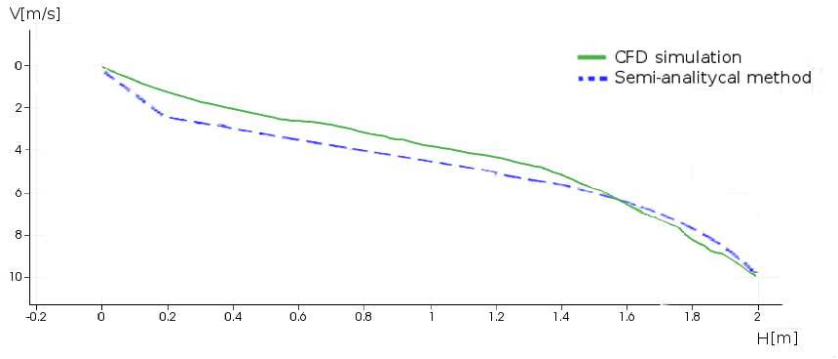

Figure 2.9: CFD simulation of the downstream evolution of the jet compared to the semi-analytical model.

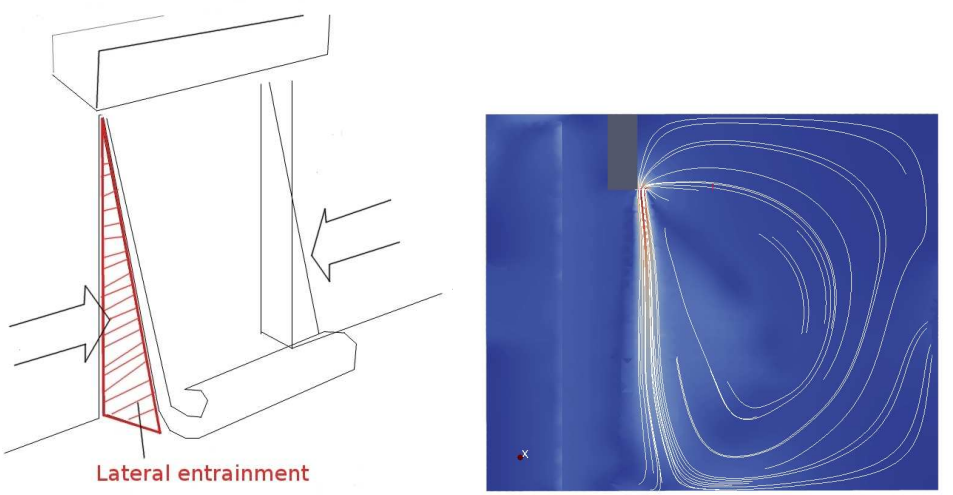

(a) (b)

Figure 2.10: (a) Scheme of the lateral entrainment due to the deflection of the air jet and (b) Jet deflection streamlines obtained from CFD simulation.

2.5.3 Corrections from CFD calculations

Contrary to semi-analytical models, CFD simulation are capable of capturing the three-dimensional behaviour of air curtains. In fact, the lateral entrainment which is responsible of affecting the ACU efficiency is not accounted for these traditional models.

The lateral entrainment is an additional flow produced through the lateral area that the air jet does not seal (see Fig.2.10(a)). Therefore the efficiency of the ACU is lower than the predicted initially by the semi-analytical approach. In this work, a modification of the initial energy balance (eq. 2.14) for considering this lateral entrainment is proposed. A new term, based on the integration of the flow through the area which is not protected by the air jet (see Fig. 2.10(b)) is introduced:

$$\dot{Q}_{ta} = \dot{H}_{ent} - \dot{H}_{jet} - \dot{H}_{env} + \dot{H}_o + \dot{H}_{lat} \tag{2.27}$$

where H_{lat} is the enthalpy flow blown into the space through the lateral unprotected area.

$$\dot{H}_{lat} = \rho_o \bar{v} A_{lat} c_p (T_i - T_o) \tag{2.28}$$

In the above equation, the mean velocity is the sum produced by the stack effect and the normal component of the wind. The lateral area where the entrainment is produced can be calculated as the integration of the jet deflection.

$$A_{lat} = \int_0^h def\,(z)\,dz \tag{2.29}$$

The CFD simulations allow the observation of the jet deflection and the entrainment produced in this lateral region(see Fig. 2.10(b)).

It is worth noting that the efficiency predicted by the model with the introduction of this additional term is closer to the results from the literature [14]. The model without the modification overestimates the efficiency achieved by the ACU in different cases (80-90%), while the modified model predicts lower efficiencies for the same cases (68-75%), which are according with the study mentioned above. The effect of the lateral entrainment diminishes the predicted efficiency of the ACU. Its effect is larger with door openings of moderate width, as it can be seen in section 5.

It has been shown that the semi-analytical model provides a reasonable agreement with both the experimental measurements and the predictions obtained by the large-eddy simulations.

2.6 Parametric study

In this section the study of the ACU behaviour for different configurations is carried out. In Fig.2.6 it is presented the reference case. In this case the discharge velocity has been fixed at 12 m/s, the door height is 3.5 m, the door width is 2 m and the discharge jet temperature is 20 °C. The geometry of the reference case is the same as in Fig. 2.1. The temperature difference between indoor and outdoor space is 15 °C. The nozzle width is 0.07m and the discharge angle is 2.5 °. For this test the intensity of wind is moderate (2 m/s).

¿From this reference case as a start point, different parameters are modified, so the effect on the ACU performance can be checked. Four parametric studies are presented:

- Influence of the door width and discharge angle (the width varies from 1 to 4 m and the discharge angle from $-15\,^\circ$ to $15\,^\circ$.
- Influence of the discharge width and the volumetric flow rate (two different nozzle width of 0.03 and 0.07 m and two mass flow rate of 0.76 and 1.53 m^3/s are investigated.
- Influence of the wind. The wind intensity varies from 0 to 4 m/s with three different discharge nozzles width.

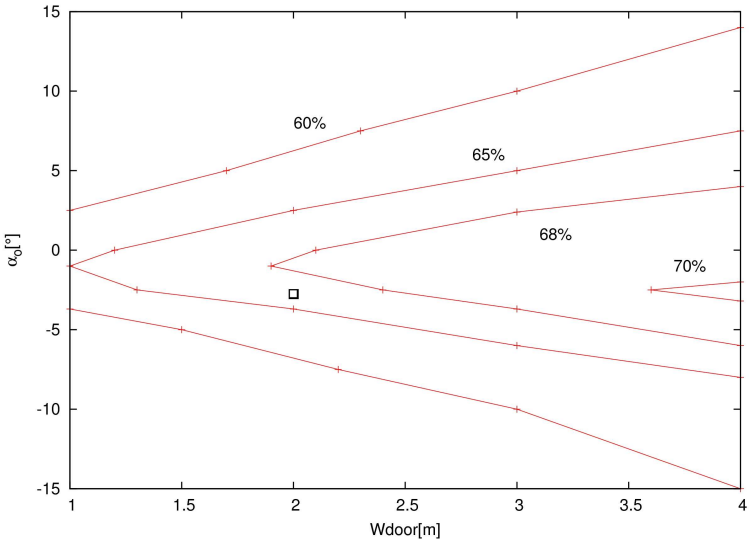

Figure 2.11: Isolines of efficiency in function of the door width and discharge angle. The square represents the reference case.

- Influence of the stack effect.The temperature difference between indoor and outdoor space varies from 4 to 20 °C.

The sealing efficiency is defined as

$$E_{ff} = 1 - \frac{Q_{ac}}{Q_d} \tag{2.30}$$

where Q_{ac} is the total thermal loss with the ACU active and Q_d is the total thermal loss through the entrance without the ACU.

2.6.1 Influence of the door width and discharge angle

The influence of the door width and discharge angle over the sealing efficiency can be studied.

The height of the door is fixed at 3.5 m. The results are depicted in Fig. 2.11.

It can be observed for a given discharge angle that if the door width is increased the ACU efficiency also increases. This is due to the attenuation of the lateral entrainment. If the door is narrower, then the lateral entrainment has a larger effect on the energy gain. For the different door width, if the angle is closer to $-2.5°$ then the efficiency achieves its maximum value.

The results obtained for the maximum efficiency (about 70%) compare well with those obtained by Jaramillo et al. [14]. It is worth mention that this study is carried out without the wind effect, which allows to isolate the effect of modifying the door geometry. Furthermore, it is shown that the smaller the door width the faster the decrease in the efficiency. This fact indicates that the air jet presents a sensitive behaviour for door openings of reduced width.

2.6.2 Influence of the discharge width and the volumetric flow rate

The intensity of wind employed is moderate (2m/s). Two different mass flows (0.76 and 1.53 m^3/s) and two different nozzle widths (0.03 and 0.07m) are employed. In this study the discharge angle is adapted in each test, considering only the results for the optimum ones. The results are presented in the Fig. 2.12.

The different curves correspond to:

- A: nozzle width=0.07 and flow rate=1.53m^3/s
- B: nozzle width=0.07 and flow rate=0.76m^3/s
- C: nozzle width=0.03 and flow rate=1.53m^3/s
- D: nozzle width=0.03 and flow rate=0.76m^3/s

In the figure, the two efficiency curves corresponding to the lower mass flow rates decrease abruptly when the door height is increased. This is due to the fact that the air jet does not have the required momentum to counteract the external pressure-induced forces. This effect is attenuated when the volumetric flow rate is increased. From the figure, the maximum efficiency for each pair of nozzle width and volumetric flow rate can also be obtained.

2.6.3 Analysis of the wind effect

The deflection produced in the air jet by the effect of the wind is here analysed. In this test there is no ventilation imbalance. In the tests, three nozzle width (0.05, 0.06 and 0.07 m)) are employed and the wind intensity is increased from 0 to 4 m/s. In Fig. 2.13) the results obtained are plotted. The efficiency is larger when the wind intensity is increased and the nozzle width is reduced. The efficiency of the ACU with wind velocities of low intensity is very poor, because the ACU is consuming a power but it is not avoiding a large potential entrainment.

For the wind intensity of 4 m/s it can be seen that the force of the wind produces the breaking of the jet for the three nozzle width.

2.6.4 Analysis of the stack effect

The difference of temperatures between indoor and outdoor space produce an additional force deflecting the air jet. In this test, the temperature difference is

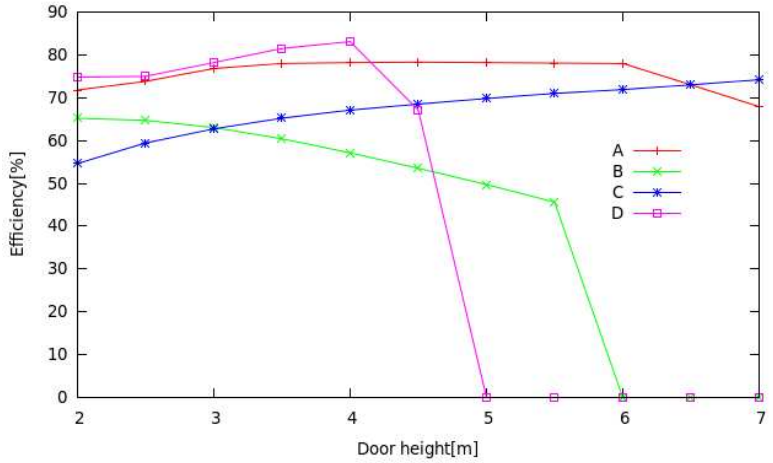

Figure 2.12: Influence of the volumetric flow rate, door height and nozzle width on the efficiency. A: nozzle width=0.07 and flow=$1.53m^3$/s, B: nozzle width=0.07 and flow=$0.76m^3$/s, C: nozzle width=0.03 and flow=$1.53m^3$/s, D: nozzle width=0.03 and flow=$0.76m^3$/s

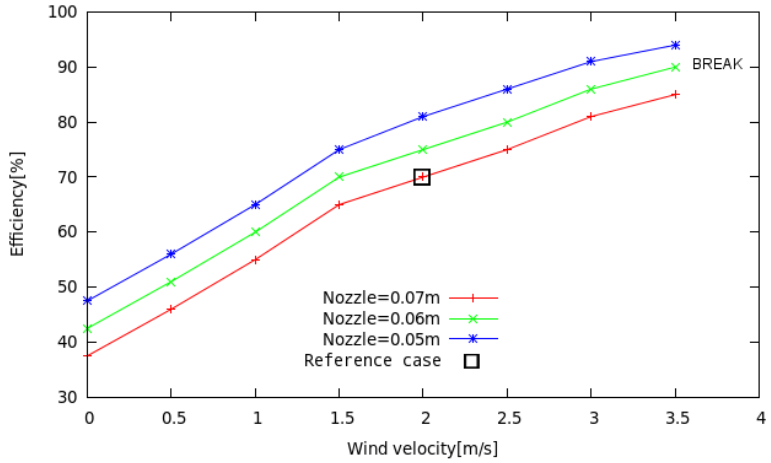

Figure 2.13: Influence of wind. Efficiency as a function of the incident wind from outdoor space. BREAK stands for jet breaking situation. The square represents the reference case.

varied so the effect on the efficiency of the ACU can be checked. The efficiency in function of the difference of temperatures is depicted in Fig. 2.14. The efficiency increases when the stack effect increases. However, after the rapid increase at lower temperature differences, the effect of this parameter on the efficiency is moderate at larger values.

2.7 Conclusions

A semi-analytical method for the prediction of air curtains efficiency has been presented. Unlike the model proposed by Sirén [5, 6], the model presented considers the effect of the entrainment through the unprotected lateral area. Furthermore, a more detailed description of the jet flow is given (the downstream evolution of the velocity considers a potential core, a developed zone and the impinging region).

The validation of the mathematical formulation has been carried out by comparison with experimental measurements and CFD simulations with advanced turbulence models (Large Eddy Simulation (LES)), both carried out by the authors. The calculations agree both with the experimental measurements and the LES results.

Several parametric studies by means of this methodology have been carried out. Specifically, the effect of modifying the door geometry, the nozzle width and the dis-

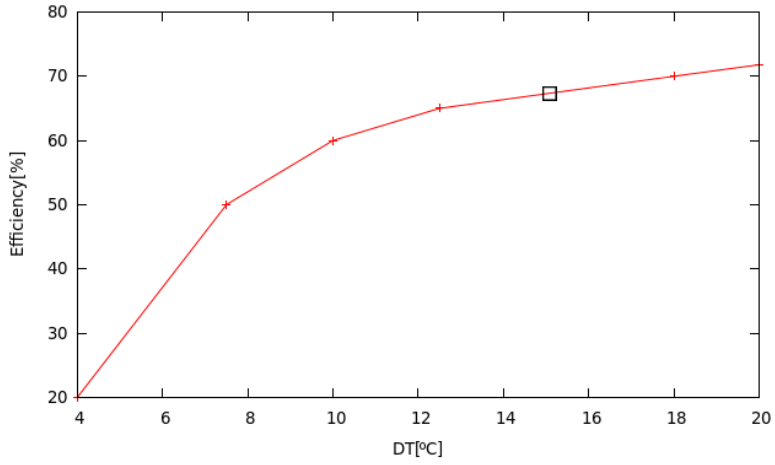

Figure 2.14: Influence of the stack effect. Efficiency as a function of the temperature difference between indoor and outdoor space. The square represents the reference case.

charge mass flow have been studied. An increase of the efficiency when the door width is increased and/or the nozzle width is decreased is observed. The effect of modifying the wind intensity or the temperature difference between indoor and outdoor spaces is also considered. An increase of the efficiency when the wind velocity or the temperature difference are increased is shown. The predicted efficiencies obtained in the parametric studies (68-75%) are more according to the results from the literature than the model without modifications(80-90%). It can be concluded that the proposed semi-analytical model is able to predict accurately the efficiency of air curtains.

Acknowledgements

This work has been financially supported by the Ministerio de Economía y Competitividad, Secretaría de Estado de Investigación, Desarrollo e Innovación, Spain (ENE-2010-17801) and by the collaboration project between the Universitat Politècnica de Catalunya (UPC) and Termo Fluids S. L. H. Giráldez also wishes to thank UPC for its support in the form of a FPI doctoral scholarship.

References

[1] G. Hetsroni and C. W. Hall. Further Studies of the Air Curtain. *ASAE Transactions*, 1:438–452, 1964.

[2] F. C. Hayes and W. F. Stoecker. Design Data for Air Curtains. *ASHRAE Transactions*, 2121:168–179, 1969.

[3] J. Partyka. Analytical Design of an Air Curtain. *Int. Journal of Modelling and Simulation*, 15(1):14–22, 1995.

[4] R. Faramarzi and K. Kemp. Comparing Older and Newer Refrigerated Display Cases. *ASHRAE Journal*, Aug.:45–49, 1999.

[5] K. Sirén. Technical Dimensioning of a Vertically Upwards Blowing Air Curtain. Part I. *Energy and Buildings*, 35:681–695, 2003.

[6] K. Sirén. Thechnical Dimensioning of a Vertically Upwards Blowing Air Curtainpart II. *Energy and Buildings*, 35:697–705, 2003.

[7] H.K. Navaz, R. Faramarzi, M. Gharib, D. Dabiri, and D. Modarress. The Application of Advanced Methods in Analyzing the Performance ot the Air Curtain in a Refrigerated Display Case. *Journal of Fluids Engineering*, 124(1):756–764, 2002.

[8] A. M. Foster, M. J. Swain, R. Barrett, and S. J. James. Experimental Verification of Analytical and CFD Predictions of Infiltration Through Cold Stores Entrances. *International Journal of Refrigeration*, 26(8):918–925, 2003.

[9] A. M. Foster, M. J. Swain, R. Barrett, P. DAgaro, L. Ketteringham, and S. J. James. Three-Dimensional Effects of an Air Curtain Used to Restrict Cold Room Infiltration. *Applied Mathematical Modelling*, 31(6):1109–1123, 2007.

[10] D. A. Carlson, J. A. Hogsette, D. L. Kline, and C. D. Geden. Prevention of Mosquitoes and House Flies from Entering Simulated Aircraft with Commercial Air Curtain Units. *Journal of Economic Entomology*, 99(1):182–193, 2006.

[11] John E. Fernandes Frank K. Lu. Visualizing the Flow Induced by an Air Curtain over a Mannequin using Stereo Particle Image Velocimetry. In *13th International Symposium on flow visualization, Nice, France*, 2008.

[12] J. E. Jaramillo, C. D. Pérez-Segarra, and A. Oliva. A Detailed Study of the Plenum and Discharge Jet Produced by Air Curtains. In *Proceedings of the 6th Internacional Conference on Engineering Computational Technology*, pages 1–12, 2008.

[13] J. E. Jaramillo, C. D. Pérez-Segarra, O. Lehmkuhl, and J. Castro. Detailed Analysis of Turbulent Flows in Air Curtains. *Progress in Computational Fluid Dynamics*, 11(6):350–362, 2011.

[14] J. E. Jaramillo, C. D. Pérez-Segarra, A. Oliva, and C. Oliet. Analysis of the Dynamic Behaviour of Refrigerated Space Using Air Curtains. *Numerical Heat Transfer, Part A*, 55(6):553–573, 2009.

[15] J. E. Jaramillo, F. X. Trias, A. Gorobets, C. D. Pérez-Segarra, and A. Oliva. DNS and RANS modelling of a turbulent plane impinging jet. *International Journal of Heat and Mass Transfer*, 55(1):789–801, 2012.

[16] J.J. Costa, L.A. Oliveira, and M.C.G. Silva. Energy Savings by Aerodynamic Sealing with a Downward-blowing Plane Air Curtain, A Numerical Approach. *Energy and Buildings*, 38(10):1182 – 1193, 2006.

[17] J.C. Gonçalves, J.J. Costa, A.R. Figueiredo, and A.M.G. Lopes. CFD Modelling of Aerodynamic Sealing by Vertical and Horizontal Air Curtains. *Energy and Buildings*, 52:153 – 160, 2012.

[18] J.C. Gonçalves, J.J. Costa, A.R. Figueiredo, and A.M.G. Lopes. Study of the Aerodynamic Sealing of a Cold Store, Experimental and Numerical Approaches. *Energy and Buildings*, 2012.

[19] Y. G. Chen and X. L. Yuan. Simulation of a cavity insulated by a vertical single band cold air curtain. *Energy Conversion Management*, 46:1745–1756, 2005.

[20] H. K. Navaz, M. Amin, S. C. Rasipuram, and R. Faramarzi. Jet entrainment minimization in an air curtain of open refrigerated display case. *International Journal for Numerical Methods for Heat and Fluid Flow*, 16(4):417–430, 2006.

[21] M. Tamm. Zur Berechnung von Luftschleiern,Dissertation. 1975.

[22] F. Nicoud and F. Ducros. Subgrid-scale stress modeling based on the square of the velocity gradient tensor. *Flow, Turbulence and Combustion*, 62:183–200, 1999.

[23] O. Lehmkuhl, C. D. Pérez-Segarra, R. Borrell, M. Soria, and A. Oliva. TERMOFLUIDS: A new Parallel unstructured CFD code for the simulation of turbulent industrial problems on low cost PC Cluster. In *Proceedings of the Parallel CFD 2007 Conference*, pages 1–8, 2007.

[24] R. W. C. P. Verstappen and A. E. P. Veldman. Symmetry-preserving discretization of turbulent flow. *Journal of Computational Physics*, 187(1):343–368, 2003.

[25] F. X. Trias and O. Lehmkuhl. A self-adaptive strategy for the time integration of Navier-Stokes equations. *Numerical Heat Transfer, Part B*, 60(2):116–134, 2011.

[26] I. Rodríguez, R. Borrell, O. Lehmkuhl, C. D. Perez-Segarra, and A. Oliva. Direct numerical simulation of the flow over a sphere at $Re = 3700$. *Journal of Fluid Mechanics*, 25(25):263–283, 2011.

[27] I. Rodríguez, O. Lehmkuhl, R. Borrell, and A. Oliva. Flow dynamics in the turbulent wake of a sphere at sub-critical Reynolds numbers. In *Proceedings of the Parallel CFD 2011 Conference*, pages 1–5, 2011.

[28] Air Movement and Control Association International. *ANSI/AMCA Standard 220-05. Laboratory Methods of Testing Air Curtain Units for Aerodynamic Performance Rating.*, 2005.

[29] H. Giráldez, C. D. Pérez-Segarra, I. Rodríguez, and A. Oliva. Optimization of the Thermal and Fluid Dynamic Behaviour of Air Curtains. Analysis of the Plenum by Means of LES. In *Proceedings of the 15th International Conference on Fluid Flow Technologies,Budapest,Hungary*, 2012.

3

Advanced mathematical models and numerical methodology

3.1 Introduction

Traditionally turbulence modeling of industrial flows in complex geometries have been solved using RANS models and unstructured meshes based solvers. The lack of precision of RANS models in these situations and the increase of computer power, together with the emergence of new high-efficiency sparse parallel algorithms, make posible the use of more accurate turbulent models such as Large Eddy Simulation models (LES). In this chapter the LES models, the numerical methodology and the data treatment is explained.

3.2 Mathematical formulation

The Navier-Stokes equations govern the flow of constant-property Newtonian fluids. The Navier-Stokes and continuity equations can be written as:

$$\rho \frac{\partial u}{\partial t} + C\left(u\right) u + Du + Gp = 0 \tag{3.1}$$

$$Mu = 0 \tag{3.2}$$

where u and p are the velocity and vector pressure, respectively.The matrices C(u), D are the convective and difusive operators, respectively.

The numerical resolution of the Navier-Stokes equations (DNS) implies, in most of the practical situations, very time-consuming calculations. In order to overcome this difficulty, a broad range of turbulence models are employed.

Historically, the first models employed are of the Reynolds Averaged Navier Stokes (RANS) type. In the RANS models the velocity field is time averaged and all the scales of the turbulence are filtered. This models require empirical information of the different flow regimes in order to determine the different constants of the model and predict accuratelly the velocity fields.

A more detailed and general description of the fluid motion is obtained with the Large Eddy Simulation (LES) technique. LES requires more time-consuming calcultions than RANS methods, but less than the DNS procedure.

3.2.1 Large Eddy Simulation

In large eddy simulation (LES), the larger three-dimensional unsteady turbulent motions are directly represented, whereas the effects of the smaller scale motions are modelled. In computational expense, LES lies between Reynolds-stress models and DNS, and it is motivated by the limitations of each of these approaches. Because the large-scale unsteady motions are represented explicitly, LES can be expected to be more accurate and reliable than Reynolds-stress models for flows in which large-scale unsteadiness is significant - such as the flow over bluff bodies. which involves unsteady separation and vortex shedding. As said above, the computational cost of DNS is high, and it increases as the cube of the Reynolds number, so that DNS is inapplicable to high-Reynolds-number flows. Nearly all the computational effort in DNS is expended on the smallest, dissipative motions, whereas the energy and anisotropy are contained predominantly in the larger scales of motion. In LES, the dynamics of the larger-scales motions (which are affected by the flow geometry and are not universal)

Large Eddy Simulation seeks to predict the large eddies behaviour while the small are modellized by means of an additional eddy viscosity.

The spatially filtered equation of momentum used in LES [1] can be written as follows:

$$\partial_t \overline{u} + (\overline{u} \cdot \nabla)\, \overline{u} + \nabla \overline{p} - 2\nu \nabla \cdot S(\overline{u}) = \nabla \cdot \left(\overline{u\overline{u}}^T - \overline{uu^T} \right) \tag{3.3}$$

Modelling the right-hand side in terms of $\overline{u}$ yields a simplified representation of the large eddies.

$$\nabla \cdot \left(\overline{u\overline{u}}^T - \overline{uu^T} \right) = 2\nabla \cdot (\nu_e S(\overline{u})) \tag{3.4}$$

In order to modellize the small eddies, some turbulence model has be to be employed: the Smagorinsky and WALE models explained below are two of the possible options.

3.2.2 Turbulence models

The classical Smagorinsky model [2] is given by

$$\nu_e = c_s^2 \Delta^2 \left| S\left(u\right) \right| \tag{3.5}$$

The Smagorinsky model suffers from several shortcomings, one of them is that it predicts a nonvanishing eddy viscosity in regions where the flow is laminar and at no-slip walls.

In order to overcome these defficiencies, in this study the Wall Adapting Local Eddy viscosity (WALE) model [3] will be employed. According to this model the expression for the eddy viscosity is given by

$$\nu_e = \left(C_w \Delta\right)^2 \frac{\left(\&_{ij}^d \&_{ij}^d\right)^{3/2}}{\left(\overline{S}_{ij}\overline{S}_{ij}\right)^{5/2} + \left(\&_{ij}^d \&_{ij}^d\right)^{5/4}} \tag{3.6}$$

where & is the traceless symmetric part of the square of the velocity gradient tensor:

$$\&_{ij}^d = \frac{1}{2}\left(\overline{g}_{ij}^2 + \overline{g}_{ji}^2\right) - \frac{1}{3}\delta_{ij}\overline{g}_{kk}^2 \tag{3.7}$$

$$\overline{g}_{ik}^2 = \overline{g}_{ik}\overline{g}_{kj} \tag{3.8}$$

and δ_{ij} is the Kronecker delta operator.

It is probed that the WALE model is a better approximation than the classical Smagorinsky model, avoiding the undesired behaviour explained above. A detailed description of the high performance parallel program Termofluids can be found in the bibliography indicated below [4].

3.3 Numerical methodology

3.3.1 Unstructured meshes

In the calculations unstructured meshes has been employed. This type of meshes allows the adaptation to curved and intrincate geometries. The employed meshes has been refined by Delanuay refinement [5]. Meshes produced by Delaunay refinement satisfy guaranteed bounds on angles, edge lengths, the number of triangles, and the grading of triangles from small to large sizes.

It is worth noting the refinement of the mesh specially in the zones where the flow may demand an important attention(see Fig. 3.1).

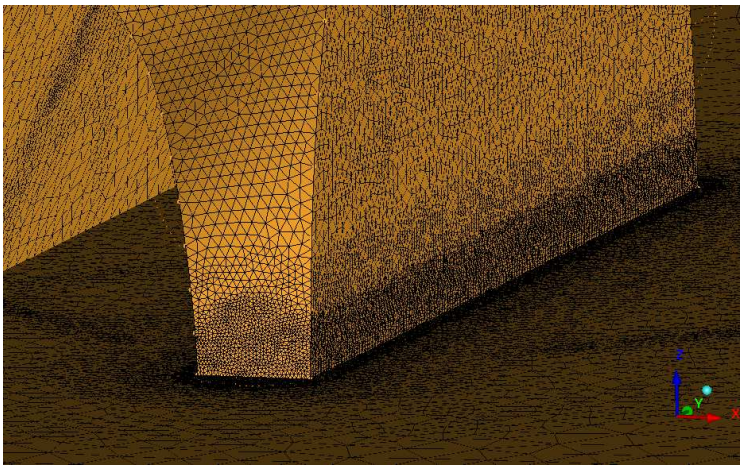

Figure 3.1: Unstructured mesh

3.3.2 Symmetry preserving discretization

The type of discretization of the Navier-Stokes equations is a key point in order to obtain accurate and stable calculations. Verstappen and Veldman [6] propose to exactly preserve the symmetry properties of the underlying differential operators. They show that such treatment ensures stability and allows the conservation of the overall kinetic energy.

This discretization is called symmetry preserving and has been employed in the convective terms of the transport equations.

3.3.3 Fractional Step Method

The fractional step method is the method employed to solve the transient state of the flow. Its essence is the following: a predictor velocity field u^* is solved without having into account the pressure field, then the corrected pressure field is generated from the divergence of this initial predictor velocity. Then, the predictor velocity is corrected with the addition of the effect of the pressure field. It is a direct method in each time step.

$$\frac{1}{\Delta t}\left[I-\frac{1}{2Re}\nabla\right]^2 u^* = \frac{1}{\Delta t}\left[I-\frac{1}{2Re}\nabla\right]^2 u^n - [\frac{3}{2}\left(u^n\cdot\nabla\right)u^n - \frac{1}{2}(u^{n-1}\cdot\nabla)u^{n-1}] \quad (3.9)$$

$$\Delta t(\nabla\cdot\nabla)p^{n+1} = \nabla\cdot u^* \quad (3.10)$$

$$u^{n+1} = u^* - \Delta t \nabla p^{n+1} \tag{3.11}$$

A detailed description of the fractional step method applied to the incompressible Navier-Stokes equations can be seen in [7].

3.3.4 Time Step

In the calculations the so called CFL condition is accomplished. This condition determine the minimum numerical stability required in order to avoid a divergent behaviour in the calculations. In comparison with other stability conditions it presents the capability to agilize the calculation procedure, not being so restrictive.

3.3.5 Boundary conditions

In order to mantain the stability of the calculations, the calculation domains employed are closed. In this way, the mass balance is easily accomplished and only inner boundaries are defined, producing the recirculation of the flow in the whole domain.

3.4 Data treatment

Once the transient calculations are carried out, the average results are extracted from them. This average is carried out from the instantaneous velocity maps once the system has acquired an statistically steady state. Also the spectral analysis of the signal in some relevant points can be carried out in order to study the possible existence of coherent structures, such as vortex shedding.

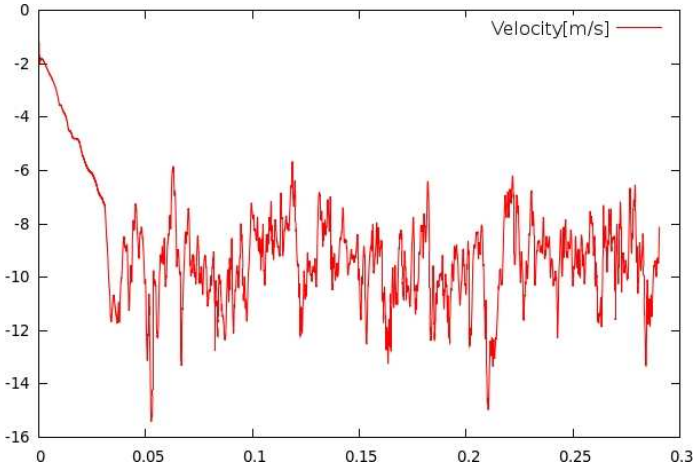

Figure 3.2: Temporal signal of the velocity at a point in the discharge nozzle.

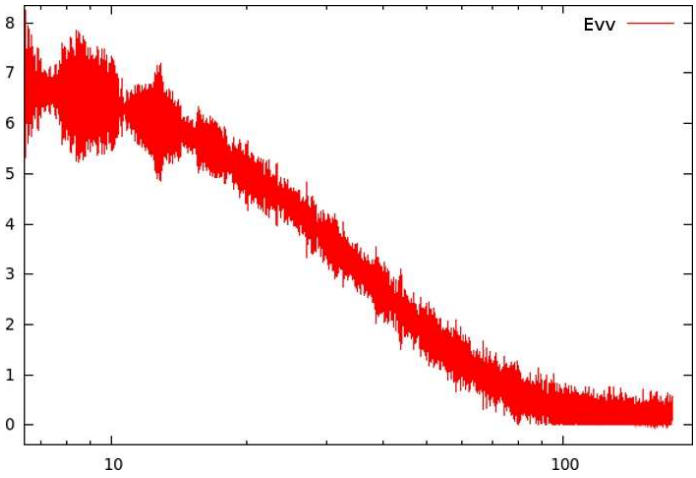

Figure 3.3: Energy spectra from the temporal signal.

3.5 TermoFluids, a general purpose CFD code

The increase in the computational power and the improvement in the numerical methods have been significant over the last decades. This fact, together with the emergence of low-cost parallel computers, has made possible the application of numerical methods to the study of complex phenomena and geometries, such as the simulation of turbulent industrial flows.

Termofluids is a general purpose CFD code with capability for parallel transient calculations with unstructured meshss. The code TermoFluids has been exhaustively validated with different benchmark cases and uses efficient algorithms, which work adequately both on slow networks of personal computers clusters and supercomputers. Governing partial differential equations are converted into algebraic ones using three-dimensional unstructured collocated meshes with symmetry-preserving discretization.

Its capability to realize calculations with unstructured meshes allow the prediction of intrincate geometries. The prediction of transient flows is possible with this code. Its capability to be parallelized for hundreds of CPU's allows to accelerate the calculation. The code TermoFluids employs a conservative formulation, being accomplished the conservation of the global kinetic-energy balance on any grid. The systems of equations are solved with full parallel direct and iterative sparse linear solvers, using transient time integration with fully explicit fractional step algorithms. Fully conservative second-order schemes are used for spatial discretization.

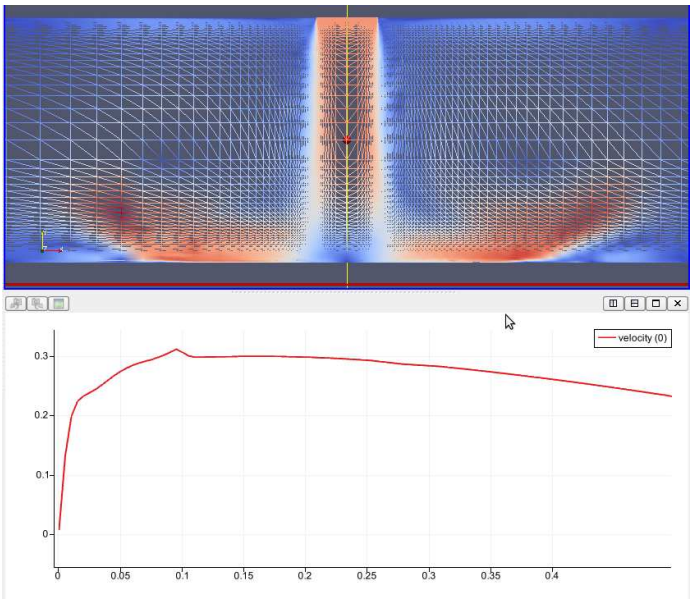

Figure 3.4: Mesh distribution for the case of the impinging slot jet and velocity profile.

3.6 Preliminar case: impinging slot jet

The impinging slot jet has been chosen to demonstrate the accuracy of the discretizations and the turbulence model.

In this benchmark case, an slot air jet impacts against the ground, spreading itself to both right and left sides. A very good agreement has been observed between the present simulations and the results from the literature [8].

This case can be considered similar to a simplified air curtain simulation: a plane air jet impinges against a solid wall. So it can be concluded that the proposed methodology is accurate enough for the simulation of air curtains.

3.7 Conclusions

In this chapter, the numerical methodology has been described. The different equations and turbulence models has been detailed. The numerical methodology and the general purpose code TermoFluids has been described and its main features has been detailed. A benchamrk case has been studied in order to verify the accuracy of the code. This code has been employed in the plenum optimization chapter to predict

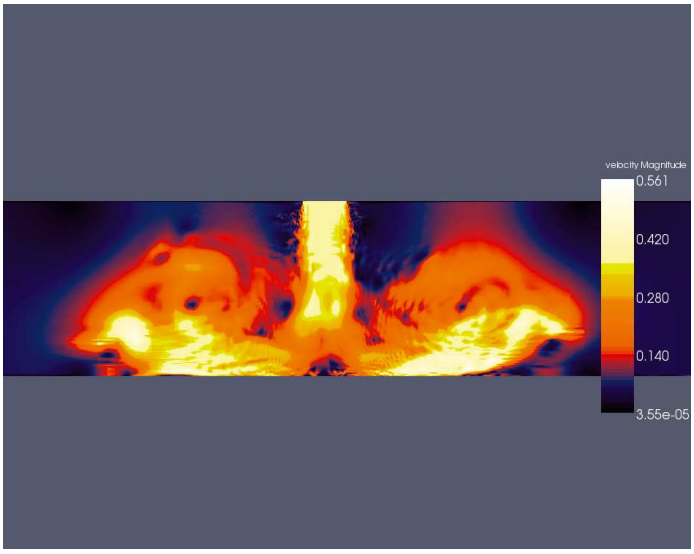

Figure 3.5: Impinging slot jet: instantaneous velocity distribution.

the air curtain behavior.

References

[1] P. Sagaut. *Large Eddy Simulation for Incompressible Flows.* Springer-Verlag, 2001.

[2] J. Smagorinsky. General circulation experiments with the primitive equations, part. I: the basic experiment. *Monthly Weather Rev.*, 91:99–164, 1963.

[3] F. Nicoud and F. Ducros. Subgrid-scale stress modeling based on the square of the velocity gradient tensor. *Flow, Turbulence and Combustion*, 62:183–200, 1999.

[4] O. Lehmkuhl, C. D. Perez-Segarra, R. Borrell, M. Soria, and A. Oliva. TERMOFLUIDS: A new Parallel unstructured CFD code for the simulation of turbulent industrial problems on low cost PC Cluster. In *Proceedings of the Parallel CFD 2007 Conference*, pages 1–8, 2007.

[5] J.R. Shewchuk. Delaunay refinement algorithms for triangular mesh generation. *Computational Geometry: Theory and Applications*, 22(1-3):21–74, 2002.

[6] R. W. C. P. Verstappen and A. E. P. Veldman. Symmetry-preserving discretization of turbulent flow. *Journal of Computational Physics*, 187(1):343–368, 2003.

[7] J. Kim and P. Moin. Application of a fractional-step method to incompressible navier-stokes equations. *Journal of Computational Physics*, 59(2):308–323, 1985.

[8] T.H. Park, H.G. Choi, J.Y. Yoo, and S.J. Kim. Streamline upwind numerical simulation of two-dimensional confined impinging slot jets. *International Journal of Heat and Mass Transfer*, 46(2):251–262, 2003.

4

Experimental characterization

4.1 Introduction

The experimental characterization of a commercial air curtain is carried out in the present chapter. For the measurements hot wire anemometry technology is employed. The results can be checked and compared with the results of other facilities thanks to the employment of the AMCA standard [1]. Moreover, it is carried out the analysis of the experimental data, obtaining information of the temporal and frequential behaviour of the flow produced by the air curtain.

4.2 Scope

Results from the tests of a commercial air curtain are presented. The measurements are carried out employing hot wire anemometry technology. The previous in-situ calibration of the sensors ensures the accuracy and reliability of the results. The required tests defined in the standard are the homoegeneity test and the maximum penetration test.

4.2.1 Homogeneity test

The homogeneity test determines the uniformity of the flow produced by the device in every transversal plane. Measurements are taken in at least five different test lines with the same distance between test lines (see Fig.4.1). An average value is calculated from this measurements and the deviation from this mean value is obtained.

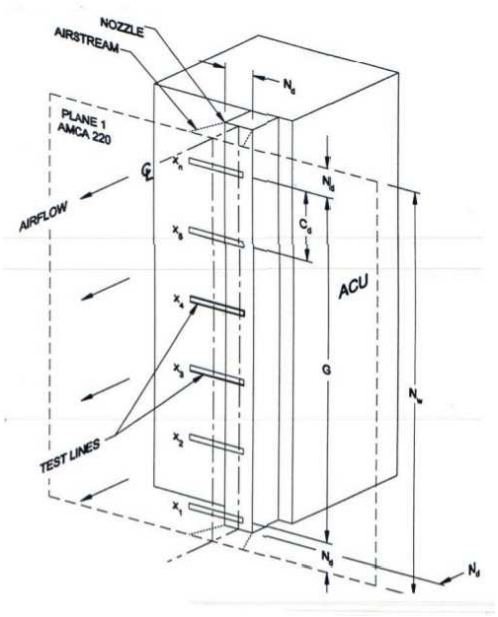

Figure 4.1: Disposition of the tets lines in the first plane according to the standard.

4.2.2 Maximum penetration test

In order to evaluate if the flow has reached some distance with some minimum velocity (target velocity), the velocity values should be measured in different distances from the nozzle of the air curtain (see Fig.4.2).

4.3 Motivation

The application of the standard method ANSI/AMCA 220-05 [1] to determine aerodynamic performance of the air curtain guarantees an accurate and comparable procedure in the characterisation of the mean features on air curtains. The standard does not restrict the technology used in the measurements, but determines the minimum precision required. All the precision requirements are accurately accomplished and the results are presented in tables following the form indicated in the normative.

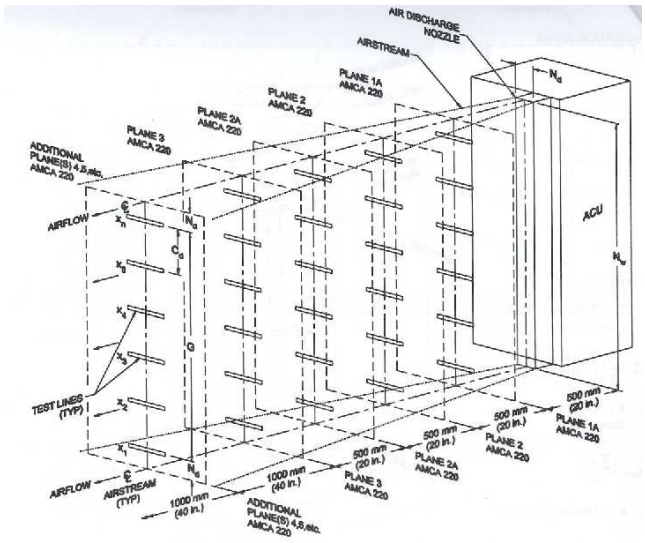

Figure 4.2: Disposition of the measurement planes according to the standard.

4.4 Hot Wire Anemometry

The technique employed to the measurement of the air curtain flow is hot wire anemometry. This technique is well known, due to the fact that it has been used in the last years with considerable success and it has become a standard tool for researchers examining the nature of turbulence.

It is based on the capacity of the flow to modify the temperature of a probe sensor. When the probe sensor is exposed to the flow, the cooling effect is proportional to the electrical tension between poles of the probe, then the element is maintained at a constant temperature. The probe can be unidimensional, bidimensional or tridimensional, in function of the number of sensors (see Fig.4.3).

Compared with other fluid velocity techniques it is a relatively cheap and effective method to measure fast velocity fluctuations.

As mentioned before, previously to the measurements, the probe should be calibrated. Then the measurements can be carried out. The deviations of the environment temperature with respect to the calibration temperature are corrected with a thermocouple attached near the probe sensor. Finally, a post analysis is used to calculate the mean velocity, normal stress, standard deviation (root mean square), turbulence intensity, skewness and flatness coefficients for all probes. Then it is possible to display time history and histograms of stored data, store time history information in

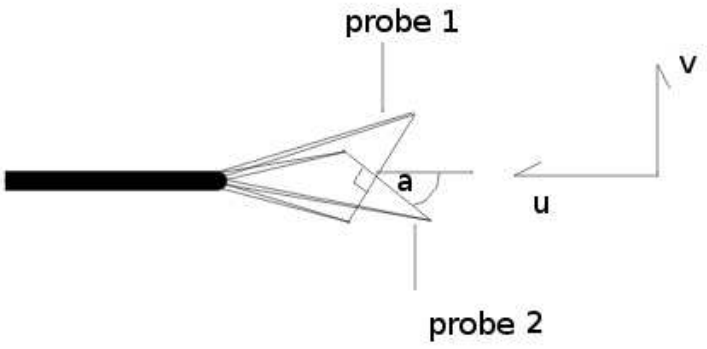

Figure 4.3: Bidimensional hot wire anemometry probe.

an ASCII file, and calculate and show power spectral density, auto-correlation and cross-correlation.

4.5 Standard AMCA 220/05

The measurements are carried out in a channel which accomplishes the AMCA standard 220-05 [1]. The standard dictates the measures of the channel, the required minimum precision on the measurements and the quantity and position of the test lines (see Fig.4.2). The experimental setup has three main components: the anemometer, the cartesian robot and the channel itself (see Fig.4.5). The cartesian robot has a rail guide in order to positionate the probe in each distance from the air curtain discharge.

In each test lines there are a number of minimum measurements required by the standard. The main objective is determining the penetration of the air curtain flow and the velocity of penetration at each distance from the discharge nozzle. It is determined from the mean velocity value in each plane. The homogeneity of the jet is the other main parameter that characterizes an air curtain. It is determined from the standard deviation of the measurements in each plane, In the table 4.4 it is presented the results of the application of this standard measurement to a comercial air curtain prototype.

Test Line	Distancia[mm]	Pla 1[70]	Pla 4[3000]	Pla 5[4000]
1	70	13,230	3,730	2,761
2	272,5	14,236	3,316	2,333
3	475	6,785	2,882	2.032
4	677,5	12,775	3,219	1,953
5	880	13,098	4,359	3,264
Vel mitja	-	12,025	3,50	2,47
Stand. Desv., s	-	2,97	0.567	0.54
Uniformitat	-	75%	84%	78%

Figure 4.4: Example of results from the application of the standard to a comercial air curtain unit.

4.6 Experimental setup

The air curtain has been placed vertically in a channel large enough to avoid any interferences with walls and surroundings. With a positioning cartesian robot and a adjusting laser, the measurements are carried out in the desired positions in reference with the air curtain discharge. See Fig.4.5 for an overall view of the setup. For further details of the experimental setup see Appendix 1.

The method employed for measuring the velocity consists in averaging the transitory signal (the flow presents unavoidably a turbulent behavior) during a time interval long enough.

The dimensions of the channel are 5 x 1.1 x 1 , with an step of 1 metre between longitudinal measurements,0.2 m in vertical and 0.03 in horizontal(see Fig.4.2).

The measurements allow to determine the homogeneity of the flow distribution in the plane of the air curtain discharge, and the following planes spaced by 1 meter from this first plane.This homogeneity is the other mean parameter demanded by the standard. Then, homogeneity and maximum distance with a target velocity are the two values which characterize the aerodynamic performance of the air curtain.

In order to capture precisely the flow behavior, the sensors supports, wires and sensor probes are previously calibrated in the same room at the same conditions of the measurements, ensuring the best reliability for this technology.

The sample rate of the data adquisition are adjusted to reproduce all the relevant turbulent scales, being 1000 Hz the best compromise between accuracy and practical purposes.

The characterization of the faster scales of the tubulence is not required in a macroscopic characterization of the flow. The total time adquiring data in each measurement is adjusted considering that the autocorrelation in time must go to zero

Figure 4.5: Overall view of the experimental setup.

inside the interval (see Fig.4.6). In this way, it is assured that the signal has reached an independent behavior in reference of its initial value.

4.7 Results

In this section a summary of the different measurements is presented.

The results from the measurements are presented in tables 4.1, 4.2 and 4.3. The maximum velocities at different distances are given in table 4.4. As can be observed, the acu with the new improved geometry (see Fig.4.13) presents a good performance. In relation with the initial geometry of the model, some modifications were carried out: smoother profile of the plenum and additional directionators in the outlet lead the flow reach higher velocities. All the results here presented have been obtained with the fastest stage of the fan (5th stage). Different measurements have been performed with other hot wire anemometers to corroborate the precision and independency of the results. It can be observed that tha flow exceeds the 12 m/s in average value at the plenum discharge and exceeds the 3,5 m/s at 3 metres from the air curtain. The homogeneity is 75% at the plenum discharge of the air curtain, which means that the values in each line of measurement do not differ significantly from the mean values of the test plane.

The presented averaged results are calculed from measurements at the 5th stage of the air curtain.

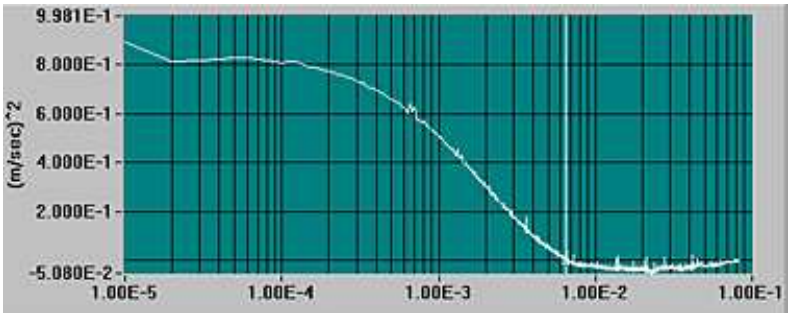

Figure 4.6: Autocorrelation of the signal.

-	X[mm]	+40	+20	axis	-20	-40
Test Line	Y[mm]	-	-	-	-	-
1	70	6,766	12,730	**13,230**	11,08	-
2	272,5	1,143	12,699	**14,236**	14,063	11,621
3	475	-	0,586	2,027	**6,785**	5,521
4	677,5	9,969	**12,775**	11,628	5,437	-
5	880	7,214	**13,098**	10,668	8,246	-
Avg.V	-	-	-	-	-	**12,025**

Table 4.1: Measurements in z=0.07 m (a nozzle width lenght) from air curtain discharge.

-	X[mm]	+120	+90	+60	+30	axis	-30	-60	-90	-120
Line	Y[mm]	-	-	-	-	-	-	-	-	-
1	70	3,65	3,50	3,80	4,04	3,88	3,77	3,38	3,67	3,44
2	272,5	3,18	2,80	2,77	3,27	3,10	3,31	3,20	2,77	3,12
3	475	1,99	2,48	2,35	2,88	2,24	2,15	2,34	2,57	2,28
4	677,5	2,62	3,06	2,98	2,58	3,14	3,22	2,55	3,16	2,53
5	880	3,47	3,82	3,95	4,02	4,49	4,29	4,17	4,26	4,30
Avg.V	-	-	-	-	-	-	-	-	-	**3,501**

Table 4.2: Measurements in z=3 m from air curtain discharge.

-	X[mm]	+120	+90	+60	+30	axis	-30	-60	-90	-120
Line	Y[mm]	-	-	-	-	-	-	-	-	-
1	70	2,38	2,25	2,76	2,66	2,38	2,55	2,53	2,31	1,83
2	272,5	2,30	2,19	2,33	1,91	2,07	2,12	2,01	1,91	1,92
3	475	1,50	2,03	1,68	1,69	1,74	1,72	1,78	1,50	1,44
4	677,5	1,95	1,73	1,56	1,74	1,87	1,44	1,79	1,72	1,94
5	880	2,25	2,67	2,45	2,69	2,46	2,76	3,26	2,99	2,99
Avg.V	-	-	-	-	-	-	-	-	-	**2,468**

Table 4.3: Measurements in z=4 m from air curtain discharge.

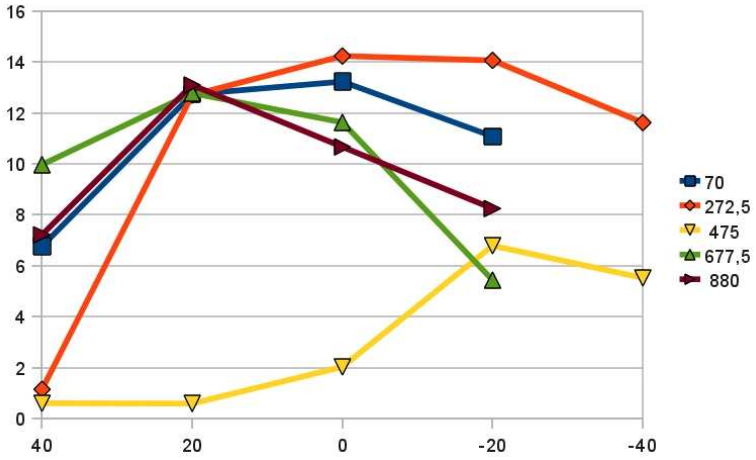

Figure 4.7: Velocity profiles in z=0.07 m from air curtain discharge.

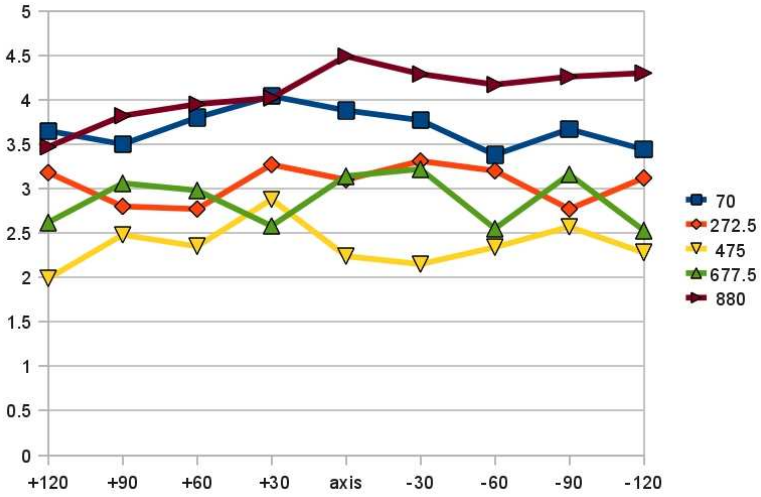

Figure 4.8: Velocity profiles in z=3 m from air curtain discharge.

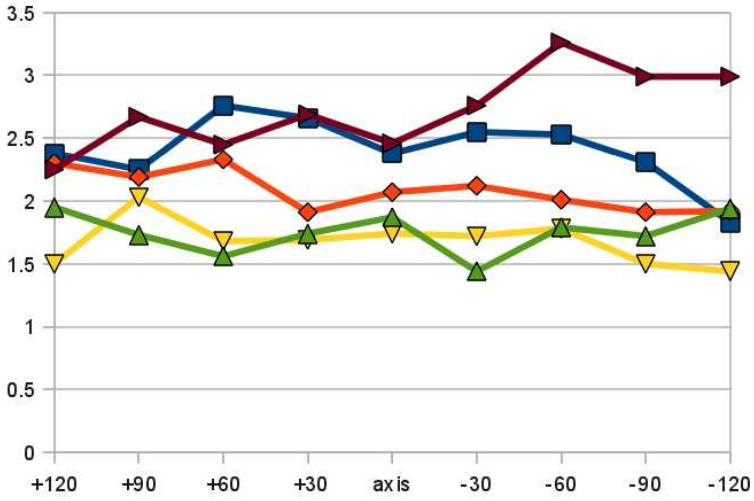

Figure 4.9: Velocity profiles in z=4 m from air curtain discharge.

Test Line	Distance[mm]	Plane1[70]	Plane 4[3000]	Plane 5[4000]
1	70	13,230	3,730	2,761
2	272,5	14,236	3,316	2,333
3	475	6,785	2,882	2.032
4	677,5	12,775	3,219	1,953
5	880	13,098	4,359	3,264
Avg. core vel	-	12,025	3,50	2,47
Stand. Dev, s	-	2,97	0.567	0.54
Uniformity	-	75%	84%	78%

Table 4.4: Maximum velocities in function of the distance from air curtain discharge.

4.8 Tentative of further improving air curtain performance. Preliminar results

Other geometry modifications has been tested (see Fig.4.10 and Fig.4.11). In order to improve the maximum velocities and the stability of the flow, some studies have been performed. To improve homogeneity is necessary a smoother section in the fan's outlet. The pieces designed to obtain the desired effect act like a diffuser when they are attached to the air curtain's plenum. The measurements show an increase of 10% in the maximun velocities and higher homogeneity between the different test lines. The results show that the new geometry avoids innecesary pressure loses due to fast expansion of the flow in the channels. More detailed studies will be carried out in the next chapters. The modified prototypes have also been tested numerically.

4.9 Flow measurements with the new geometry

Measurements carried out in the axis of the plane at 4000 mm from the discharge prove that the new geometry (see Fig.4.11) improves the performance of the device at least 13%. The comparison between measurements (see table4.5) with and without the new improvements corroborates that statement. Measurements are carried out with two different sensors (A and B columns), ensuring the reliability of the results.

Future tests will be centered in the addition of the current flaps to the new geometry.

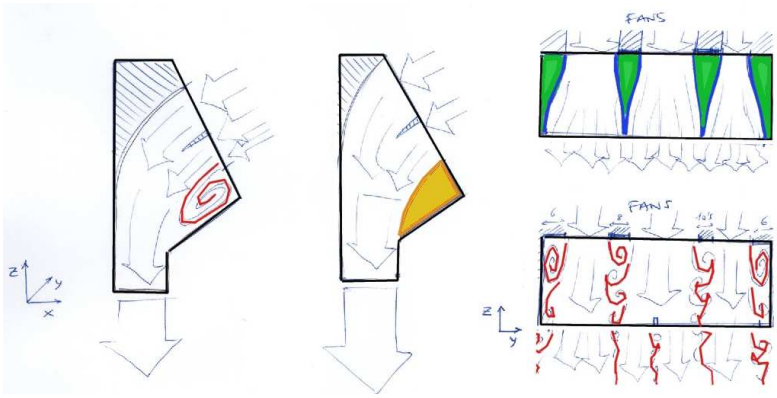

Figure 4.10: Avoiding recirculations with the new geometry for the fan's outlets.

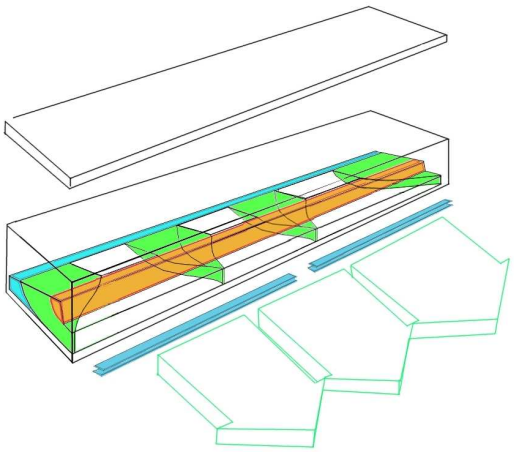

Figure 4.11: New proposed geometry for the fan's outlets.

Test Line	Test	Current Geom	New Geom (A)	New Geom (B)
1	70	3,264	3,696	3,673
2	272,5	1,953	2,708	2,416
3	475	2,032	1,882	2,160
4	677,5	2,333	2,234	2,561
5	880	2,761	3,095	3,543
Avg. core vel	-	2,468	2,795	2,871%
Stand. Dev, s	-	0,54	0.71	0.68%
Uniformity	-	78%	74%	76%
Improvement	-	-	13,2%	16,3%

Table 4.5: Comparison between current geometry and the new geometry proposed.

4.10 Numerical simulations with the new geometry

Some numerical preliminar simulations are carried out to compare the new proposed geometry with the current geometry. The numerical calculations compare the plenum discharge, quantifiying the mean value, the standard deviation from the mean value and the assimetrical behavour of the flow. The calculations indicate that the new geometry improves the homogeneity of the plenum discharge.

Test	Current Geom	New Geom (Inner curve)
Mean value	-0.34	-0.35
Standard deviation	0.075	0.079
Skewness	1.9835	1.5117
% Improvement Skew	-	31.1%

Table 4.6: Numerical results. Comparison between current geometry and the new geometry proposed.

Fig.4.12 shows the standard plenum geometry and flow configuration using CFD models. Fig.4.13 shows the same air curtain after introducing some relevant modifications. As can be seen, not only an smoother channel is presented, but also different directionator blades has been added (two in the fans discharge and two more in the nozzle discharge).

The introduced modifications has been designed in order to avoid the defficiencies (lack of homogeneity) described by the experimental measurements carried out in this chapter.

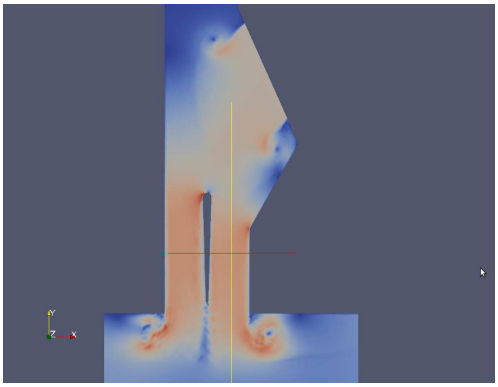

Figure 4.12: Standard geometry of the air curtain plenum and numerical solution of the flow.

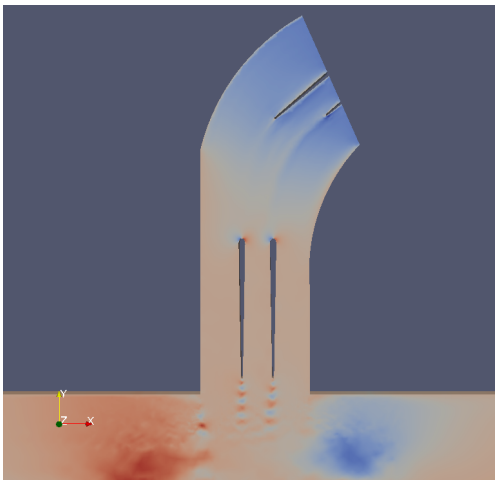

Figure 4.13: Modified geometry of the air curtain plenum and numerical solution of the flow.

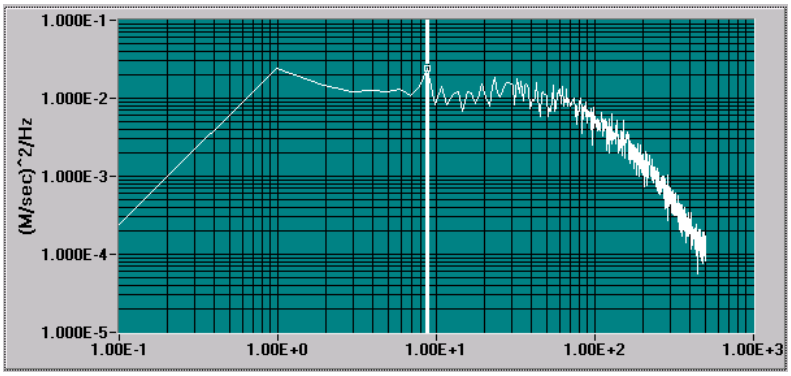

Figure 4.14: Energy espectra experimentally obtained.

4.11 Analysis of experimental data

The post-analysis of the experimental data allows the determination of mean velocity values, turbulence or coherent structures in the main flow (see Fig.4.14). The spectral analysis shows if there is an excessive vortex shedding after the nozzle discharge. It is worth noting that the main objective of the study is designing an air curtain with low levels of turbulence and high mean velocity values.

4.12 Conclusions

In this chapter, the experimental procedure to measure air curtain flows has been described. Hot wire anemometry technology has been employed and the application of the AMCA standard has been explained. The post-analysis of the data has been also detailed. The numerical validation has been employed in order to evaluate the flow behaviour inside the plenum once its design has been modified.

References

[1] Air Movement and Control Association International. *ANSI/AMCA Standard 220-05. Laboratory Methods of Testing Air Curtain Units for Aerodynamic Performance Rating.*, 2005.

5

Plenum optimization and analysis of the wind effect

Main contents of this chapter have been published as

H. Giraldez, C.D. Perez Segarra, I. Rodriguez and A. Oliva. Optimization of the thermal and fluid dynamic behaviour of air curtains. Analysis of the plenum by means of LES. *Proceedings of the Conference on Modelling Fluid Flow (CMFF'12),Budapest,Hungary*, 2012.

5.1 Introduction

The improvement procedure of an air curtain unit (ACU) is described in the present chapter. The procedure is based on Large Eddy Simulations (LES) and Hot Wire Anemometry (HWA) measurements. Initially, the flow provided by the air curtain is evaluated experimentally according to the AMCA standard [1] and employing HWA technology. The initial measurements indicate an undesired behavior of the device: the velocity at the discharge exhibits a non homogeneous distribution. According to the literature, the efficiency of air curtains is closely related to its capacity to provide an homogeneous jet with high enough velocity and with low turbulence levels [2].

On this study, the criteria for optimization applied to the plenum chamber consist in finding out what design increases both the homogeneity and the mean velocity values produced at the discharge. An air curtain producing a jet with these features will minimize the air interchange between outdoor and indoor spaces.

Alternative plenums are evaluated by means of fully 3D LES. Previous works indicate that a fully three-dimensional treatment is required in the simulations of

ACUs [3], due to its no-bidimensional behaviour. The results of the simulations indicate that a more smooth plenum is required to avoid recirculations. The prototype of the designs with the best behavior, according to the simulations, are constructed and its flow are characterized with HWA measurements. The measurements show consistent results with LES. It is concluded that the proposed plenum geometry improves the initial design both in homogeneity and in mean velocity values at the discharge. The downstream jet evolution is characterised with semianalytical and experimental approaches. The code TermoFluids [4] has been used for the simulations of the plenum.

5.2 Definition of the main objectives

An air curtain unit (ACU) is a device which acts as an ambient separator producing a plane air jet. The entrainment is produced by the difference of temperature and pressure between indoor and outdoor spaces and the presence of wind. In order to minimize the entrainment of external air to the protected indoor space, the jet should have a velocity high enough to counteract these effects. It also must be as homogeneous as possible. The homogeneity of the flow at the discharge affects directly the downstream evolution of the jet. A low level of turbulence is also a desired characteristic in the jet [5].

The part of the ACU that gives the jet its desired characteristics is the plenum. The plenum is an inner chamber which is situated between the fans and the nozzle discharge (see Figure 1).

The ACU studied in this paper is characterised according to the AMCA standard [1]. A lack of homogeneity at the discharge is observed in the measurements .

The cause of this behaviour is determined by means of LES, showing that the main cause of inhomogeneity is the fast expansion after the fans outlet. This expansion produces ring vortices, which spreads and affects the discharge and hence the overall efficiency of the device. To solve this problem an alternative plenum design will be evaluated by means of LES.

The best designs according to the simulations are constructed (here refered as m1 and m2 prototypes) and its flow is measured with HWA, so the difference in the flow produced by the plenum modifications can be checked. The HWA measurements show consistent results with the numerical simulations, so the plenum that produces a high homogeneous discharge has also higher downstream velocity values.

The comparation of the energy spectras possibly highlight the effect of the mesh, showing that some peaks at the energy spectra may be produced numerically.

In the economical sense, it is worth notice that the more sofisticated is the plenum design, the more expensive can be its production. This is the main cause that the proposed designs must be quantitative evaluated, in order to ensure that the improve-

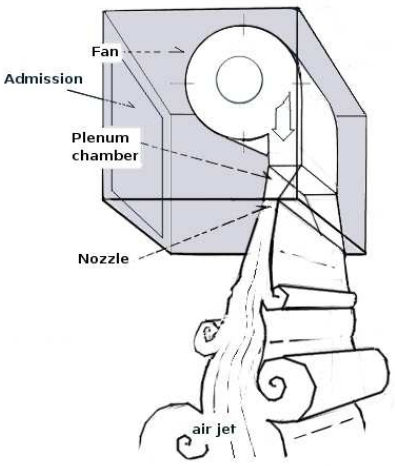

Figure 5.1: Scheme of the basic parts of an air curtain.

ments in efficiency imply higher savings than its associated manufacturing costs.

The numerical techniques employed has been a tool to predict the behaviour of the device and the overall methodology has probed itself as an acceptable procedure to improve ACU designs.

5.3 Methodology

The actions carried out consist in:

- Measuring the flow produced by the air curtain with HWA. Identification of possible flow deficiencies.
- Searching the possible causes of the non optimal behaviour with LES. Application to the plenum.
- Proposing alternative plenum designs in order to overcome the persisting deficiencies.
- Prediction of the behaviour of alternative designs with LES.
- Construction and experimental evaluation of the produced air flow with HWA of the bests designs according to the numerical simulations.

Figure 5.2: The experimental setup where the HWA measurements are carried out.

- Checking the design by means of comparison with the initial behaviour.

The measurements are carried out according to the AMCA standard requirements.The HWA probes are calibrated at the same laboratory, ensuring the accuracy of the measurements.

The simulations are performed with a high performance parallel code developed by Termofluids S.L. [4], capable of calculations with unstructured three-dimensional meshes, in unsteady conditions and with different LES models (e.g. the Wale model [2]). In the LES models, the larger scales of the turbulence are solved, while the smaller ones are filtered and modelled by means of a turbulent viscosity, which adds the additional transport of momentum contained in the small vortices.

5.4 Experimental Setup

An experimental setup to evaluate the flow produced by the ACU is constructed (see Figure 2). The dimensions of the channel are 5 x 1.1 x 1 , with a step of 1 metre between longitudinal measurements, 0.01 metres between transversal measurements. The main parts of the experimental setup are the channel itself, the probe positioning cartesian robot and the HWA system. Obviously, the ACU is fixed at the beginning of the channel.

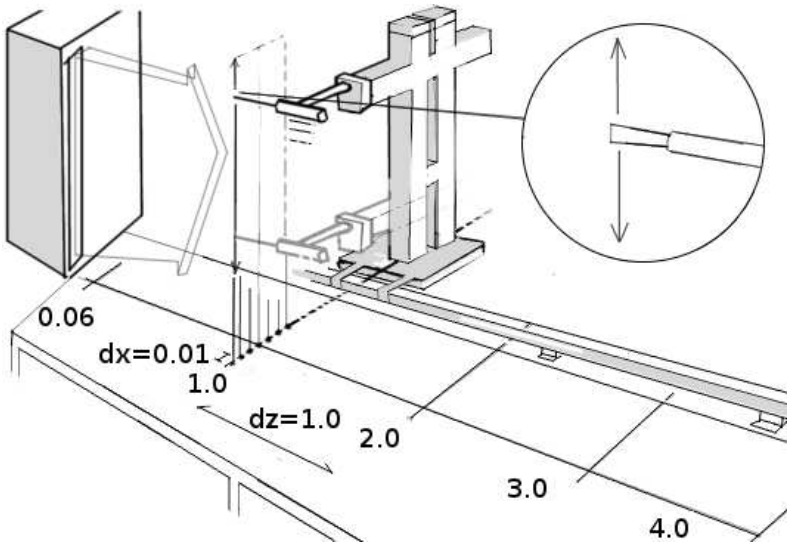

Figure 5.3: Velocity measurement procedure scheme.

The experimental setup allows the characterization of the flow in the range between the discharge (z=0m) and the end of the channel itself (z=4m), without external perturbations by the action of the baffles situated at each side of the ACU.

The cartesian robot allows a positioning with resolution of 10^{-6}m. The measurements are taken in every transversal section programming the cartesian robot to cover all the required domain in a time interval equal to the adquisition time. The relative movement of the robot do not affect the measurement of the velocity because the probe only captures the components of the velocity which acts in the plane normal to its wire (see Figure 2). The measurements are carried out with unidimensional probes at a sample rate of 1000 Hz, during an adquisition time of 128 s in each test line. The test lines have a length of 1.0 m, covering all the spanwise direction of the ACU discharge and with a separation of 0.01 m between each test line. The separation between measurement planes is 1 m, being the first plane at a distance equal to the nozzle width.

Moreover, adjoint to the probe there is also a termocouple, which allows to correct the discrepances produced by the possible deviations between the ambient temperature in the moment of calibration of the probe and the ambient temperature in the moment of data adquisition.

5.5 Mathematical Formulation

5.5.1 Large Eddy Simulation

The spatially filtered equation of momentum used in LES [6] can be written as follows:

$$\partial_t \overline{u} + (\overline{u} \cdot \nabla)\,\overline{u} + \nabla \overline{p} - 2\nu \nabla \cdot S(\overline{u}) = \nabla \cdot \left(\overline{u\overline{u}^T} - \overline{uu^T} \right) \tag{5.1}$$

Modelling the right-hand side in terms of $\overline{u}$ yields a simplified representation of the large eddies.

$$\nabla \cdot \left(\overline{u\overline{u}^T} - \overline{uu^T} \right) = 2\nabla \cdot (\nu_e S(\overline{u})) \tag{5.2}$$

The classical Smagorinsky model [7] is given by

$$\nu_e = c_s^2 \Delta^2 |S(u)| \tag{5.3}$$

The Smagorinsky model suffers from several shortcomings, one of them is that it predicts a nonvanishing eddy viscosity in regions where the flow is laminar and at no-slip walls.

In order to overcome these defficiencies, in this study the Wall Adapting Local Eddy viscosity (WALE) model [8] will be employed. According to this model the expression for the eddy viscosity is given by

$$\nu_e = (C_w \Delta)^2 \frac{\left(\&_{ij}^d \&_{ij}^d\right)^{3/2}}{\left(\overline{S}_{ij}\overline{S}_{ij}\right)^{5/2} + \left(\&_{ij}^d \&_{ij}^d\right)^{5/4}} \tag{5.4}$$

where & is the traceless symmetric part of the square of the velocity gradient tensor:

$$\&_{ij}^d = \frac{1}{2}\left(\overline{g}_{ij}^2 + \overline{g}_{ji}^2\right) - \frac{1}{3}\delta_{ij}\overline{g}_{kk}^2 \tag{5.5}$$

$$\overline{g}_{ik}^2 = \overline{g}_{ik}\overline{g}_{kj} \tag{5.6}$$

and δ_{ij} is the Kronecker delta operator.

It is probed that the WALE model is a better approximation than the classical Smagorinsky model, avoiding the undesired behaviour explained above. A detailed description of the high performance parallel program Termofluids can be found in the bibliography indicated below [4].

5.6 Results

5.6.1 Description of the prototypes

In the present study there are three geometries involved: the current plenum geometry and the two modified prototypes, here refered as m1 and m2 designs. It is worth noting that the plenum is the inner chamber which conditiones the air flow, and it is located between the fan and the discharge.

The modified plenum design m1 introduces only an inner curve, in order to isolate and evaluate its effect (see Fig.4). Additionally, the modified design m2 introduces lateral diffusors and a more thin nozzle discharge (see Fig.7).

The results obtained in every step of the optimization procedure are summarised below.

5.6.2 HWA measurements of the initial flow field

The measurements allow to determine the mean velocity and the homogeneity of the flow along the air curtain discharge, being those the mean parameters demanded by the AMCA standard [1].

The velocity measurements of the initial design show some undesired phenomena (see Table.4.1). As a consequence of the lack of homogeneity at the discharge, the jet spreads transversally faster, and the decrease of the core velocity is also larger. This characteristic produces a jet too much weak and, hence, a low sealing efficiency. In order to find out the reasons of this undesired behaviour, LES of different plenum designs are evaluated. The analysis of the results of the simulations are following described.

Distance[m]	0.06	1.0	2.0	3.0	4.0
Avg. core vel	12.03	6.55	4.65	3.50	2.47
Uniformity	75%	80%	84%	84%	78%

Table 5.1: Mean core velocities in function of the distance from the air curtain discharge. Initial design.

5.6.3 Numerical simulation of the modified plenum geometry m1

A new plenum design is proposed and the simulation of its produced flow is carried out. The meshes employed in the present study are unstructured and each one has roughly 1,8 M control volumes. Once the system has acquired an statistical steady state, the results captured are averaged from that moment and during an interval of time long enough to ensure that the temporal autocorrelation of the signal goes to zero. The inlet boundary condition is emulated situating a previous channel long enough to develope a turbulent profile with a mass flow equal to the provided by the

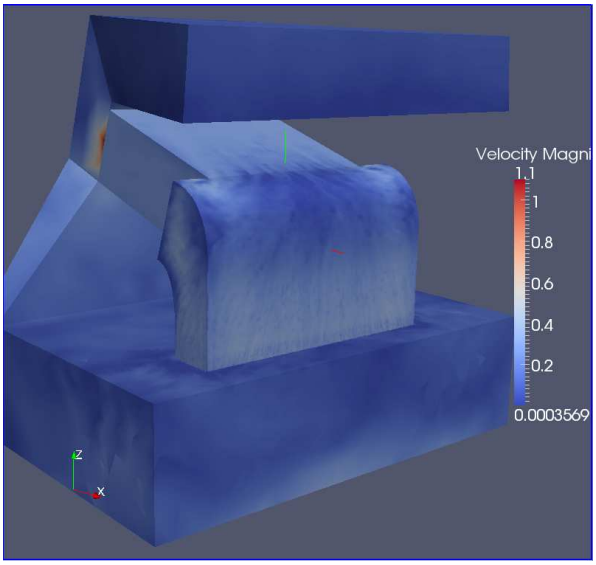

Figure 5.4: Instantaneous velocity distribution with the modified plenum design m1.

actual fans. The characteristic Reynolds of the simulations is 20.000, defined with the characteristic length of the fan's discharge, its mean velocity and the physical properties of air at ambient temperature (20°C).

It can be seen the presence of strong inhomogeneity of the mean velocity values at the discharge section of the flow. It is produced by a fast expansion after the fans. This recirculation spread down and modifies the whole flow's structure, having a destructive effect in a supposedly ideal bidimensional airjet. To make the jet behaviour more bidimensional further modifications of the plenum are required.

5.6.4 Numerical simulation of the modified plenum geometry m2

A new design is modelled and the flow produced is predicted by means of LES. The modified plenum m2 includes a smoothing lateral diffusors, that avoid fast changes of section in the path from the fans to the ACU discharge. In the Figures 7 and 8 it can be seen that the initial lack of homogeneity is diminished with this design.

5.6.5 HWA measurements of the proposed geometries

A prototype of the proposed designs is constructed and evaluated by means of HWA. The results for the model m1 without lateral diffusors have been summarized

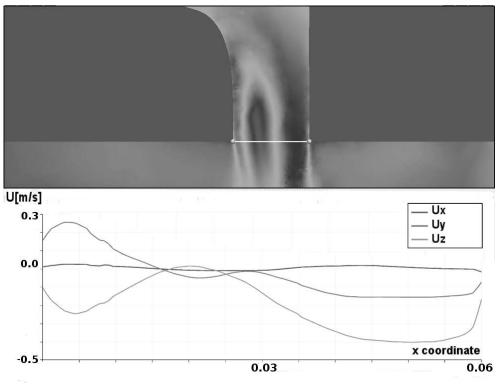

Figure 5.5: Mean velocity components profile in x middle section of the discharge (see white line on the upper figure) with the modified plenum design m1.

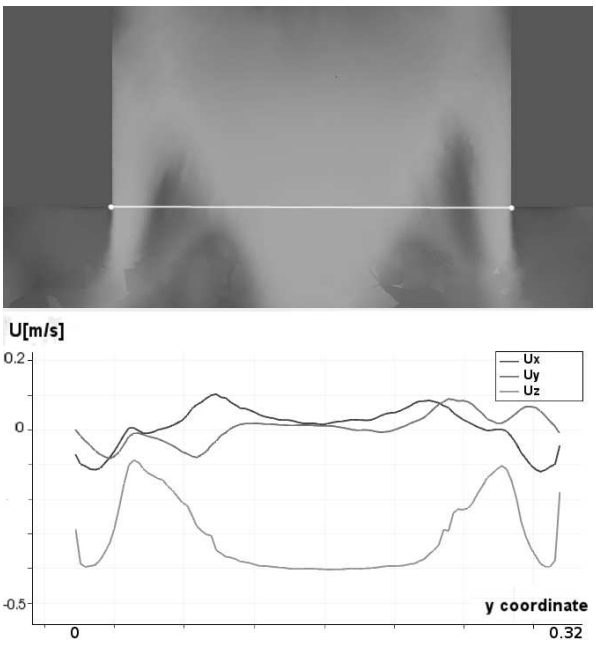

Figure 5.6: Mean velocity components profile in y middle section of the discharge (see white line on the upper figure) with the modified plenum design m1.

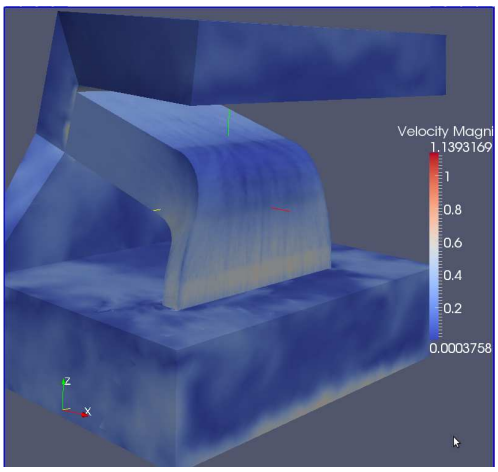

Figure 5.7: Instantaneous velocity distribution with the modified plenum design m2.

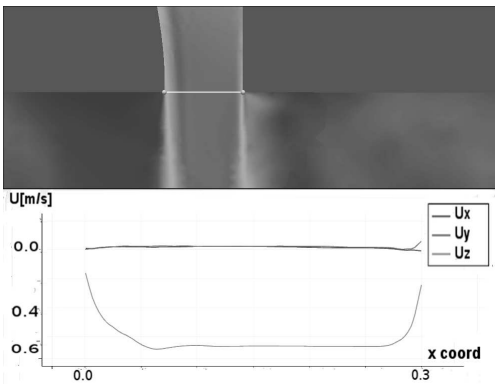

Figure 5.8: Mean velocity components profile in x middle section of the discharge (see white line on the upper figure) with the modified plenum design m2.

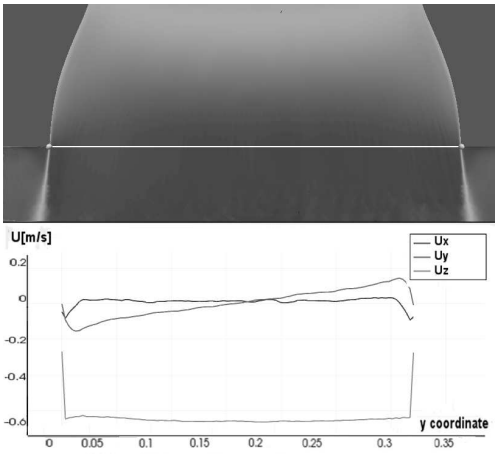

Figure 5.9: Mean velocity components profile in y middle section of the discharge (see white line on the upper figure) with the modified plenum design m2.

below (see Table.4.2). The results for the model m2 with lateral diffusors are also summarized below (see Table.4.3).

It can be seen in the present comparative (see Table.4.4) that the new design has a better behavior than the initial design. The modified plenum m1 does not improve much more the results, but after lateral diffusors and a thin nozzle are introduced (modified plenum m2) the results are satisfactory even at the most demanding distance (4 metres from the discharge).

5.6.6 Experimental and numerical velocity profiles

The velocity at the discharge is characterised at five different locations and its mean value is compared with the results of the numerical simulations (see Fig.)

5.6.7 Experimental and numerical energy spectras

The energy spectra at some locations at the discharge have been studied in order to evaluate the possible coherent strutures of the flow with the proposed design. The energy spectra at the central point of the discharge is presented (see location as white point on Fig. 11). The study is carried out employing the technique of the Lomb periodogram, which generates the energy spectra from an uneven temporal signal [9]. The evaluation of the proposed design m2 indicates a possible vortex shedding in two different frequencies (see Fig. 10). A plausible explanation for this phenomena is that the vortex shedding of low frequency is produced by the lateral ring vortices and

Distance[m]	0.06	1.0	2.0	3.0	4.0
Avg. core vel	15.99	6.78	5.09	3.29	3.07
Uniformity	73%	79%	85%	84%	81%

Table 5.2: Mean core velocities in function of the distance from the air curtain discharge. Prototype without lateral diffusors.

Distance[m]	0.06	1.0	2.0	3.0	4.0
Avg. core vel	17.65	8.85	7.02	5.63	4.4
Uniformity	83%	83%	85%	85%	86%

Table 5.3: Mean core velocities in function of the distance from the air curtain discharge. Prototype with lateral diffusors and thin nozzle.

Prototype	Initial	m1	m2
Avg. core vel at 4 m	2.47	3.07	4.4
Improvement	-	24%	80%

Table 5.4: Comparative of the results obtained by the initial geometry and the proposed prototypes.

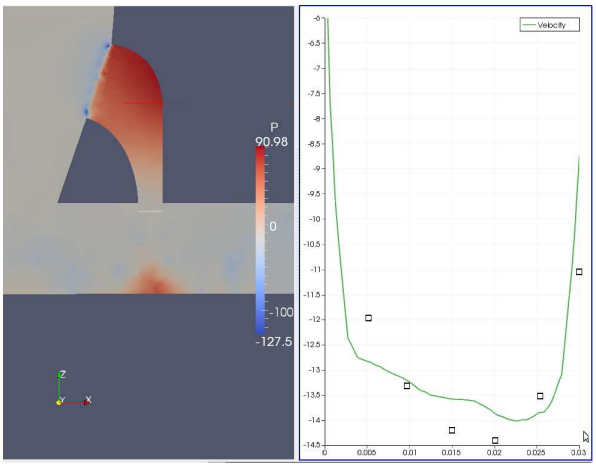

Figure 5.10: Mean velocity value at the discharge. Numerical profile and mean value experimentally obtained.

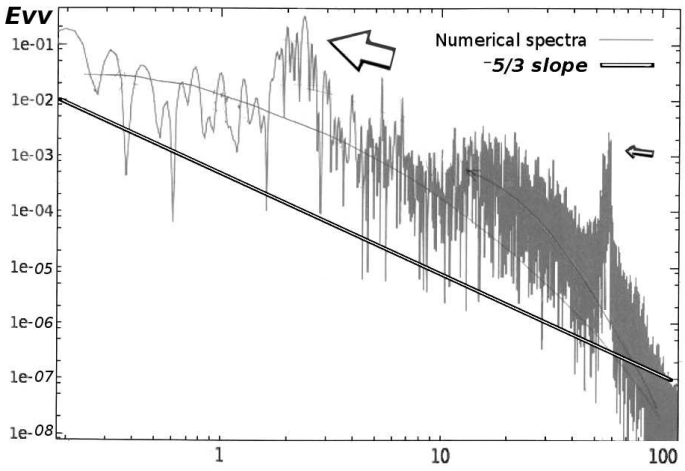

Figure 5.11: Energy spectra numerically obtained at middle point of the discharge with the modified plenum design m1.

the vortex shedding of high frequency is produced by the inner curve (see Fig.12). The observation of the streamlines indicates a similar behavior. In order to check the frequency associated with the vortex shedding produced by the inner curve:

$$St = fD/v \tag{5.7}$$

So, as the other parameters are known, the frequency associated is

$$f = St * v/D = 0.2 * 20.0/0.3 = 53s^{-1} \tag{5.8}$$

The spectra obtained experimentally at the same location show a different energy distribution, not appearing the observed peaks. The difference between spectras possibly indicate that the peaks (see Fig.5.11 and 5.12) are numerically induced. Another possibility is that discrepancies are generated by the boundary conditions. The numerical simulations can only partially emulate the real boundary conditions.

The observation of the spectra obtained numerically (see Fig.5.11) indicates a possible backward cascade of energy from high frequencies. It can also be observed that the -5/3 slope is not an acceptable approximation in the studied region of the spectra. This indicates that the flow exhibits a non isotropic turbulence, possibly due to the proximity of solid walls.

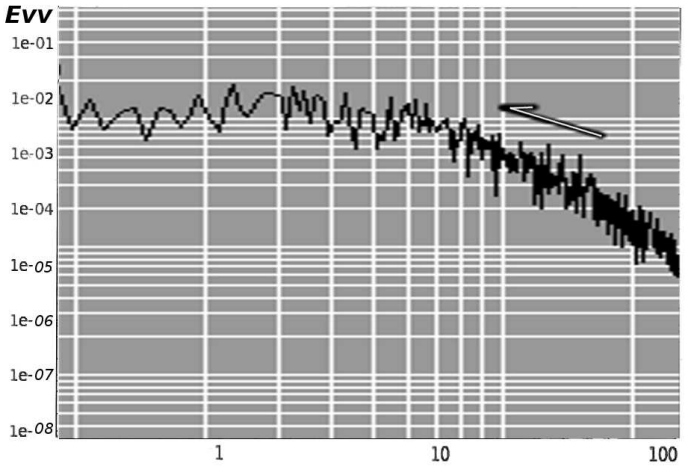

Figure 5.12: Energy spectra experimentally obtained at middle point of the discharge with the modified plenum design m1.

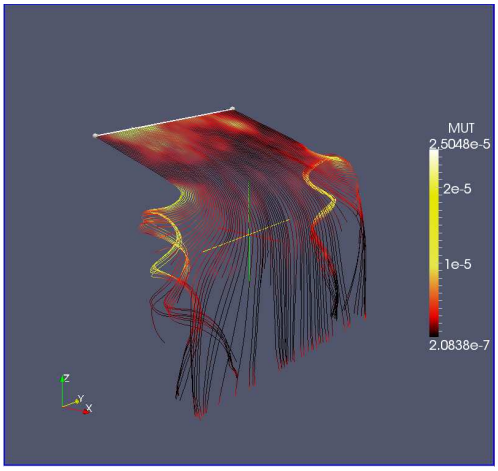

Figure 5.13: Streamlines obtained with the modified design m1.

5.7 Analysis of the wind effect by means of semi-analytical models

In the present section it is analyzed the effect of the incident wind in the air curtain deflection. The trajectory of the jet in every case is studied. The study is carried out by means of semianalytical models and advanced numerical 3D simulations.

Results of the analysis of the jet deflection by the effect of the wind are presented. The deflection produced in the air jet by the effect of the wind can be checked with the semianalytical approach. Once fixed the other parameters such discharge velocity(10m/s) and discharge angle, it can be observed the effect of the wind on the air jet (see Figs.5.14-5.18). The deflection produced in the air jet is directly proportional to the wind velocity. For the cases of wind velocity=0m/s to 3m/s (see Fig. 5.14, 5.15, 5.16 and 5.17)there is no breakthrough of the jet, but in the case of wind velocity=4m/s (see Fig.5.18) there is an excessive deflection and the consequent breakthrough. It is worth mention that the expressions employed in the semianalytical model do not describe the 3D nature of the air jet, being the treatment bidimensional and, hence, very optimistic about the deflection produced (the air jet presents less resistence to the wind with a 3D simulation). Despite the lack of accuracy of this method, the results are very according to the experiments and the numerical simulations, and this method has the advantage of being much less time consuming than the Large Eddy Simulations.

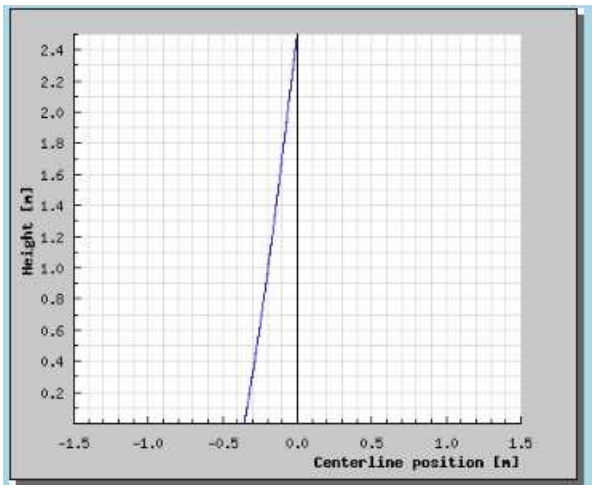

Figure 5.14: Jet without the effect of the wind.Semianalytical.

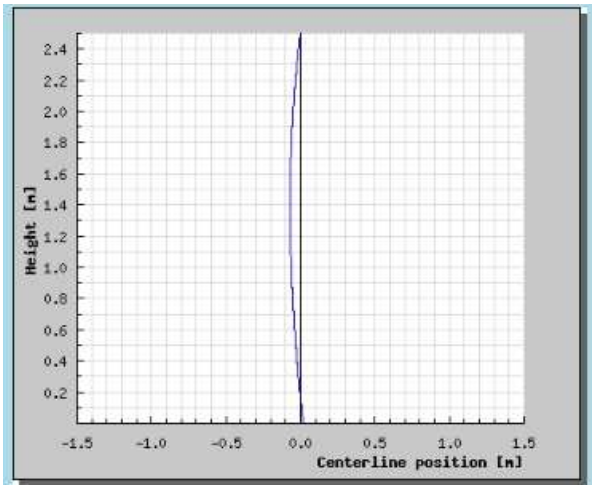

Figure 5.15: Jet deflection by the effect of the wind.Semianalytical.Wind velocity=1m/s.

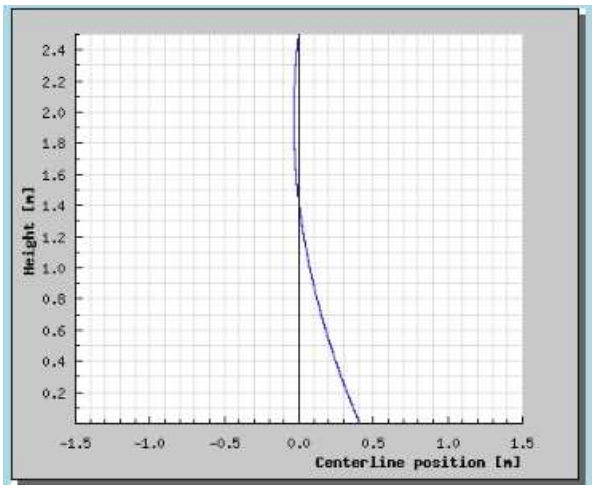

Figure 5.16: Jet deflection by the effect of the wind.Semianalytical.Wind velocity=2m/s.

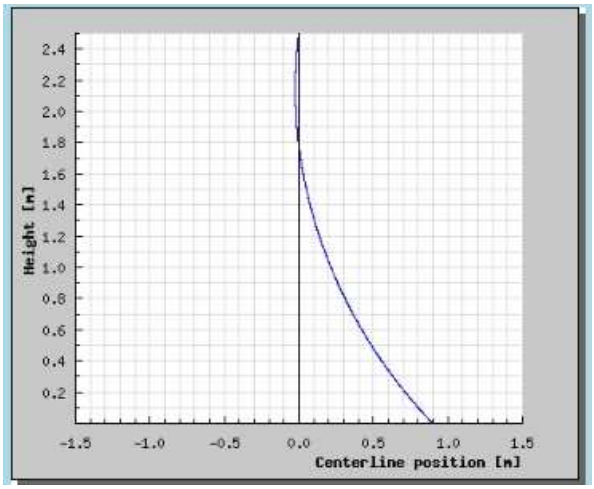

Figure 5.17: Jet deflection by the effect of the wind.Semianalytical.Wind velocity=3m/s.

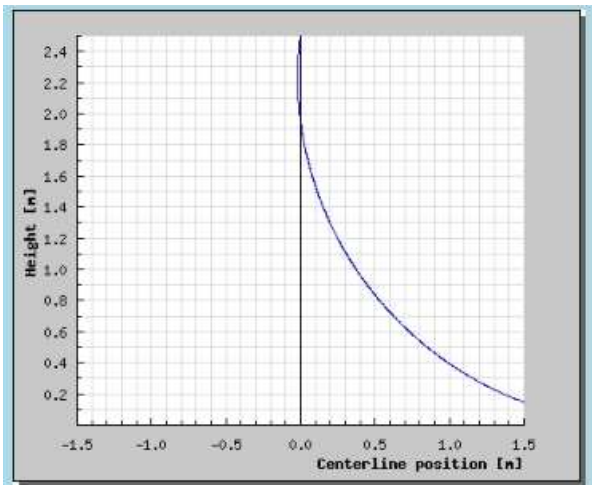

Figure 5.18: Jet deflection by the effect of the wind.Semianalytical.Wind velocity=4m/s.

5.8 Analysis of the wind effect by means of Large Eddy Simulation

In this section the deflection of the jet by the effect of the wind is predicted with Large Eddy Simulation. The simulations are performed with a high performance parallel code developed by Termofluids S.L., for further details about the code see [4]. The simulations are carried out in 3D meshes of roughly one million control volumes in unsteady regime. The turbulence model employed is the Wale model [8] and the discretization is symmetry-preserving. The solver employed for the Poisson equation is the iterative conjugate gradient method and the global algorithm is the fractional step method.

5.8.1 Domain geometry

The geometry of the physical domain consists of two adjacent rooms with different dimensions, 2 m x 2 m x 2.5 m the inner protected room, and 4 m x 0.75 m x 2.5 m the outer room,connected by a door featuring 1.0 m width and 2 m height, with the air curtain unit installed on the top. The first room represents the interior space to maintain sealed, and the other corresponds to the outdoor environment, where a inner boundary condition emulate the incident wind. The two rooms are connected by a by-pass ventilation duct, which avoid the difference of pressure between the two spaces (see Fig.5.19). The discharge nozzle of the air curtain has a thickness of 0.06 m and the discharge angle is fixed at 0 degrees for all the simulations. A length of 1.0 m was considered for the discharge nozzle to ensure that the jet covers the whole door width.

5.8.2 Results

It is worth mention that the air jet suffers deformation by the effect of the wind not only in the jet direction. In the direction of the door width there is an additional deflection, which increases the lateral unprotected area. In the following pictures, the slice of the domain at the middle section of the door is presented. The pictures show the average solution of the flow. In the first simulation (wind velocity=1m/s) it can be seen that there is no excessive lateral entrainment caused by the jet deflection. In the second simulation (wind velocity=2m/s) it can be seen that the jet suffers breakthrough by the effect of the wind force. In the third and fourth simulations (wind velocity=3m/s and 4m/s) the deflection is progressively larger than in the previous cases. In all the simulations it can be seen how the whole room suffers the flow recirculation produced by the air curtain unit, but this effect is clearly increased by the small dimensions of the space. In real situations, this recirculation contributes to the destruction of the thermal stratification in the whole domain, being this a common undesirable side-effect. A possible way to avoid this phenomena is the installation of a receptor vent in the floor, but the system complexity and the installation and maintenance costs inhibit its common use [10]. Another solution to diminish this

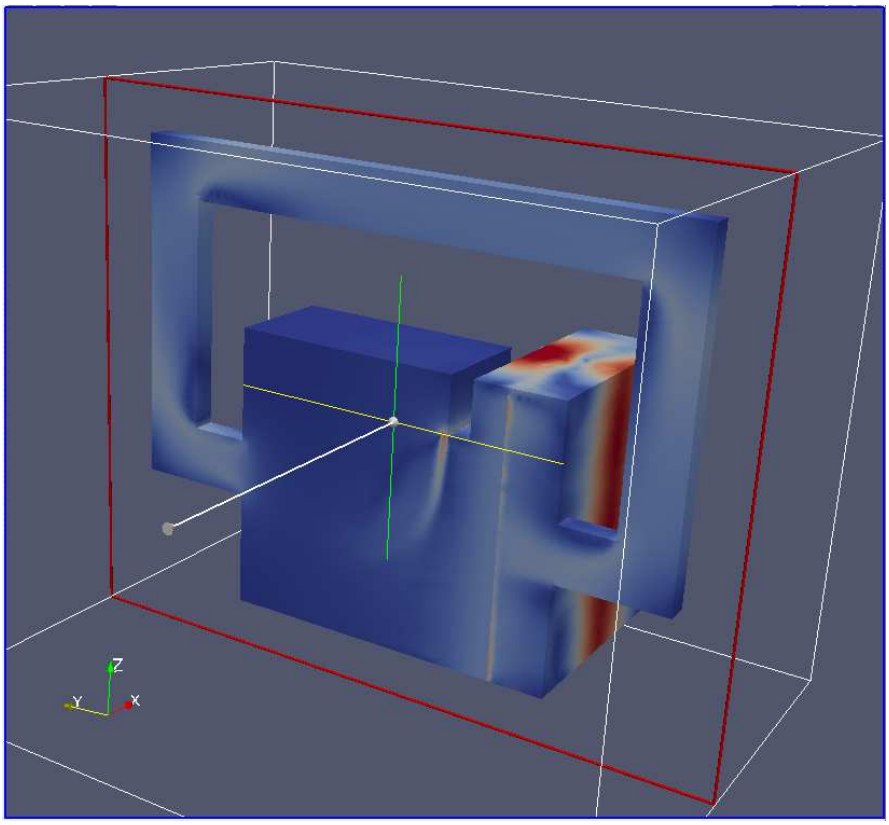

Figure 5.19: Geometry of the calculation domain.

recirculation is the lateral suction configuration in the air curtain unit, which produces a lower vorticity inside the room.

5.9 Conclusions

The airflow ejected by an air curtain has been characterized according to the AMCA standard requirements [1]. The measurements of the flow produced by the initial design has been observed as a non homogeneous, with very low velocity values in some regions. It have been detected by means of LES the main reasons of the problem. Alternative geometries have been numerically characterized and the best candidate

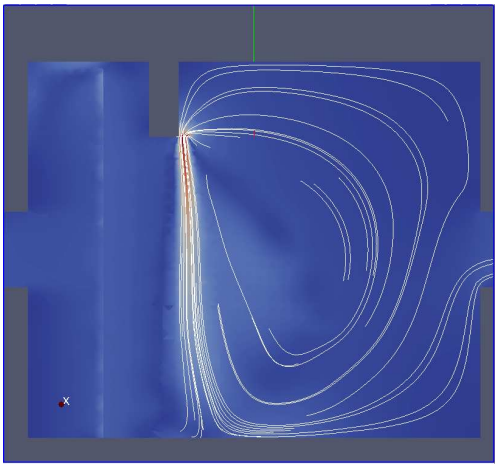

Figure 5.20: Jet deflection by the effect of the wind.LES.Wind velocity=1m/s.

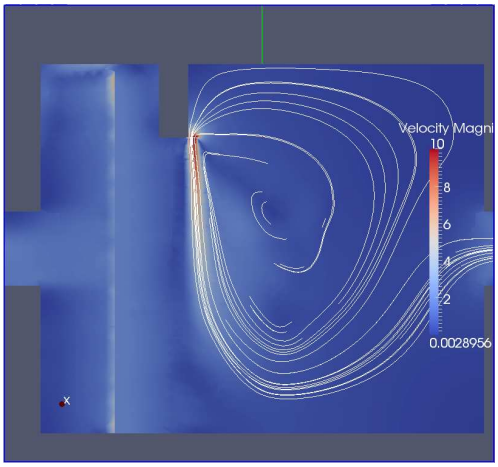

Figure 5.21: Jet deflection by the effect of the wind.LES.Wind velocity=2m/s.

according to the predictions has been constructed. The prototype has been checked experimental and numerically, showing concordance between the simulations and the measurements. The prototype of the proposed geometry improves the homogeneity

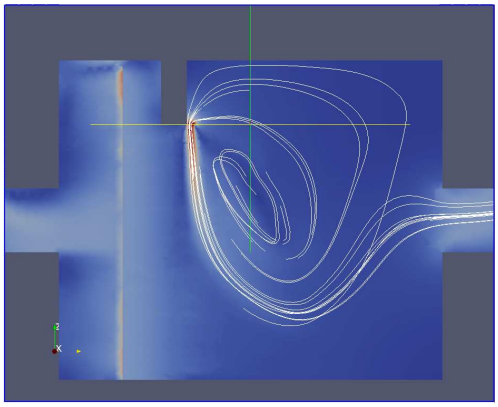

Figure 5.22: Jet deflection by the effect of the wind.LES.Wind velocity=3m/s.

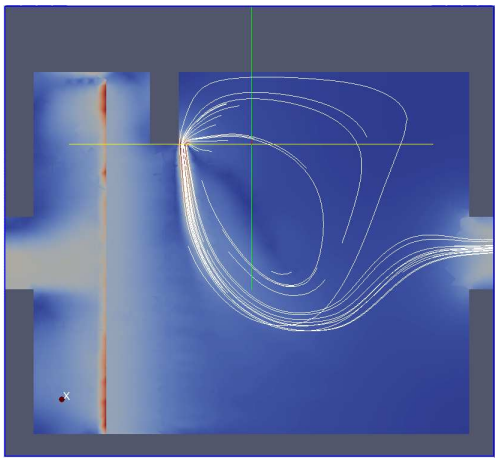

Figure 5.23: Jet deflection by the effect of the wind.LES.Wind velocity=4m/s.

and the mean velocity values in the discharge.

It is worth noting the optimization procedure described here is iterative. It includes experimental measurements, numerical simulations and the production of new prototypes.

The different plenum geometry modifications (both the inner curve and lateral

Wind Velocity [m/s]	1	2	3	4
Air flow entrainment [m^3/s]	0.13	1.5	2.75	3.75

Table 5.5: Air flow entrainment in function of the wind velocity.

difusors as well) have been checked. After the present study, the air curtain presents a configuration with two major modifications introduced so far: outer and inner curves, and next prototypes may include the lateral diffusors proposed.

LES has been employed in the optimization procedure of the air curtain plenum.

The deflection of the air jet by the effect of the wind has been studied. The air curtain has been studied based on semianalytical and CFD-based methods. Both numerical and semianalytical results are obtained for steady conditions. The CFD approach and the semianalytical analysis show similar results for the study of the wind effect but it is worth noting that the CFD simulations predict a slightly larger deflection than the semianalytical approach.

References

[1] Air Movement and Control Association International. *ANSI/AMCA Standard 220-05. Laboratory Methods of Testing Air Curtain Units for Aerodynamic Performance Rating.*, 2005.

[2] K. Sirén. Technical Dimensioning of a Vertically Upwards Blowing Air Curtain. Part I. *Energy and Buildings*, 35:681–695, 2003.

[3] J. E. Jaramillo, C. D. Pérez-Segarra, A. Oliva, and C. Oliet. Analysis of the Dynamic Behaviour of Refrigerated Space Using Air Curtains. *Numerical Heat Transfer, Part A*, 55(6):553–573, 2009.

[4] O. Lehmkuhl, C. D. Perez-Segarra, R. Borrell, M. Soria, and A. Oliva. TERMOFLUIDS: A new Parallel unstructured CFD code for the simulation of turbulent industrial problems on low cost PC Cluster. In *Proceedings of the Parallel CFD 2007 Conference*, pages 1–8, 2007.

[5] A. M. Foster, M. J. Swain, R. Barrett, P. D'Agaro, and S. J. James. Effectiveness and optimum jet velocity for a plane jet air curtain used to restrict cold room infiltration. *International Journal of Refrigeration*, 29(5):692–699, 2006.

[6] P. Sagaut. *Large Eddy Simulation for Incompressible Flows.* Springer-Verlag, 2001.

[7] J. Smagorinsky. General circulation experiments with the primitive equations, part. I: the basic experiment. *Monthly Weather Rev.*, 91:99–164, 1963.

[8] F. Nicoud and F. Ducros. Subgrid-scale stress modeling based on the square of the velocity gradient tensor. *Flow, Turbulence and Combustion*, 62:183–200, 1999.

[9] Lomb, N.R. Least-squares frequency analysis of unequally spaced data *Astrophysics and Space Science*, 39(2):447–462, 1976.

[10] J.C. Gonçalves, J.J. Costa, A.R. Figueiredo, and A.M.G. Lopes. CFD Modelling of Aerodynamic Sealing by Vertical and Horizontal Air Curtains. *Energy and Buildings*, 52:153 – 160, 2012.

6

Air curtains in the refrigeration field

6.1 Introduction

An air curtain unit (ACU) is a device which produces a plane impinging jet acting as an ambient separator. The efficiency of the ACU is understood as its capability to seal properly a room from heat and moisture entrainment. The efficiency of ACUs applied to the refrigeration field has been studied by several authors from the 60's.

The studies of Hetsroni [1] and Hayes [2] are the first attempts to characterise ACUs by means of simplified models. Later, Siren [3] [4] introduced a semi analytical method which allows a more accurate dimensioning of ACUs.

Among others, Navaz et al. [5] studied the flow field produced by an ACU by means of Particle Image Velocimetry (PIV) and CFD. A combination of CFD and experimental techniques applied to refrigerated rooms was presented by Foster et al. [6]. They indicated some discrepancies between the two approaches, but also pointed out that a more accurate simulation of the chamber was not possible due to the computing resources. In a different study, Foster [7] studied the three-dimensional behaviour of ACUs applied to restrict refrigerated room infiltration. In their study, the effect of the discharge velocity on the efficiency and the three-dimensional behaviour of the air jet are studied by means of Reynolds Averaged Navier Stokes (RANS) approach, concluding that the jets produced by ACUs in this application can not be considered as bi-dimensional. Jaramillo et al. [8] analysed these devices applied to refrigerated chambers by means of RANS calculations. Their studies showed satisfactory results when compared with experimental measurements.

A more detailed review of the employed methods in each of the indicated studies are presented in a previous article by the authors [9], where the jet deviation was

studied in detail. The jet produced by an ACU can be deviated by the effect of the wind, the difference of pressure inside/outside the building and/or the difference of temperatures. It was observed how the jet curvature diminishes the ACU efficiency. The air jet behaviour was studied by means of experimental measurements and LES calculations.

The main objective of the present study is to present an analysis of the efficiency of air curtains applied in refrigerated rooms, obtained by vertical downward blowing air curtain units. Fully three-dimensional Large Eddy Simulations are used to describe the interaction between an ACU and a refrigerated room.

Velocity and energy fields are typically calculated in different situations by means of CFD simulations. The additional magnitude implied in this coupled heat and moisture calculation is the water vapour concentration, which is transported both by diffusion and convection through the protected door and into the whole room.

The thermal and vapour entrainment efficiency of the installation can be determined by comparing the entrainment with the ACU turned on at different configurations and the ACU turned off.

The optimum discharge velocity and discharge angle for minimizing the entrainment produced by the temperature and moisture differences between the inner space and the outside are also evaluated. In order to compare the different ACU configurations, the reference case is calculated with a recirculating ACU and a twin-jet ACU. Different simulations are carried out in order to compare the obtained efficiency with and without recirculating ducts.

Once the moisture has entered the inner space, and as a function of the dew point temperature, it is determined the water condensation in the walls.

The basic structure of the following sections consists in the description of the employed numerical model, the validation of this model and a numerical study of an ACU protecting a refrigerated space under condensation conditions.

6.2 Mathematical formulation and numerical model

The mathematical formulation and its numerical resolution are presented in this section. The methodology consists of the numerical simulation of the fully three-dimensional turbulent flow originated by the ACU. The calculations are based on the solution of the filtered Navier-Stokes equations. The technique employed is the Large Eddy Simulation using the WALE model for the subgrid scales.

6.2.1 Governing equations

Assuming incompressible air flow behaviour and constant viscosity, the spatially filtered equation of mass and momentum used in LES can be written as follows:

$$\nabla \cdot \bar{\mathbf{u}} = 0 \tag{6.1}$$

$$\frac{\partial \bar{\mathbf{u}}}{\partial t} + \nabla\left(\bar{\mathbf{u}}\bar{\mathbf{u}}\right) + \frac{1}{\rho_o}\nabla\bar{p} - \nu\nabla^2\bar{\mathbf{u}} - \frac{\rho\mathbf{g}}{\rho_o} = \nabla\cdot\boldsymbol{\tau} \tag{6.2}$$

where $\bar{\mathbf{u}}$ represents the volume average velocity. The right-hand side of the momentum equations stands for the turbulent scales which are smaller than the mesh size.

$$\boldsymbol{\tau} = \bar{\mathbf{u}}\bar{\mathbf{u}} - \overline{\mathbf{u}}\overline{\mathbf{u}} \tag{6.3}$$

This subgrid scales has been modelled using an eddy viscosity approach,

$$\boldsymbol{\tau} = \frac{1}{3}\boldsymbol{\tau} : \boldsymbol{\delta} + 2\rho\nu_e\overline{\mathbf{S}} \tag{6.4}$$

$$\overline{\mathbf{S}} = \frac{1}{2}\left[\nabla\bar{\mathbf{u}} + \nabla\bar{\mathbf{u}}^T\right] \tag{6.5}$$

where $\mathbf{S}$ is the rate of stress tensor. In this study, the Wall Adapting Local Eddy viscosity (WALE) model [11] is employed. According to this model, the expression for the eddy viscosity is given by

$$\nu_e = \left(C_w\Delta\right)^2 \frac{\left(\overline{\boldsymbol{\mathcal{S}}} : \overline{\boldsymbol{\mathcal{S}}}\right)^{3/2}}{\left(\overline{\mathbf{S}} : \overline{\mathbf{S}}\right)^{5/2} + \left(\overline{\boldsymbol{\mathcal{S}}} : \overline{\boldsymbol{\mathcal{S}}}\right)^{5/4}} \tag{6.6}$$

where Δ is the length scale of the filter, C_w is the turbulent model constant, and $\boldsymbol{\mathcal{S}}$ is the traceless symmetric part of the square of the velocity gradient. In tensor notation:

$$\overline{S_{ij}} = \frac{1}{2}\left(\bar{\gamma}_{ij}^2 + \bar{\gamma}_{ji}^2\right) - \frac{1}{3}\delta_{ij}\bar{\gamma}_{kk}^2 \tag{6.7}$$

$$\bar{\gamma}_{ij} = \frac{\delta\bar{u}_i}{\delta x_j} \tag{6.8}$$

The energy equation governs the temperature distribution in the whole domain:

$$\frac{\partial\bar{T}}{\partial t} + \bar{\boldsymbol{u}}\cdot\nabla\bar{T} = \nabla\cdot\left[\left(\frac{\nu}{Pr} + \frac{\nu_e}{Pr_t}\right)\nabla\bar{T}\right] \tag{6.9}$$

where Pr is the Prandtl number and Pr_t is the turbulent Prandtl number, which has a value of 0.4.

The transport of water vapor concentration in humid air can be described by its transport equation:

$$\frac{\partial \bar{Y}_v}{\partial t} + \bar{\boldsymbol{u}} \cdot \nabla \bar{Y}_v = \nabla \cdot \left[\left(\frac{\nu}{Sc} + \frac{\nu_e}{Sc_t} \right) \nabla \bar{Y}_v \right] \tag{6.10}$$

where Y_v is the water mass fraction and Sc and Sc_t are the Schmidt number and the turbulent Schmidt number respectively. A value of 0.4 has been taken for the latter.

6.2.2 Boundary Conditions

In the outside region, a mixed inflow/outflow boundary has been imposed far away from the air curtain. At the outflow zones, pressure is given while the gradient in the normal direction of the different variables (velocity, temperature and vapour concentration) is set to zero. At the inflow zones, fixed values of the different scalar variables are imposed.

At the air curtain discharge, the three velocity components are fixed. In the discharge, the temperature and vapour concentration are prescribed according to their values upstream the discharge.

Inside the refrigerated chamber, the solid walls have a fixed temperature. In these walls a non-slipping condition has been assumed.

In every time step, if the wall presents a temperature lower or equal to the dew point temperature, the calculation imposes the saturation concentration in the solid surface, otherwise the mass gradient is set to zero.

This implies that when the dew point temperature is reached, the wall acts as a sink for the water vapour concentration. The water produced by condensation is removed from the computational domain. The detailed analysis of the droplets accumulation at the walls is out of the scope of this paper. Therefore the walls of the refrigerating space do not produce an accumulation of water in the ground.

6.2.3 Numerical model

All the simulations are carried out using the CFD & HT code Termofluids [12], which is an unstructured and parallel object-oriented code for solving industrial flows. In Termofluids, the governing equations are discretized on a collocated unstructured grid arrangement, by means of second-order spectro-consistent schemes [13]. Such discretization preserves the symmetry properties of the continuous differential operators, and ensure both stability and conservation of the global kinetic-energy balance on any grid. For the temporal discretization, a two-step linear explicit scheme on a fractional-step method has been used for the convective and diffusive terms [14], while for the pressure gradient term an implicit first-order scheme has been implemented. This methodology has been previously used with accurate results for solving the flow over bluff bodies with massive separation and in different cases of natural/mixed convection in enclosures [15], [16], [17]. A CFL condition has been employed for the determination of the time step.

6.3 Validation of the model

For the simulation of the refrigerating chamber, the model includes the transport of water vapour, which enters the protected space through the doorway. In order to validate the mathematical model, three different situations have been taken into account:

- Isolated plane air jet without interactions with the environment.
- Surface evaporation of water vapour in presence of air on a horizontal pool.
- Evaporation from a water film in a vertical wall.

The second and third cases have been specifically chosen to analyse the mass diffusion effect of humid air with the produced water vapour transport from liquid surfaces.

6.3.1 Previous study of the plane air jet

Before the coupled simulations of moisture and thermal entrainment are carried out, the dynamics of the plane air jet produced by the ACU has been studied. In this stage, the plane air jet has been analysed as an isolated entity, without the effect of the rest of the whole domain.

The accuracy of the predicted velocity distribution for the air jet have been experimentally validated in a setup designed by the authors [19].

In those previous works, the experimental measurements are carried out according with the standard procedure for air curtains characterization [18].

The studies showed the mean core velocity evolution of a plane air jet, which presents different regions, progressively reducing the maximum velocity and spreading the air jet in the spanwise direction. This effect diminishes its capability to act as a separator. It was seen that low discharge velocities produce weak air jets, which can not avoid the entrainment of external air. As an example, Fig.6.1(a) shows the typical deflection and air entrainment produced by external forces acting against a weak air jet. In the case of an air curtain with a high discharge velocity (see Fig.6.1(b)), the external forces cause a lower deflection and do not break the jet. Therefore, the conditioned space is properly protected from a large external air entrainment.

The obtained results of the previous works showed that the air jet behaviour predicted by the mathematical models employed here (LES with WALE model) agrees with the experimental measurements (see [19] for details).

6.3.2 Surface evaporation of water vapour in presence of air on a horizontal pool

In order to validate the mathematical model considering mass transfer, the same case as reference [20] is considered. This case consists in a water pool partially evaporating with a parallel dry air stream flowing above it. As expected, the initially

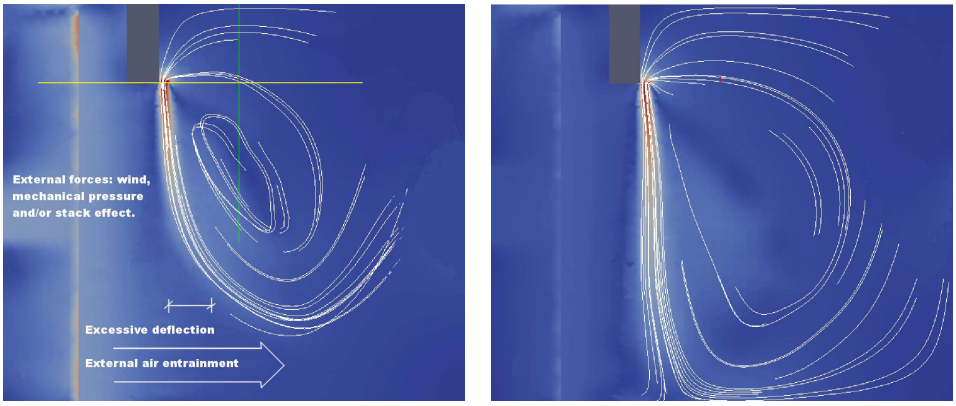

(a) (b)

Figure 6.1: Average streamlines produced by the ACU. (a)Weak air jet which presents an excessive deflection. (b)Strong air jet which seals properly a refrigerated chamber. Source: numerical tests carried out by the authors.

dry air stream progressively increases its water mass fraction as it flows through the domain. In this case, the velocity, temperature and water vapour concentration for the tridimensional moist air flow are calculated.

The geometry of the system (see Fig.6.2) is a horizontal 3D rectangular duct with a water pan centered in the bottom of the channel. All the other surfaces of the channel are considered adiabatic.

For the air flow, a velocity profile is imposed at the entrance with a uniform temperature and relative humidity. The flow is assumed to be steady and laminar.

At the bottom wall (y = 0), the water is at rest and its initial temperature is 16°C.

The simulation was carried out using an structured mesh of 50 x 50 x 100 control volumes. This mesh was progressively concentrated near the solid walls of the channel and near the water surface in order to capture accurately the physical phenomena.

The present results are compared with the experimental measurements carried out by Talukdar et al. [20](see Fig.6.3). Ten different situations are simulated, which present different initial boundary conditions in each case. The figure shows the values of temperature and relative humidity of the air flow at the outlet section of the domain. See [20] for further details of the different inlet conditions in each case.

In all the situations a good agreement between the results from the reference study and the calculations presented here can be observed.

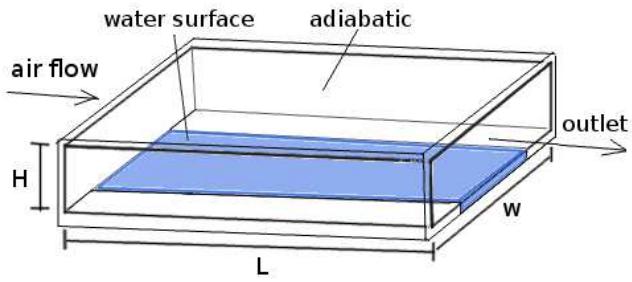

Figure 6.2: Overall scheme of the second validation case: pool.

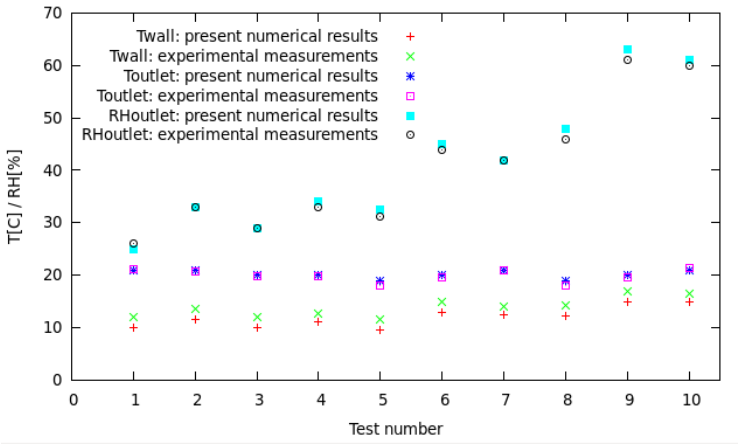

Figure 6.3: Air flow temperature and relative humidity at the exit of the duct. Experimental measurements from [20] compared to the numerical results.

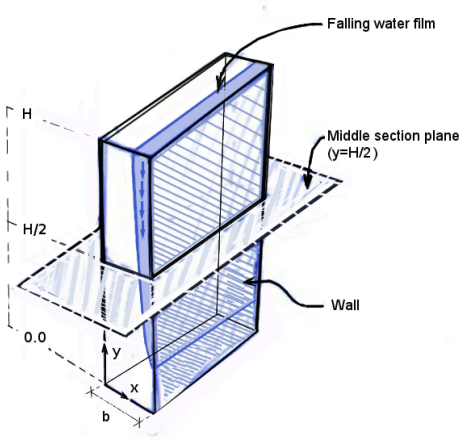

Figure 6.4: Scheme of the falling film case.

The simulations showed that the temperature and concentration fields evolve in the streamwise direction, being the dry air just above the pool progressively humidified by the water vapour coming from the pool. Therefore relative humidity of air at the outlet increases because of evaporation. It can be seen from Fig.6.3 that the water temperature found from the simulation is slightly lower than that measured in the experiments. According to Talukdar [20] this indicates that there could be a heat gain from surroundings in the experimental setup or could be caused by errors in the measurement of the water temperature.

6.3.3 Evaporation from a water film in a vertical wall

In the cool surfaces of a distillation unit it can be formed a liquid film by condensation of the water vapour. Once the film has been created, the mass of water will be transported by the gravity effect and by the partial evaporation to the surrounding air. This third case, referred to falling film, describes this transport phenomena (see Fig.6.4).

The details of the tested case can be found in [21].

In this case, as explained above, the liquid film falls vertically attached to a wall under the gravity effect and suffers evaporation which diminishes its total mass flow.

A comparison of the numerically predicted and experimentally obtained temperature distributions of the gas mixture with respect to the abcissa x, in the horizontal middle section (y=H/2) (see Fig.6.5(a)) and along the wall (see Fig.6.5(b)), are presented.

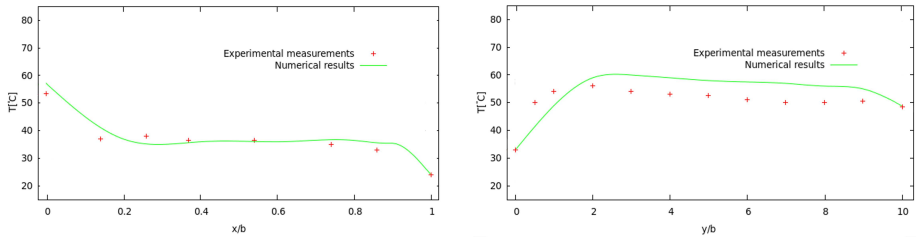

(a) (b)

Figure 6.5: Falling film. Comparison of the numerical results and measurements from [21]. (a)Temperature distribution in the horizontal middle section (y=H/2). (b)Temperature distribution along the wall.

There is some deviation between the results (see Fig.6.5(b)). This is, according [21], because the calculation gives a value of the liquid-gas interface temperature, though the measurement of the reference study concerns the mean film temperature at that level, as this latter is effectively given by the thermocouple sticked to the wetted wall.

The numerical calculations slightly overestimate the temperature in central region of the wall (see Fig.6.5(b)), but the differences are reduced and, in the opinion of Jabrallah et al., the discrepancies are due to the adopted hypothesis assuming that the flux applied to the wall is totally transmitted to the film.

It can be seen that the present numerical results agree well with the experimental measurements from the literature [21].

Althought the experimental measurements in the wall are slightly lower than the values predicted by the numerical calculations, it can be concluded that the model can be employed for an accurate prediction of the water vapour transport in the surfaces of the refrigerating room.

For the refrigerating space the mathematical formulation is exactly the same and the obtained numerical results in the two previous validation tests (pool within a rectangular duct [20] and falling film in a cavity [21]) confirm the capabilities of the mathematical model proposed.

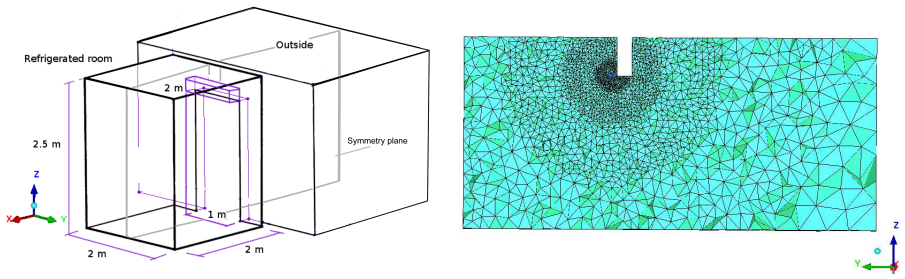

Figure 6.6: (a) Geometry of the calculation domain and (b) sketch of the discretization mesh in the symmetry plane.

6.4 Numerical study of air curtain in refrigerating spaces under condensation conditions

Air curtain analysis considering both heat and moisture transport are presented in this section. The heat and moisture entrainment produced through the door are determined for different situations and configurations. The efficiency of the ACU is calculated by comparison with the situation where the ACU is turned off. The water vapour condensation produced in the inner space walls is calculated.

6.4.1 Problem definition and mesh generation

Three configurations have been studied: recirculating, non-recirculating and twin-jets ACU. The geometry of the physical domain consists of two adjacent rooms connected by a door featuring 1.0 m width and 2.0 m height (see Fig.6.6(a)). An ACU is installed on the top of the door. One of the rooms represents the refrigerated space and the other represents the outdoor environment. The discharge nozzle, on the lower face of the air curtain, has a width of 6 cm and a length of 1.0 m, covering the whole door width. In the recirculating configuration, the ground has a receptor vent that allows the air flow to return to the ACU suction by means of ducts which are located inside the walls (see Fig. 6.7). In the twin-jets configuration, the ACU has two jets of 3 cm wide with a separation of 3 cm between them. It should be indicated that the positive discharge angles are corresponding towards the inside of the chamber, so the negative angles towards the outside.

An unstructured mesh is employed, the mesh has approximately 400000 control volumes, most of them in the region which covers the air jet (see Fig.6.6(b)). It is employed a high mesh concentration near the device in order to correctly describe the

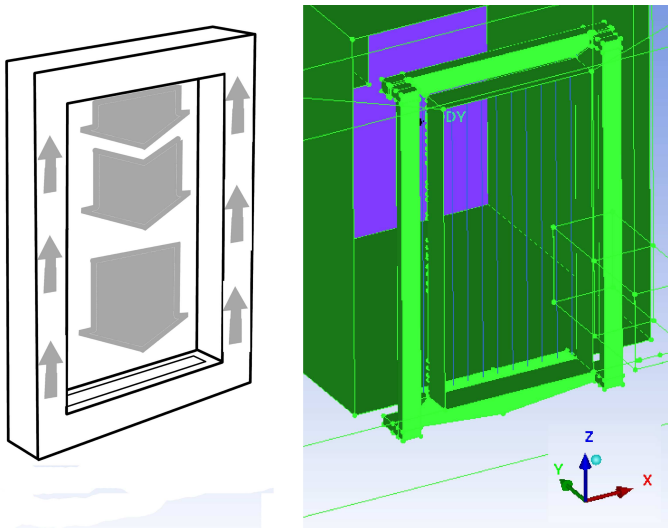

Figure 6.7: Geometry of the recirculating air curtain.

air jet behaviour. In order to check the mesh independency of the solutions, three different mesh concentrations have been studied and compared. It can be seen that the employed mesh produces the same results as the mesh with a higher concentration (see Fig. 6.8). Therefore, the mesh proposed it is suitable for carrying out the calculations.

6.4.2 Boundary and initial conditions

The purpose of the following boundary conditions is to allow the observation and the study the entrainment and the phenomena of condensation in the interior walls as the external air enters the refrigerated room through the door. The external air contains a water concentration which will exceed the saturation conditions as the air flow enters the refrigerated chamber.

As initial conditions, the air has been assumed stagnant all over the whole domain. The concentration of water vapour and temperatures are imposed in both inside and outside spaces. For the inner refrigerated space, an initial temperature of 278 K and a humidity ratio of 5 g/kg of dry air (which corresponds to 90% of relative humidity) are given. The outside space has an intial temperature of 298 K and a humidity ratio of 18 g/kg of dry air (which corresponds to 90% of relative humidity). All the domain is considered at atmospheric pressure.

The envelope of the calculation domain has been taken as impervious, except the inflow/outflow boundary far from the room, air changes being allowed only through

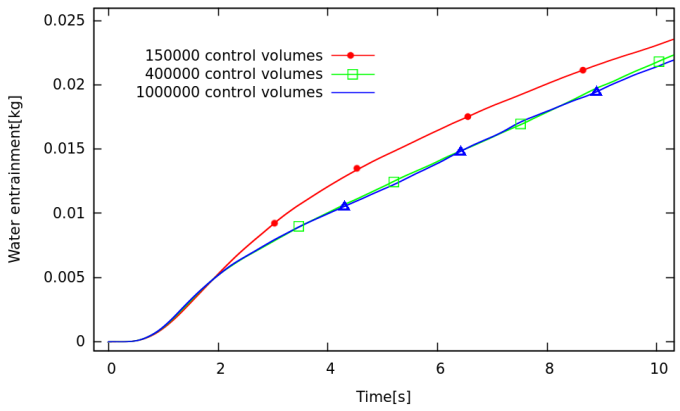

Figure 6.8: Comparison between three meshes with different concentrations.

the doorway between the two spaces. Despite the solid surfaces of a refrigerating chamber are usually considered adiabatic [8],for this simulations, inside the room the walls have been considered at a fixed temperature of 281 K. This is because it has been observed a behaviour different from totally adiabatic, as it is explained in the following.

Thermal inertia of the walls Although the walls of a refrigerating chamber have been usually treated as adiabatic, in this study, a fixed temperature is imposed as a more representative condition in fast transients including the thermal inertia of the walls. The effect of the thermal inertia, according to a preliminar simulation carried out by the authors, generates a temperature in the surface which is similar to 281 K ((see Fig.6.9) for the time span under study (about 25 s).

The temporal evolution for the initial moments has been simulated by a unidimensional transient model, and the temperature increase in the surface is relatively slow. The solid has an initial linear profile corresponding to a wall in steady state with differents temperatures between the inner space and the outside of 278 K and 298 K, respectively. Convective heat transfer coefficients are estimated by natural convection correlations [22]. The inner face of the wall is submitted to a sudden increase of the temperature to 298 K. In this way, it can be seen the effect of the thermal inertia of the wall in the temperature profile evolution. It can be seen that the surface temperature remains similar to 281 K for more than a minute. In this period of time, the walls act as an energy sink, due to its low temperature. If an adiabatic boundary condition would be assumed, this energy sink would not be taken

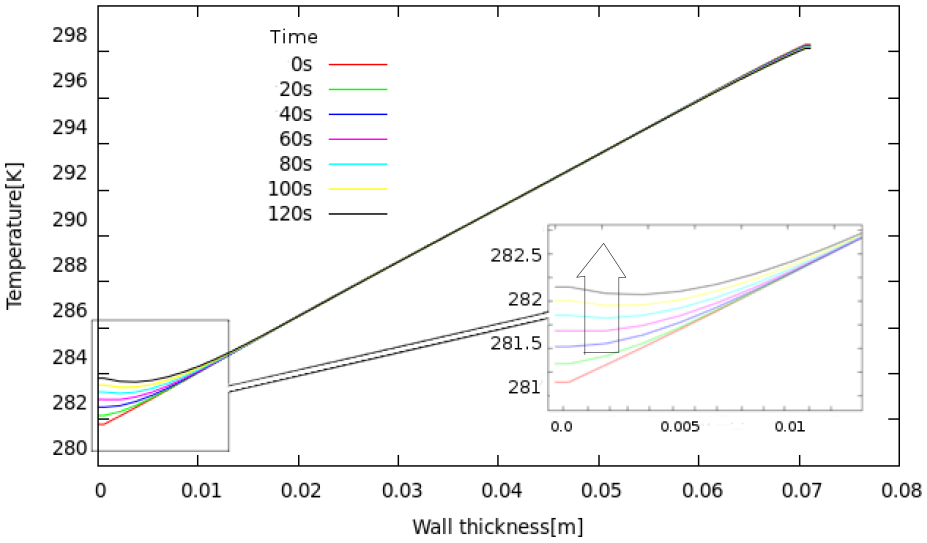

Figure 6.9: Time evolution of the transversal temperature profile inside the wall.

into account. In fact, the heat flux in the initial period is of the order of five times that of the steady and with reversed direction.

Therefore, for this study, a boundary condition with fixed temperature is considered more descriptive of the phenomena than an adiabatic condition.

As a further simplification, in the walls where condensation is produced it is assumed an instantaneous drain of the mass of liquid water.

6.4.3 Parametric studies

In this section, three parametric studies are presented.

In the first study, different velocities and discharge angles are prescribed at the ACU. The thermal and moisture entrainment are studied and the condensation produced in the walls of the refrigerated room is determined.

In the second parametric study, the velocity and dicharge angles have been fixed. The input parameters are the moisture and temperature in the outside environment.

In the third study, recirculating, non-recirculating and twin-jet ACU's are compared, obtaining the efficiency of every of them in the same scenario.

The thermal efficiency of the ACU can be defined as:

$$Eff_Q = 1 - \frac{Q_{on}}{Q_{off}} \tag{6.11}$$

where Q_{on} and Q_{off} are the thermal gain with the air curtain turned on and the air curtain turned off at the same conditions respectively. The mass entrainment efficiency can be defined as:

$$Eff_M = 1 - \frac{M_{on}}{M_{off}} \tag{6.12}$$

where M_{on} and M_{off} are the water mass entrainment with the air curtain turned on and the air curtain turned off respectively.

The efficiency tests carried out in the present study are summarised in the Table 6.1.

Study	$v[m/s]$	$\alpha[^\circ]$	$H_{out}[\%]$	$T_{out}[^\circ C]$	$Type$
First	2.5	-15.0	90.0	298.0	Single jet
	2.5	0.0	90.0	298.0	Single jet
	2.5	15.0	90.0	298.0	Single jet
	5.0	-15.0	90.0	298.0	Single jet
	5.0	-7.5	90.0	298.0	Single jet
	5.0	0.0	90.0	298.0	Single jet
	5.0	7.5	90.0	298.0	Single jet
	5.0	15.0	90.0	298.0	Single jet
	10.0	-15.0	90.0	298.0	Single jet
	10.0	0.0	90.0	298.0	Single jet
	10.0	15.0	90.0	298.0	Single jet
Second	5.0	0.0	50.0	288.0	Single jet
	5.0	0.0	70.0	288.0	Single jet
	5.0	0.0	90.0	288.0	Single jet
	5.0	0.0	50.0	308.0	Single jet
	5.0	0.0	70.0	308.0	Single jet
	5.0	0.0	90.0	308.0	Single jet
Third	5.0	0.0	90.0	298.0	Single jet
	5.0	0.0	90.0	298.0	Twin-jet
	5.0	0.0	90.0	298.0	Recirculating

Table 6.1: Parametric studies

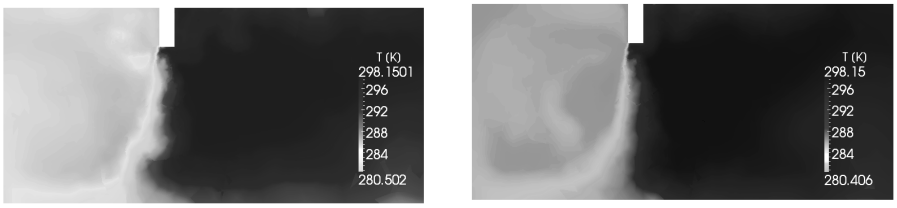

(a) (b)

Figure 6.10: (a) Temperature distribution in the inner space with discharge velocity 5m/s. (b) Temperature distribution in the inner space with discharge velocity 10m/s.

First parametric study: effect of the angle and the discharge velocity in the entrainment to the refrigerating space This first parametric study is focused on the thermal energy entering a refrigerated chamber with a door sealed by an ACU. The acumulation of energy inside the protected space is equal to the energy transfer through the door. The modified input parameter are the discharge velocity and the discharge angle of the ACU. The different discharge velocities are 0, 2.5, 5.0 and 10.0 m/s. The different discharge angles are -15, -7.5, 0, 7.5 and 15 °. The initial temperature inside the refrigerated chamber is 278 K and the outside temperature is fixed at 298 K.

The thermal distribution for the case of 5.0 m/s can be seen in Fig.6.10(a). The distribution with a discharge velocity of 10.0 m/s can be seen in Fig.6.10(b).

Comparing the two figures it can be seen that a higher discharge velocity does not necessarily mean a higher sealing of the door. The case with the ACU operating at 10.0 m/s exhibits a refrigerated room with higher temperatures due to the external entrainment. This is because the discharge velocity of 10.0 m/s (see Fig.6.10(b)), produces an excessive fast jet, which partially seals, but also partially accelerates the entrainment of external air. An analogue behaviour has been observed for the water vapor concentrations.

The energy and mass entrainment can be seen in Figs.6.11 and 6.12. From the results it can be seen that the different discharge velocities are not equally effective for different times of aperture in the door. It can be distiguished three stages: the initial moments where the air has not been yet accelerated by the stack effect, so the ACU is not reducing the entrainment compared to the ACU turned off. Once the air jet is completelly developed, it produces the desired effect insulating the inner space. In the second stage the curves of entrainment exhibits a pronounced slope, because the ACU is not covering the whole door and even can slightly accelerate the arrival

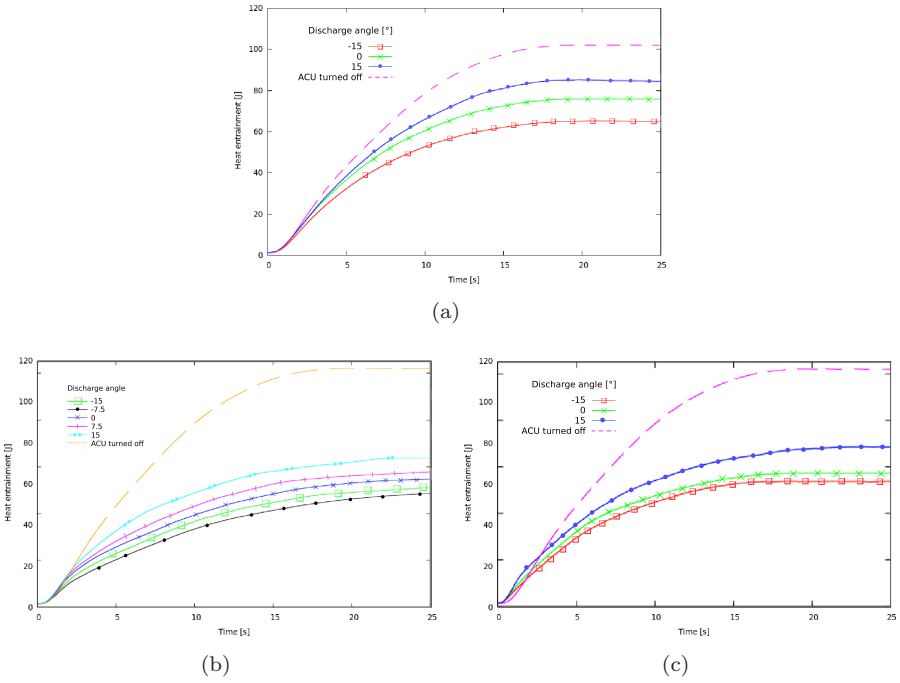

Figure 6.11: (a) Heat entrainment with a discharge velocity of 2.5 m/s. Different angles. (b) Heat entrainment with a discharge velocity of 5 m/s. Different angles. (c) Heat entrainment with a discharge velocity of 10 m/s. Different angles.

of humid air to the room. In the third stage, the evolution acquires its steady state, because the inner space has acquired a relatively high temperature due to the external entrainment.

The efficiency for the different discharge velocities and discharge angles can be seen in Fig.6.13 and Fig.6.14 for the thermal and mass efficiencies respectively. It is worth indicating that the calculations predict a higher sealing of the refrigerated room not for the maximum velocities. This is due to the fact that excessive velocities enhance the mixing between the outside air and the air in the interior space. In the other side, the lowest velocities will not produce an air jet strong enough to act as a separator with external forces deflecting it. For this particular configuration, the optimum is found in the discharge velocity of 5.0 m/s with an angle of 7.5 degrees towards the outside (see Figs.6.13 and 6.14).

The accumulated condensation produced in the different walls of the inner space

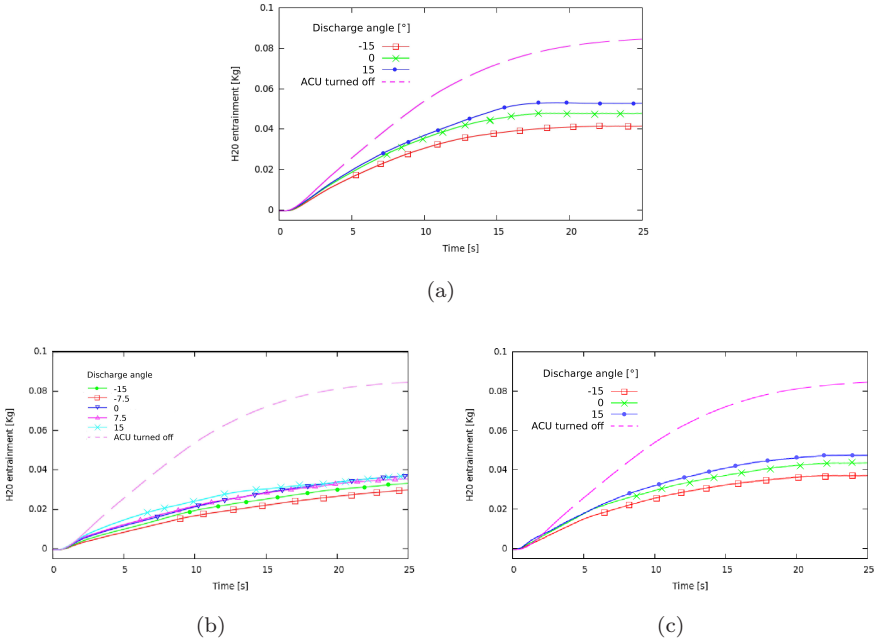

Figure 6.12: (a) Mass entrainment with a discharge velocity of 2.5 m/s. Different angles. (b) Mass entrainment with a discharge velocity of 5 m/s. Different angles. (c) Mass entrainment with a discharge velocity of 10 m/s. Different angles.

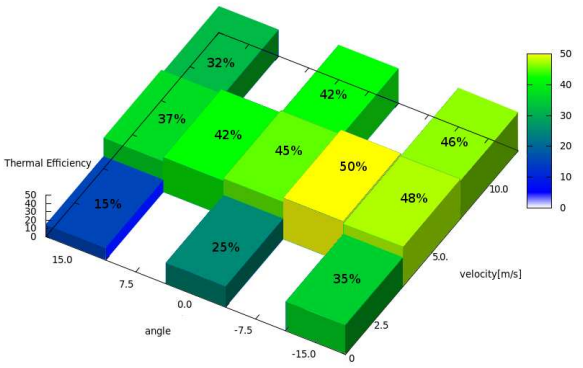

Figure 6.13: Thermal efficiency for each ACU discharge velocity and discharge angle.

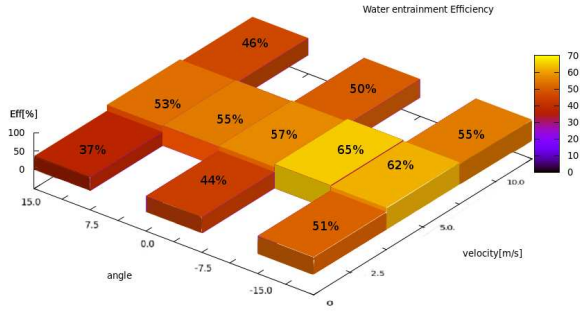

Figure 6.14: Water entrainment efficiency for each ACU discharge velocity and discharge angle.

is presented. The moisture penetrating through the door collides against the surfaces, and if they are below the dew point temperature, occurs the phenomena of surface condensation. The amount of condensed water per area in each of the surfaces after 20.0 seconds of opening are summarised in the following figures (see Fig.6.15, 6.16 and 6.17). It can be seen that the negative discharge angles (towards the outside the chamber) produces lower quantities of condensation in the surfaces than with the positive angles. It is observed that the condensation of water in the ground is lower than the amount condensed in the ceiling and in the walls. For the discharge velocity of 2.5 m/s (see Fig.6.15), when the angle is increased, the condensation in the ground follows an opposite trend than the condensation in the ceiling. It could be produced because of the trajectory followed by the draught of moist air: it first flows near the ground, collides against the walls and finally it impacts against the ceiling. All the quantity of water which does not condensate in the ground, or in the walls, is available to concensate in the ceiling. This explanation will describe the trajectory in the case of a weak jet. The jet is not covering completely the entrance, so the draught of outside air can penetrate into the room through the lower region of the door.

For the case of 5.0 m/s (see Fig.6.16), it can be seen low levels of condensation in the negative angles. As the angle is modified, the trend of the condensation in the different surfaces does not present a clear pattern.

For the case of 10.0 m/s (see Fig.6.17), also it can be seen low levels of condensation with the negative angle. The condensation in the ceiling increases as the angle is increased.

The discharge angle of the ACU has been also modified in order to determine the required position that produces the higher efficiency of the device. It can be seen that the best performance is obtained with negative discharge angles (towards the outside), according with the experience. The air jet produced by the ACU is deflected, therefore the discharge angle towards the outside increases the efficiency. It is worth mention that in the case of recirculating air curtains, the angle should be smaller than the indicated here.

If a difference of mechanical pressure, between the refrigerated chamber and the outside, or other external forces (e.g. wind) were applied, higher angles than the indicated here could be required in order to compensate the deflection of the air jet.

6.4.4 Differences of temperature and moisture effect

This section is focused in the effect of the temperature and moisture differences between the outside and the refrigerated chamber.

The input parameters are the temperature and moisture at the outside space, mantaining the refrigerated chamber at 278 K. The velocity is prescribed at 5.0 m/s and the discharge angle is 0°.

In Fig.6.18(a) the time evolution of the thermal entrainment is described. It can be seen that the thermal entrainment is not highly affected by the modifications of

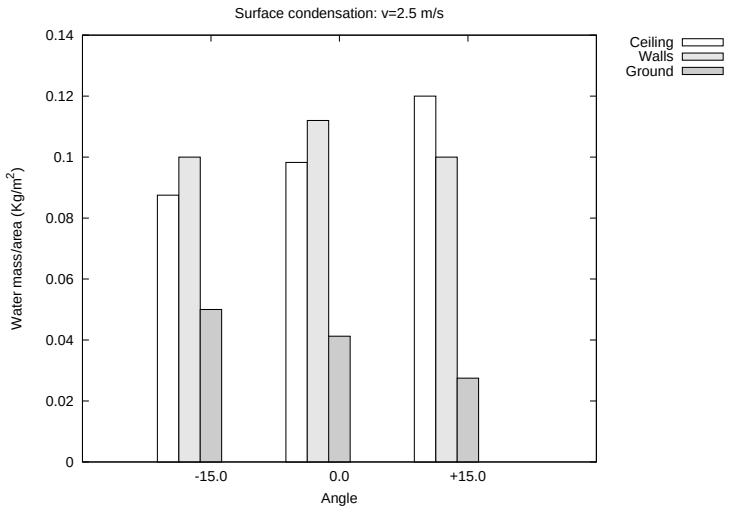

Figure 6.15: Condensation in the different surfaces of the protected room with different angles. ACU at 2.5 m/s.

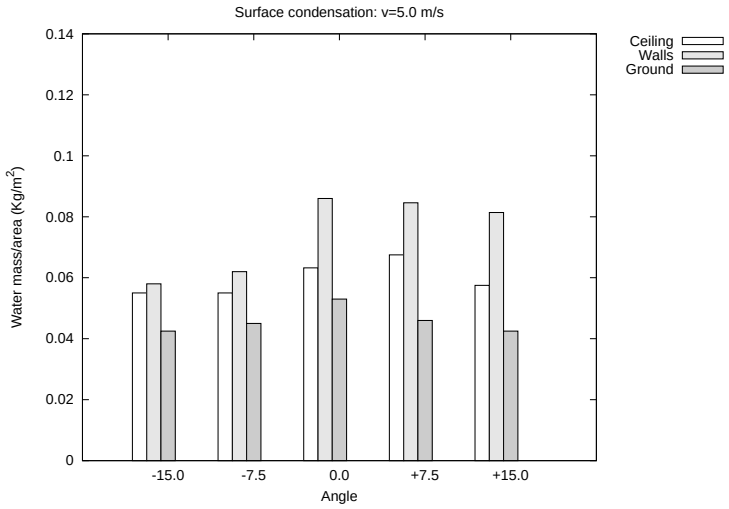

Figure 6.16: Condensation in the different surfaces of the protected room with different angles. ACU at 5.0 m/s.

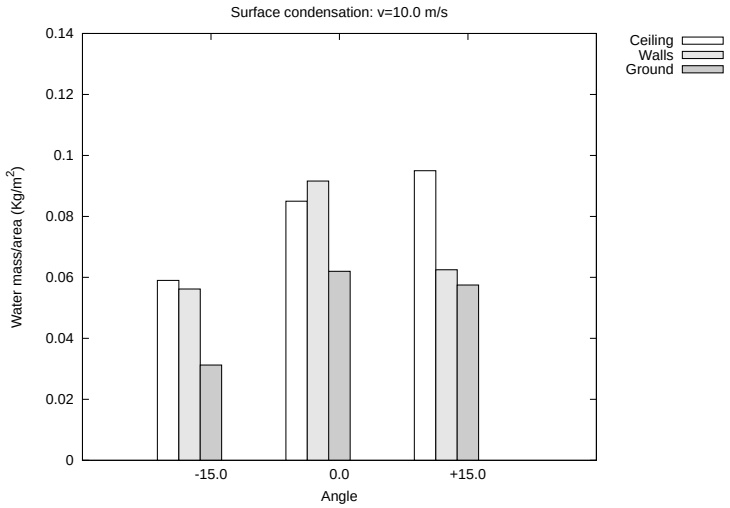

Figure 6.17: Condensation in the different surfaces of the protected room with different angles. ACU at 10.0 m/s.

the moisture level at the outside. This is a logical result, because the stack effect is due to the difference of density mainly produced by the difference of temperature between inside and outside.

In Fig.6.18(b) the time evolution of the water vapour entrainment is described. It can be seen that the effect of modifying both the levels of moisture and temperature at the outside clearly affects the amount of water vapour entering the refrigerated room, logically increasing the amount of water penetrating through the door as the temperature difference is increased and/or as the relative humidity difference is increased.

The condensation in the surfaces of the refrigerated room can be seen in Fig.6.19(a) and 6.19(b). The effect of a higher temperature in the outside increase the amount of condensation inside, with a higher increase in the walls and in the ground than in the ceiling. The same effect is observed for the relative humidity present at the outside. This results indicate that the ACU is partially preventing the thermal and mass entrainment, but not totally. As it has been pointed out in the previous section, in these studies only the stack effect is acting as external force. If any other external force acts against the air jet, it could be required additional adjustments.

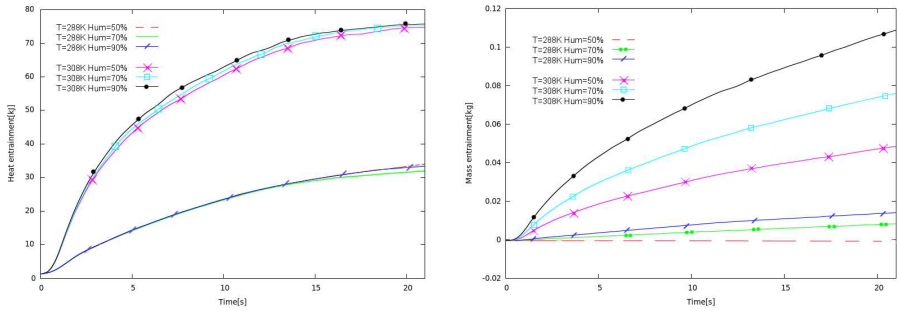

(a) (b)

Figure 6.18: (a) Thermal entrainment with different levels of temperature and relative humidity at the outside. (b) Mass entrainment with different levels of temperature and relative humidity at the outside.

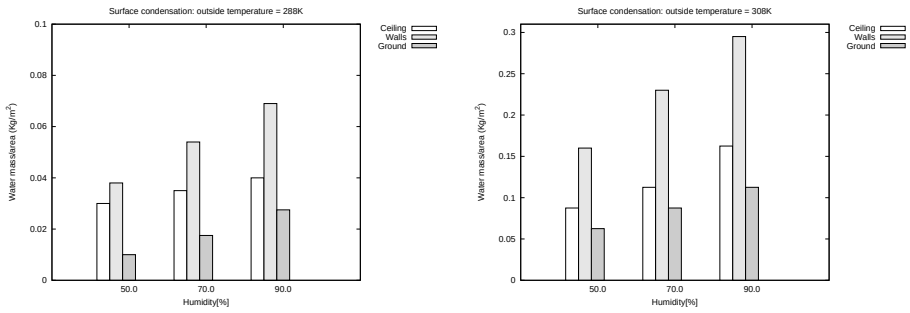

(a) (b)

Figure 6.19: (a) Surface condensation with a temperature of 288K at the outside. (b) Surface condensation with temperature of 308K at the outside.

6.4.5 Evaluation of different air curtain configurations

In this section three different configurations are evaluated: recirculating, non-recirculating and twin-jet configurations. The efficiency obtained with the three different configurations have been determined.

The first configuration is the non-recirculating single jet, which is the reference configuration employed in the previous sections. The second configuration is the non-recirculating twin-jets, which consists in a double jet with a separation between jets of 3 cm. The third configuration is the recirculating ACU, which is a more complex system. This system has ducts placed inside the walls to redirectionate the air jet collected in the receptor vent(see Fig.6.20) to the ACU suction.

The velocity is prescribed at 5.0 m/s and the discharge angle is 0°. The obtained results are summarised in Fig.6.21. The twin-jets improves the sealing capability of the ACU compared to the non-recirculating single jet. This is due to the additional protection that the jet placed in the external side gives to the internal jet. In this way, the curvature of the jet is lower than in the single jet. It is worth notice that, far away from the discharge, the two jets finally merge in a single air stream. This is due to the deformation of the rectangular jets as they advance: their shapes are progressively changed from rectangular to circular. Once this state is achieved, it can be seen how the two jets are overlapping with each other (see Fig.6.22).

On the initial seconds of simulation, when the air jets are not totally closing the door, the efficiency of the single and the twin-jets is exactly the same (see Fig.6.23).

In its turn, the recirculating system presents a higher sealing capability than the other configurations. An instantaneous temperature distribution obtained for the recirculating system is presented in Fig.6.24. Even when the installation of the recirculating ACU is more expensive than the non-recirculating model, the present results pointed out that this type of installation can produce an overall energy efficiency benefit. The receptor vent has a double effect: it diminishes the mixture of the inside/outside air and, moreover, it diminishes the curvature of the jet due to the produced suction effect. It is worth indicate that the receptor vent should be wide enough to receive all the air stream of the jet.

6.5 Conclusions

CFD calculations using LES modelling for the prediction of air curtains efficiency have been presented. The model considers the effect of the moisture entrainment through the protected opening. Furthermore, a description of the water vapour entrainment and condensation is carried out.

The validation of the moisture transportation and condensation has been carried out in the previous sections.

The validation of the mathematical formulation for the air jet has been carried out

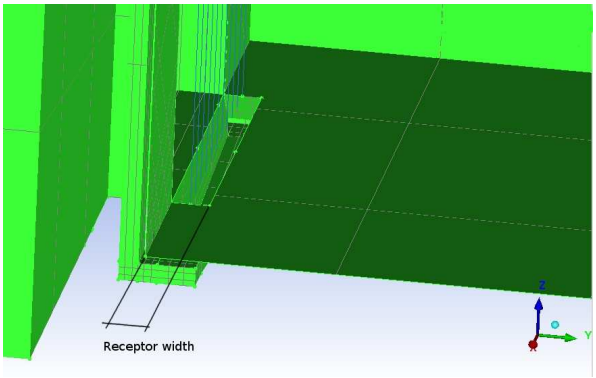

Figure 6.20: Detail of the recirculating ACU: receptor vent.

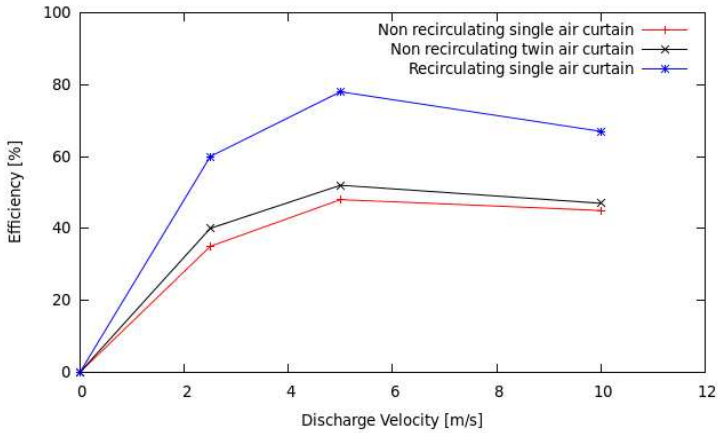

Figure 6.21: ACU efficiency with different velocities and configurations: single jet, twin-jet and recirculating ACU.

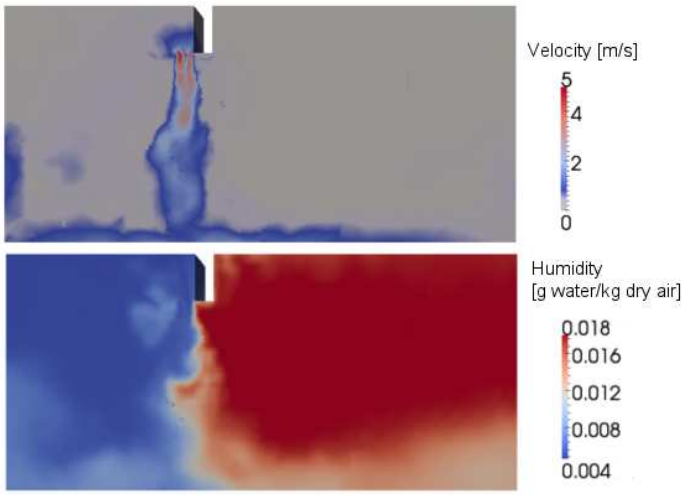

Figure 6.22: Twin-jets ACU. Instantaneous velocity and humidity distributions in the middle plane.

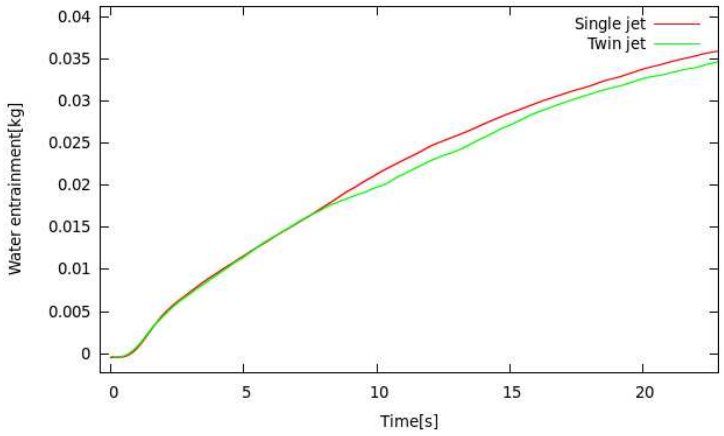

Figure 6.23: Temporal evolution of the mass entrainment: comparison between single jet and twin-jet. Discharge velocity fixed at 5m/s.

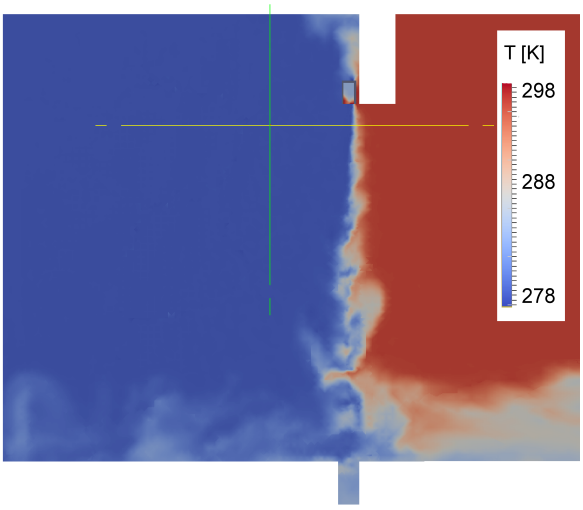

Figure 6.24: Recirculating ACU. Instantaneous temperature distribution in the middle plane.

in previous works by comparison with experimental measurements from the literature. The calculations agree with the measurements.

The effect of modifying the discharge velocities has been studied, being determined the optimum one for obtaining the highest level of protection against humidity and thermal entrainment through the door. The discharge angle has been modified in order to determine the position that produces the higher efficiency. It has been observed that low discharge angles towards the outside of the chamber produce the best performance.

In the present study the behaviour of three different configurations have been described by means of CFD simulations. In the case of twin-jets, they have produced a higher efficiency than the single jet configuration. In the case of recirculating air curtains, they exhibit higher efficiencies than non-recirculating devices. The direct air recirculation system provides a maximum sealing performance of 80% for the optimum discharge velocity.

All these results are obtained for steady boundary conditions.

It can be concluded that the air curtains are able to protect refrigerated spaces from heat and moisture entrainment, diminishing the energy consumed to maintain the refrigerated space at the required moisture and temperature levels.

Acknowledgements

This work has been financially supported by the Ministerio de Economía y Competitividad, Secretaría de Estado de Investigación, Desarrollo e Innovación, Spain (ENE-2010-17801) and by the collaboration project between the Universitat Politècnica de Catalunya (UPC) and Termo Fluids S. L. H. Giráldez also wishes to thank UPC for its support in the form of a FPI doctoral scholarship.

References

[1] G. Hetsroni and C. W. Hall. Further Studies of the Air Curtain. *ASAE Transactions*, 1:438–452, 1964.

[2] F. C. Hayes and W. F. Stoecker. Design Data for Air Curtains. *ASHRAE Transactions*, 2121:168–179, 1969.

[3] K. Sirén. Technical Dimensioning of a Vertically Upwards Blowing Air Curtain. Part I. *Energy and Buildings*, 35:681–695, 2003.

[4] K. Sirén. Thechnical Dimensioning of a Vertically Upwards Blowing Air Curtainpart II. *Energy and Buildings*, 35:697–705, 2003.

[5] H.K. Navaz, R. Faramarzi, M. Gharib, D. Dabiri, and D. Modarress. The Application of Advanced Methods in Analyzing the Performance ot the Air Curtain in a Refrigerated Display Case. *Journal of Fluids Engineering*, 124(1):756–764, 2002.

[6] A. M. Foster, M. J. Swain, R. Barrett, and S. J. James. Experimental Verification of Analytical and CFD Predictions of Infiltration Through Cold Stores Entrances. *International Journal of Refrigeration*, 26(8):918–925, 2003.

[7] A. M. Foster, M. J. Swain, R. Barrett, P. DAgaro, L. Ketteringham, and S. J. James. Three-Dimensional Effects of an Air Curtain Used to Restrict Cold Room Infiltration. *Applied Mathematical Modelling*, 31(6):1109–1123, 2007.

[8] J. E. Jaramillo, C. D. Pérez-Segarra, A. Oliva, and C. Oliet. Analysis of the Dynamic Behaviour of Refrigerated Space Using Air Curtains. *Numerical Heat Transfer, Part A*, 55(6):553–573, 2009.

[9] H. Giráldez, C. D. Pérez-Segarra, I. Rodríguez, and A. Oliva. Improved semi-analytical method for air curtains prediction. *Energy and Buildings*, 60:256–266, 2013.

[10] J.C. Gonçalves, J.J. Costa, A.R. Figueiredo, and A.M.G. Lopes. CFD Modelling of Aerodynamic Sealing by Vertical and Horizontal Air Curtains. *Energy and Buildings*, 52:153 – 160, 2012.

[11] F. Nicoud and F. Ducros. Subgrid-scale stress modeling based on the square of the velocity gradient tensor. *Flow, Turbulence and Combustion*, 62:183–200, 1999.

[12] O. Lehmkuhl, C. D. Pérez-Segarra, R. Borrell, M. Soria, and A. Oliva. TERMOFLUIDS: A new Parallel unstructured CFD code for the simulation of turbulent industrial problems on low cost PC Cluster. In *Proceedings of the Parallel CFD 2007 Conference*, pages 1–8, 2007.

[13] R. W. C. P. Verstappen and A. E. P. Veldman. Symmetry-preserving discretization of turbulent flow. *Journal of Computational Physics*, 187(1):343–368, 2003.

[14] F. X. Trias and O. Lehmkuhl. A self-adaptive strategy for the time integration of Navier-Stokes equations. *Numerical Heat Transfer, Part B*, 60(2):116–134, 2011.

[15] I. Rodríguez, R. Borrell, O. Lehmkuhl, C. D. Perez-Segarra, and A. Oliva. Direct numerical simulation of the flow over a sphere at $Re = 3700$. *Journal of Fluid Mechanics*, 25(25):263–283, 2011.

[16] D. Kizildag, F.X. Trias, I. Rodríguez, A. Oliva. Large eddy and direct numerical simulations of a turbulent water-filled differentially heated cavity of aspect ratio 5. *International Journal of Heat and Mass Transfer*, 77:1084–1094, 2014.

[17] Trias, F.X., Lehmkuhl, O., Oliva, A., Pérez-Segarra, C.D., Verstappen, R.W.C.P. Symmetry-preserving discretization of Navier-Stokes equations on collocated unstructured grids. *Journal of Computational Physics*, 258: 246–267, 2014.

[18] Air Movement and Control Association International. *ANSI/AMCA Standard 220-05. Laboratory Methods of Testing Air Curtain Units for Aerodynamic Performance Rating.*, 2005.

[19] H. Giráldez, C. D. Pérez-Segarra, I. Rodríguez, and A. Oliva. Optimization of the Thermal and Fluid Dynamic Behaviour of Air Curtains. Analysis of the Plenum by Means of LES. In *Proceedings of the 15th International Conference on Fluid Flow Technologies,Budapest,Hungary*, 2012.

[20] Talukdar, P., Iskra, C.R., Simonson, C.J. Combined heat and mass transfer for laminar flow of moist air in a 3D rectangular duct: CFD simulation and validation with experimental data. *International Journal of Heat and Mass Transfer*, 51(11-12):3091–3102. 2008.

[21] S. Ben Jabrallah, A. Belghith, J.P. Corriou Convective heat and mass transfer with evaporation of a falling film in a cavity. *International Journal of Thermal Sciences*,45, Issues 1,16–28, 2006.

[22] Eckert, E. R. G. and Drake Jr., R. M. Analysis of Heat and Mass Transfer. *McGraw-Hill*,1972.

7

Final conclusions and future research

7.1 Concluding remarks

The main objective of the present thesis has been the study and optimization of ACUs. In the chapters 2, 3, 4 it has been completed the characterization stage by means of semianalytical methods, numerical simulations and experimental measurements respectively.

In the chapter 2, it has been proposed a modification of an existing semianalytical method, obtaining a good agreement with experimental measurements. The semianalytical method has allowed predictions of the air jet behaviour with very low time consuming calculations.

In the chapter 3, the numerical simulations by means of Large Eddy Simulations(LES) have provided a more detailed description of the flow field produced by ACUs. The numerical simulations do not describe just the air jet behaviour as in the semianalytical methods, it also describes the surroundings of the installation, allowing the study of the interaction between the device and other agents.

In the chapter 4, by means of hot wire anemometry measurements, actual ACUs has been characterised according to the standard provided in the industry. For this purpose, an experimental setup has been constructed, employing the standard as a reference. This experimental setup isolates the air jet, allowing direct measurements without any external perturbation.

In the chapter 5 the ACU inner chamber (plenum) has been optimized according to the possible flaws in the initial design. It has been observed that an overall new design was needed, being not small modifications a solution to avoid unnecesary pressure losses inside the device. The proposed prototype is characterised by means of numerical simulations and also by means of experimental measurements, demonstrating an improved behaviour in its sealing capability.

In the chapter 6 the application of ACUs in the refrigeration field has been studied. The efficiency of the ACU has been evaluated for energy and moisture entrainment. Recirculating and non-recirculating ainstallations have been compared. Several parametric studies has been carried out in order to determine the efficiency of the device to protect refrigerated rooms in different situations.

It is worth noting the good agreement between the different methodologies employed in the present thesis to predict and optimize air curtains.

7.2 Future actions

The study of other configurations such as different orientating blades effect are topics that could be treated in following stages.

The study of the fans inside the air curtains units also remains as a challenge due to the required moving adaptable meshes, in order to correctly characterize the flow behaviour around the blades.

In the future, detailed studies of the air curtain interaction with pedestrians could be carried out.

Also it is worth noting that the environment where the air curtain is placed it is also a region of interest for more detailed studies. One of the more interesting aspects is the volume condensation produced inside the refrigerating chambers protected by air curtains.

From the information of more detailed simulations, the semianalytical models could be further refined.

Appendix A

Experimental setup facility and plenum design

A.1 Experimental setup

The experimental setup is constructed according to the AMCA standard [1]. In this section it is shown the overall aspect of this experimental setup, especifically designed for the purposes of this thesis, which includes a cartesian robot, an anemometer, its calibrator and the channel itself.

The cartesian robot is mounted over a platform especifically designed for this experiment. The platform has attached two tensors which allow its movement in the sreamwise direction.

This platform has been constructed with a stainless steel of 2 centimeters of width, ensuring its capability to support the weight of the cartesian robot without suffering deformation, which will make the positioning not accurate.

Attached to the platform of the cartesian robot there is also a couple of tensors, which allow the positioning of the robot in the streamwise direction. This tensors can be moved by means of two motors, one in each extrem of the channel.

Other component of the experimental setup is the calibrator. The calibrator ensures the precision and fiability of the measurements. The calibration of all the sensors probes has been carried out according to the indications of the manufacturers. The calibration has been carried out at similar conditions of pressure and temperature as the conditions of the measurements.

Figure A.1: Overall view of the experimental setup.

A.2 Plenum design

The plenum of a commercial air curtain has been modified in order to produce a more homogeneous jet. The geometric details of the new design are presented in this section.

The air curtain studied has three fans that produce the air jet (see Fig. A.6). The plenum is the inner chamber of the air curtain which connects the fan's discharge with the discharge nozzle. Its main funtion is to conditionate the air flow to obtain a plane air jet that present some desired characteristics. These characteristics are required in order to obtain an air jet which acts as an efficient ambient separator.

The characteristics are spatial and temporal homogeneity, low turbulence, high mean velocity, flat profile and low noise. The initial design has not the desired charcaterisitcs due to a unefficient geometry: sharp angles and unnecesary changes of section produce an air jet with a low capability of sealing.

The new plenum presents a smoother profile than the initial model, without sudden sharps of section neither sharp angles. The direct acoplation of this new plenum with the fans of the air curtain allow a continuous directionating of the flow from the fan discharge to the discharge nozzle (see Fig. A.7).

The progressive growth of the plenum channel in the spanwise direction produces an air jet with a high homogeneity and low turbulence. In the other hand, the progressive contraction in the other direction makes that the jet increases its mean velocity, allowing an strong air jet.

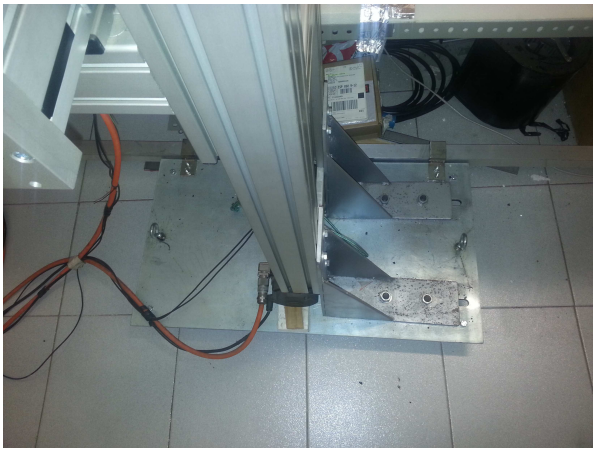

Figure A.2: Platform detail.

Figure A.3: Cartesian robot positioning system.

Figure A.4: Calibrator of the probes.

Finally, the curvature of the plenum directionates the air jet in the smoother way possible, due to the reduced space of the air curtain housing. A total of three fans with its three attached plenums are distributed in a complete air curtain of 1 meter.

It is worth noting that the directionating blades has also been studied in this optimization procedure. The different blades profiles and blades orientation has been modified in order to minimise the vortex shedding and obtain the desired angle of inclination for the jet in every position. There are two directionating blades in the fans discharge and two more in the nozzle discharge. The two in the nozzle discharge can be positioned manually by the user in the desired angle. The two in the fans are fixed.

The design procedure was a work of several months of iterative improvements. Different designs were tested, modified and numerical and experimentally compared to the previous model.

In the Fig. A.8 it can be seen some of the drawings carried out during the conception of the modified designs.

References

[1] Air Movement and Control Association International. *ANSI/AMCA Standard 220-05. Laboratory Methods of Testing Air Curtain Units for Aerodynamic Performance Rating.*, 2005.

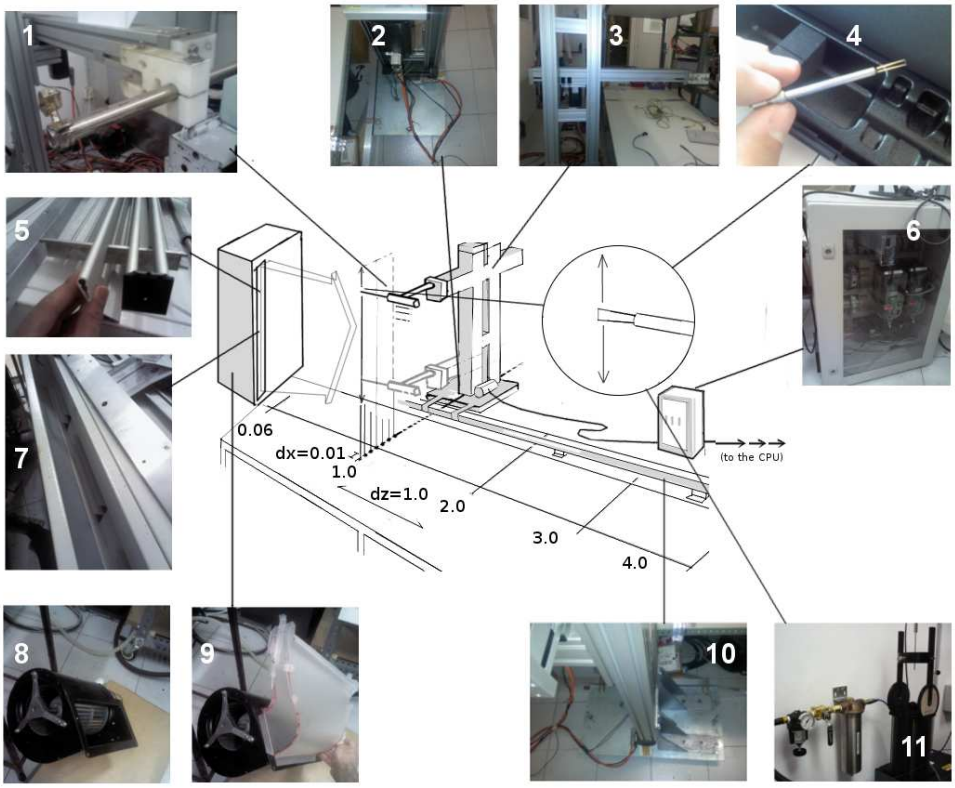

Figure A.5: 1.Fitting the probe support in the end of the robot arm. 2.The cartesian robot connections. 3.Robot horizontal arm. 4.Sensor probe detail. 5.Directionator blades of different sections and sizes. 6.Robot controller 7.Air curtain discharge nozzle with the directionator blades removed. 8.One of the centrifugal fans of the air curtain. 9.The centrifugal fan with the modified plenum attached in its discharge. 10.Platform of the cartesian robot. 11.Sensor probes callibrator.

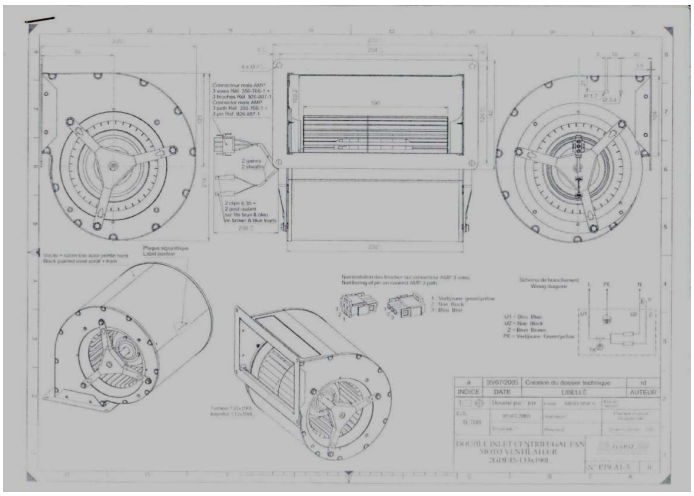

Figure A.6: Air curtain fan. Schemes and characteristics.

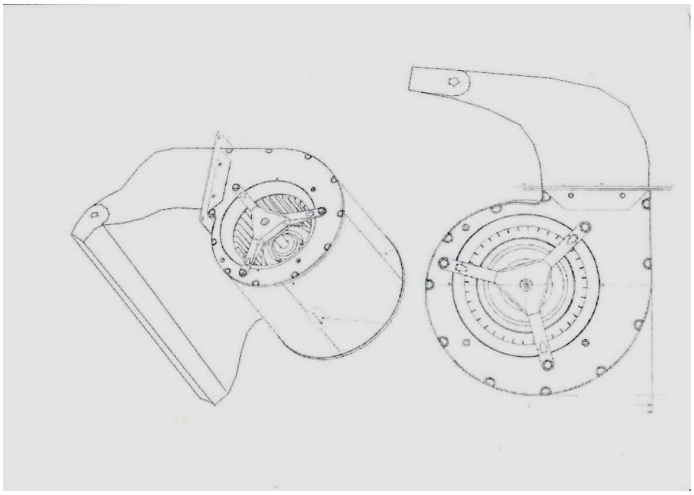

Figure A.7: Schematic of the plenum design.Plenum attached to the fan.

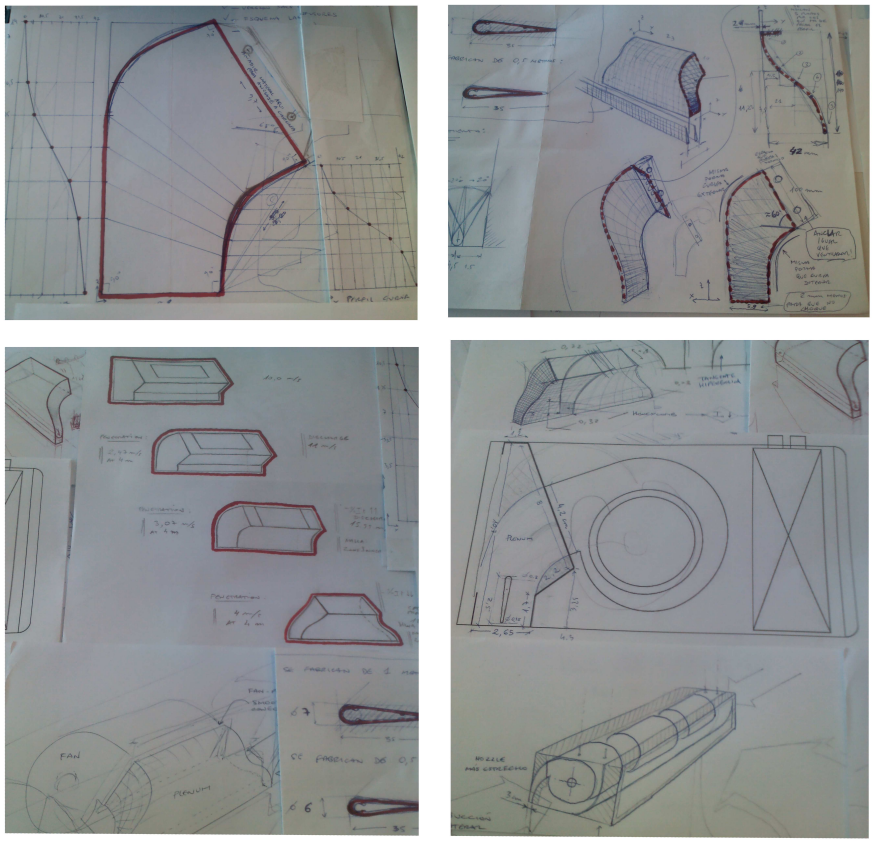

Figure A.8: Design procedure. Drawings of the concepts: hyperbolic tangent expansion to avoid pressure loses and directionating blades to fix the discharge angle, successive modifications of the design and acoplation with the fans.

Appendix B

Thermal anemometry: calibration and measurement

B.1 Principles of operation of thermal anemometry

Thermal anemometers measure fluid velocity by sensing the changes in heat transfer from a small, electrically-heated element exposed to the fluid. In the "constant temperature anemometer," the cooling effect caused by the flow passing the element is balanced by the electrical current to the element, so the element is held at a constant temperature (see Fig.B.1).

The change in current due to a change in flow velocity shows up as a voltage at the anemometer output.

One of the most important characteristics of the thermal anemometer is its ability to measure very rapid changes in velocity. This is accomplished by coupling a very fine sensing element (typically a wire four to six microns in diameter or a platinum thin film deposited on a quartz substrate) with a fast feedback circuit which compensates for the drop in the natural sensor response. Time response to flow fluctuations as short as a few microseconds can be achieved. For this reason, the thermal anemometer is employed in the study of turbulent flows.

The small sensor size, normally only a millimeter in length, also makes the technique useful in applications where access is difficult or larger sensors obstruct the flow. Since the actual measurement is of heat transfer between the sensor and its environment, the thermal anemometer will respond to changes in parameters other than velocity, such as temperature, pressure, and fluid composition. While this adds

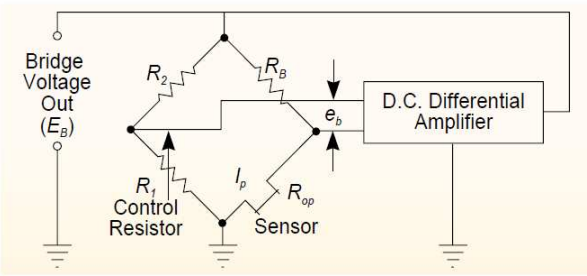

Figure B.1: Schematic of constant temperature anemometer.

to versatility, it also means that when more than one parameter is changing, special techniques must be used to extract velocity.

The anemometer has nearby attached a thermocouple in order to correct the velocity reading for temperature changes. When selecting a thermal anemometry probe, the user must choose between film and wire sensors. The choice is based on the fluid characteristics, the velocity range, the number of velocity components, contamination in the flow, and access to the flow.

The traditional sensor for research thermal anemometry has been a fine wire. For very low turbulence intensities, the wire sensor is still superior and the smaller the wire, the better the results. For those applications that require a wire sensor, a 4 micrometer-diameter platinum-coated tungsten wire is employed for measurements at normal room temperatures and below. Tungsten is very strong and has a high temperature coefficient of resistance.

It will, however, deteriorate at high temperatures in oxidizing atmospheres (such as air). Platinum wires, though weaker, can also be made very small and will resist high temperature in an oxidizing atmosphere.

If more strength is needed at high temperatures, an alloy such as platinum-iridium should be selected. The rigidity and strength of cylindrical film sensors, relative to wire sensors, make them useful in a wide range of thermal anemometry applications.

Film sensors are less susceptible to damage or coating by particles in the flow than are wire sensors.

B.2 Procedure of selection of the sensor probe

The following steps indicate the key measurement and environmental parameters that must be known in order to select the required probe and probe support for an specific application. The selection process then becomes relatively straightforward.

Figure B.2: The sensor probe is connected to the anemometer, whose software captures and records data that can be processed using signal analysis techniques.

1. Identify environmental conditions (determines the applicable sensors)

   High temperature gases

   Sensors are normally operated well above the environment temperature. The maximum operating temperature of film sensors is 425∘C, while for tungsten wires it is 300∘C. Platinum wires can operate at much higher temperatures but are much weaker than tungsten. Platinum iridium is stronger than platinum but has a lower temperature coefficient (providing lower S/N ratio). The probe must also be selected for the appropriate temperature range.

   Clean liquids

   Most liquids are sufficiently conductive that the sensor element must be insulated. Thus, only coated film sensors ("W" designation) can be used. Standard construction techniques for probes used in conductive liquids limits the fluid temperature to approximately 30∘C. In a insulating liquid, a non-coated sensor should be used since it tends to collect less contamination. In liquids, boundary layer lag can substantially reduce the expected frequency response.

2. Number of velocity components to be measured (there are limits to the magnitude of the turbulence intensity that can be accurately measured)

   A single cylindrical sensor perpendicular to the flow will give a good measurement of the instantaneous velocity in the mean flow direction.

   Two cylindrical sensors, properly oriented, will measure two components of velocity.

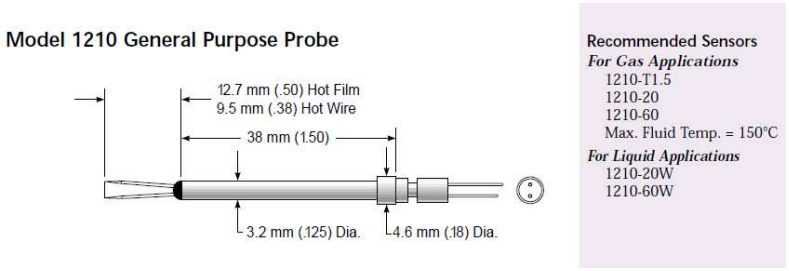

Figure B.3: Scheme of the sensor probe model 1210.

Three cylindrical sensors,properly oriented, will measure all three velocity components.

3. Hot wires versus cylindrical film sensors where either can be used

   Hot wires provide the best S/N ratio and generally better frequency response than film sensors. With multiple sensors, they do not stay positioned as well (lengthen and bend when heated), causing errors in velocity component calculations.

   Cylindrical film sensors generally do not contaminate as easily(due to larger diameter) and will not shift resistance due to strain in a high velocity environment or due to particle impact.

4. Probe and support selection

   Once the type and number of sensors is determined, further selections depend on the access to the flow and where the measurement is made. Right angle adapters, miniature probes, andcross flow designs are variations that fixes the sensor where it is required with minimum flow field disturbance.

A TSI probe model 1210-20 General Purpose Probe is the probe type employed in most of the measurements carried out in the present study. A probe model 1210-1.5 has been employed for low velocity measurements and a dual sensor probe model 1241-20 has been employed in regions where the air curtain flow has exhibit non-unidirectional behaviour.

The dual sensor probe has two sensors in close proximity, in “X” configuration, for measuring two components of flow and the correlation between them.

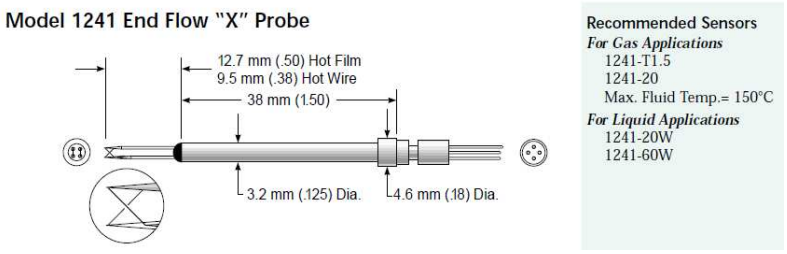

Figure B.4: Scheme of the sensor probe model 1241.

Figure B.5: Sensor probe model 1210.

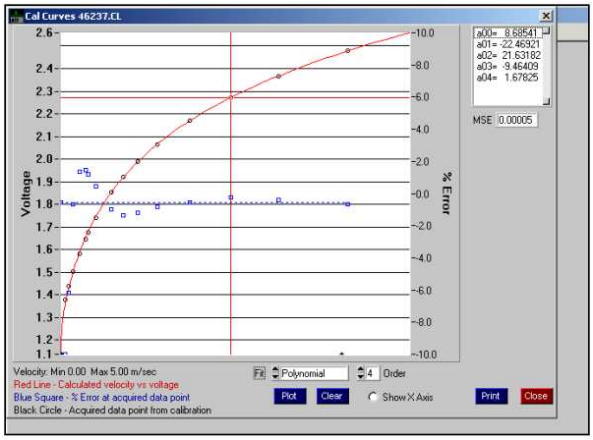

Figure B.6: Calibration curve. Voltage as a function of the flow velocity and the related error between the fitting and the actual measurement in every calibration point.

B.3 Calibration of the probes: theory and procedure

In this section the theoretical principles of operation of the calibrator and the calibration procedure are detailed. The calibration procedure is explained with every detail in order to serve as a guide for the author himself in the future.

B.3.1 Calibration curve

Before the measurements the sensor probes should be calibrated. As said before, the cooling effect caused by the flow passing the element is balanced by the electrical current to the element, so the element is held at a constant temperature. But the exact relationship between the electrical current and every flow velocity should be determined in a previous calibration. This voltage-velocity relationship can be depicted by means of the calibration curve (see Fig. B.6).

So the point of the calibration is determining the exact shape of this calibration curve. For this purpose, the sensor should be exposed to different known velocities. In every velocity the electrical tension is measured so a new point of the calibration is determined. A fitting of the different points will produce the calibration curve. The calibrator user can select the "Fit" that he wants (e.g., 4th Order Polynomial, Kings Law, etc.)

B.3.2 Imposing known velocities

The velocity emerging from the exit nozzle of the calibrator are established measuring the differential pressure between the settling chamber and the room. The velocity is calculated using differential pressure as well as absolute (barometric) pressure, temperature, and certain air properties such as gas constant and ratio of specific heats as follows:

$$a_0 = \left(\gamma \cdot R \cdot (T + 273.15)\right)^{1/2} \tag{B.1}$$

$$M = \left(2 \frac{\left(\frac{P - \Delta p}{P}\right)^{\frac{\gamma - 1}{\gamma}} - 1}{\gamma - 1} \right)^{1/2} \tag{B.2}$$

$$a = \left(\frac{a_0^2}{1 - \left(\frac{\gamma - 1}{2} M^2\right)} \right)^{\frac{1}{2}} \tag{B.3}$$

$$U = M \cdot a \tag{B.4}$$

Where P is the absolute pressure, T is the stagnation pressure, γ is the ratio of specific heats, R is the gas constant for specific gas, a is the speed of sound, a_o is the speed of sound at stagnation conditions, M is the Mach number and U is the velocity. These equations give the same result as Bernoulli's equation for velocities less than 50 m/s. At velocities greater than 50 m/s, the Bernoulli equation starts to introduce sigfnificant error because of compressibility effects. Once the theory of calibration has been detailed, the following section is a brief description of the procedure for calibrating a hot-wire probe with the automated air velocity calibrator employed in this thesis.

B.3.3 Calibration procedure

The calibrator is controlled by means of its software. The procedure will be detailed in this section. The different screenshots of each step of the calibration procedure are included in order to facilitate the comprehension of the whole process.

• Fill the information of the probe, selecting Probe Data from the calibration menu.

• If the probe is connected in channel 1, the pressure should go to channel 2. For "Cal

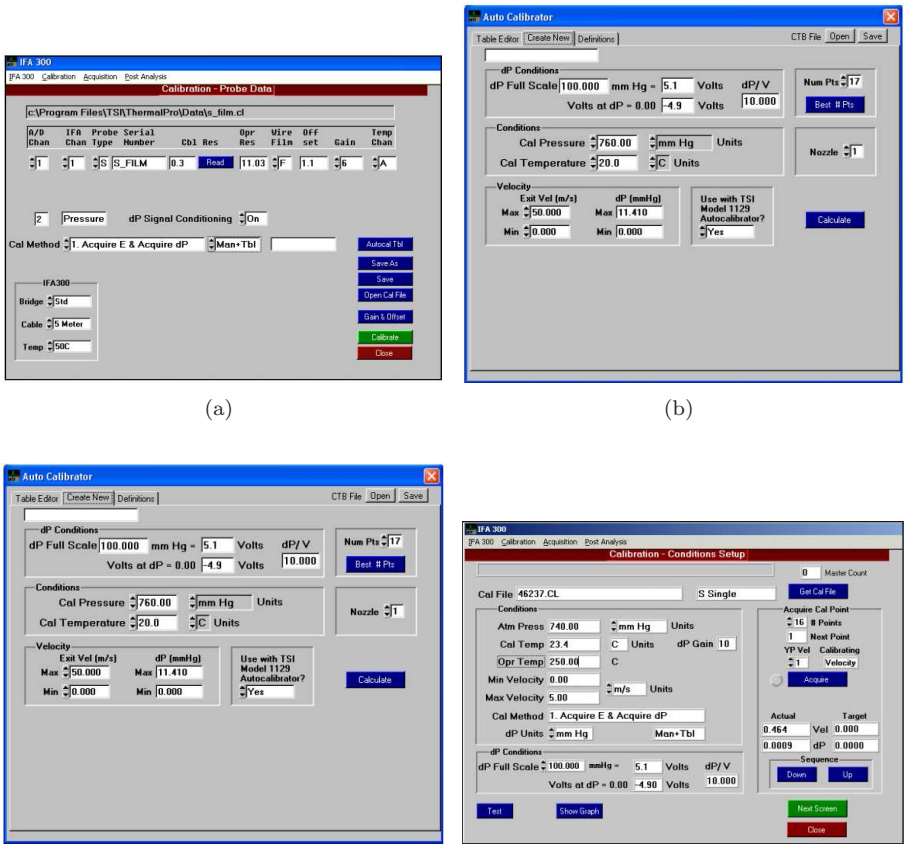

(a) (b)

(c) (d)

Figure B.7: (a)first step (b) second step (c) third step (d) fourth step.

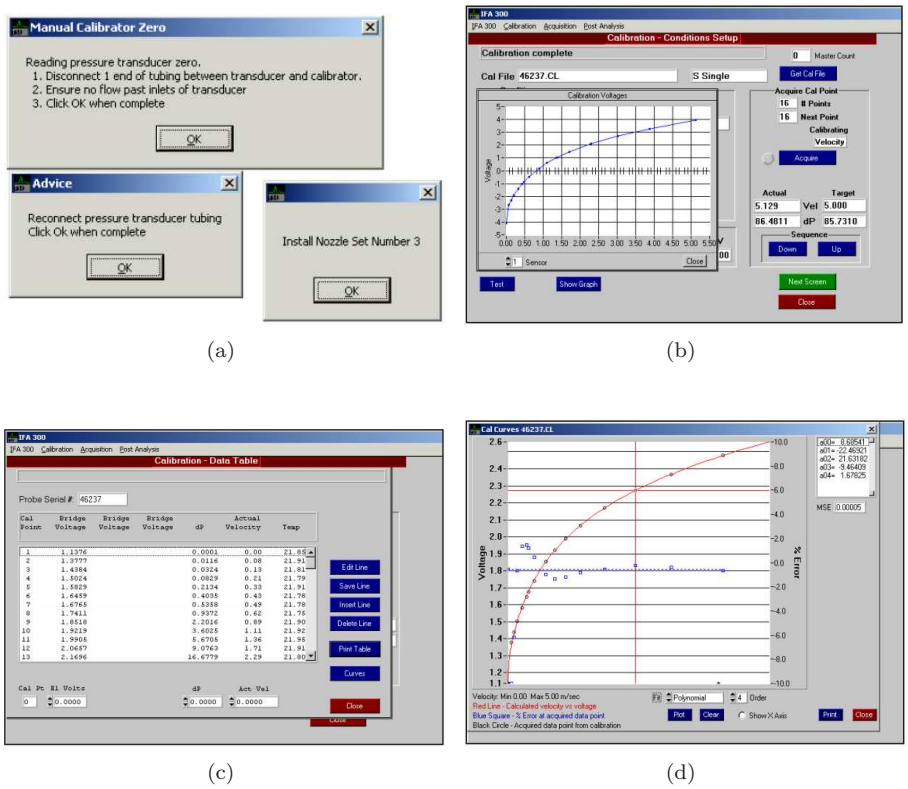

Figure B.8: (a)fifth step (b) sixth step (c) seventh step (d) eight step.

Method": "1. Acquire E and Acquire dP" is the method used with the calibrator. In the field of calibration method, Auto is used with an auto calibrator as the one employed in this thesis (model 1129).

• In Calibration, select the Autocalibration Table and create a new table with the information of the calibrator, the atmospheric temperature, pressure and min and max velocity.

• On the Probe Data screen, go to the calibration file and select the saved one. The next screen looks like Fig.B.7(d). Enter the atmospheric pressure and the temperature of the room.

• In the field Points, goes the number of calibration points. A calibration has at least 15 points. Two windows appear and the first calibration point will be obtained.

• When all the calibration points are obtained, a table showing the calibration points appears (see Fig.B.8(b)).

• On Curves it can be selected and viewed the curve fit for the data. On the calibration curves screen, select the required fit.

• The red line is the curve fit, the blue squares are the % error of each data point from the curve. When using the calibrator, the error should be less than 2 % for all but the very lowest calibration points.The calibration has been carried out taking into account the velocity range produced by the ACU. The lowest point of the calibration curve should be near 0.0 m/s and the highest velocity point of the calibration curve should be higher than the maximum velocity produced by the ACU.

B.4 Mounting the probes in the robot arm: support and connections to the anemometer

The adjustment in the precise position of the sensor probes is a key factor for a correct measurement. This is carried out by means of the cartesian robot and other additional pieces specifically designed by the authors for the present work. In the following figures (see Figs. B.9, B.10, B.11)it can be seen two details of the setup and an overall scheme of the acoplation of the different components. It is worth noting that the sensor probe is connected to the electronic anemometer by means of its wire,

which is disposed in order to not disturb the flow measurement. Adjoint to the sensor probe there is also a thermocouple, which allows to correct the discrepancies between the temperature in the moment of the sensor calibration and the room temperature in the moment of the measurements. This thermocouple is also connected to the electronic anemometer.

In the Fig. B.11, it is indicated the relative position of the different pieces:

1. The cartesian robot, which has two perpendicular axis and is mounted in a rail allowing the positioning in the three-dimensions.
2. An adaptator, the first piece is placed at the end of the robot to mantain the probe support in its position.
3. The second piece of the adaptator allows the posibility of angular inclination. This piece also mantains the thermocouple in its exact position. The termocouple and the sensor probe should be always as near as possible in order to correct the signal with the velocity properly.
4. A metal cilinder, which containd the probe support and the wires that are connected to the support. The wires should not interfere in the measurements, and this is the main reason for this metal cilinder, which conducts in its inner space the wires of the sensor probe and the thermocouple.
5. The probe support, directly connected to the sensor probe and to the electronic anemometer.
6. The sensor probe, which obtains the signal and send it to the anemometer in order to be processed.

B.5 Air flow measurement procedure

Once the sensor probe has been calibrated and placed in the required position the measurements can be carry out. There are different parameters that should be determined a priori in order to carry out the measurements. The first parameter is the total time of data adquisition. This parameter determines how long the sensor probe will be adquiring the signal. If the time is too long, the quantity of data can be excessive and redundant, if the time is too short the signal cannot be significative, being the mean value of the velocity not properly determined, for example. The second parameter is the sample rate. The data adquisition is not fully continuous in time. This parameter determines the time between succesive adquisitions. If the sample rate is too large, the quantiy of dat will be excessive and also unnnecesary. If the sample

Figure B.9: Positioning of the sensor probes by means of a cartesian robot.

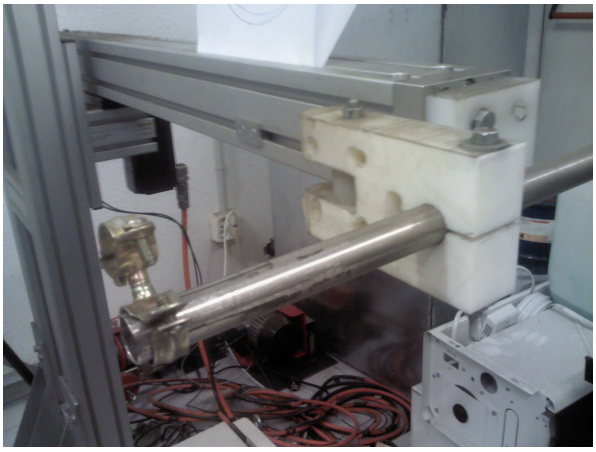

Figure B.10: Adjustment of the probe to the robot.

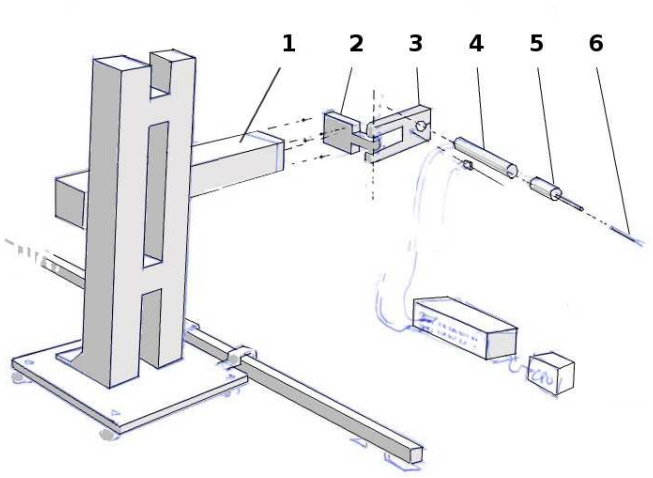

Figure B.11: Scheme of the different pieces of the probe positioning system.

rate is too little, the signal will not properly described, being the turbulence level unrealistic, as an instance. The third parameter is the pressure in the room where the measurements are carried out. This is manually introduced. The temperature is measured directly measured by the thermocouple, so it is not required to introduce it manually.The fourth parameter is the channels of the electronic anemometer where the sensor probe and the termocouple are connected. They should be indicated and its proper behaviour should be check out before the measurements.Other parameters, such as type of sensor, are determined in a similar way as the procedure explained in the previous appendix.

B.6 Data analysis

Post-processing gives complete statistics, including mean velocity, turbulence intensity, standard deviation, skewness, flatness, and normal stress for one-, two-, and three component probes, and shear stress, correlation coefficient and flow direction angle for two- and three component probes.

In addition, power spectrum, autocorrelation, and crosscorrelation can be calculated and displayed.

The software includes an algorithm used for sensor probe analysis which is based

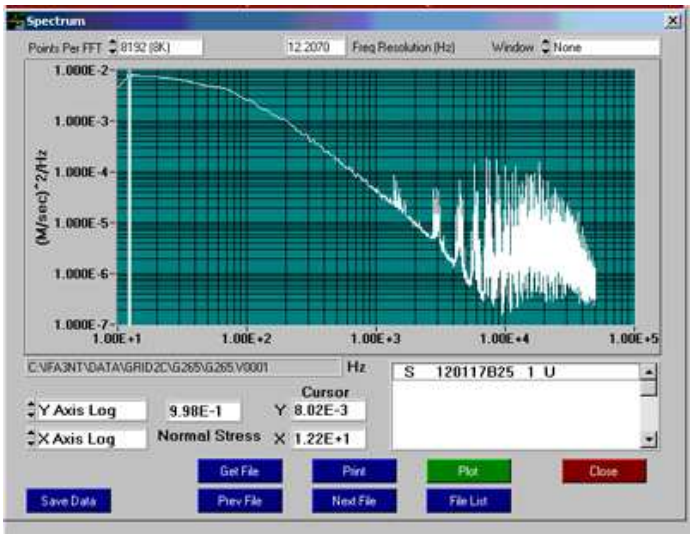

Figure B.12: Screenshot of the spectra obtained fin the post process of a measurement.

on work done by Fingerson [2], with further refinement by Lekakis [3] and Walter [4].

B.7 Indicators of non-valid measurements

There are different causes that can produce non valid measurements. The most common cause are from electric origin or from disturbances in the flow to be measured. If the processed signal presents excessive turbulence levels (roughly more than 40 per cent), a second measurement can be a good practice. An excessive turbulence could be produced by the nature of the measured flow but also by undesired exterior disturbances. Another causes of non valid signal can be an parasite voltages which produce unrealistic levels of electric intensity in the wires. All the wires and the probe support should not be in contact with metal parts, in order to minimise possible disturbances. If the signal is completelly flat, the channels of the electronic anemometer can be the wrong ones or the connections have not being properly initiated. It is also recommended to repeat the measurements, even when the mean velocity is different from zero. If the problem persist the sensor probe should be checked because it can be broken (see Fig. B.13). The wires should be checked also.

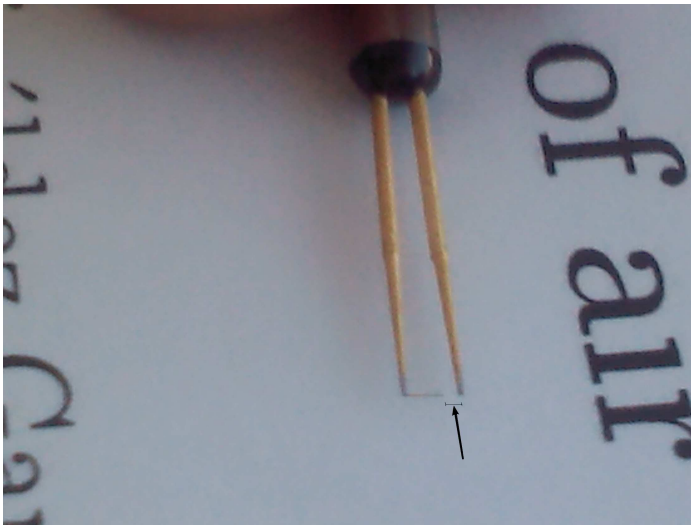

Figure B.13: A broken probe. The wire is thin so an accidental breaking is unfortunately very usual.

If the probe is not broken, the electronic anemometer should be shut down and initiated again employing other channels for the sensor probe, in order to check a possible problem with the connection channels.

B.8 Conclusions

In this chapter the theory and employment of hot wire anemometry technology has been presented. The principles of operation of thermal anemometry has been explained. The main parameters affecting the type of sensor which should be employed in the measurements has been also detailed. The calibration of the probes, connections and measurement procedure has been explained. Finally, the data analysis and the possible indicators in the signal of a flawed measurement has been pointed out.

References

[1] J. Jaramillo. *Suitability of Different RANS Models in the description of Turbulent Forced Convection Flows. Application to Air Curtains.* PhD thesis, Universitat Politecnica de Catalunya, 2008.

[2] Fingerson LM *Practical extensions of anemometer techniques.* Advances in Hot-Wire Anemometry: 203–218, 1968.

[3] Lekakis IC. Adrian RJ. Jones BJ. *Measurement of velocity vectors with orthogonal and nonorthogonal triple-sensor probes.* Experiments in Fluids, 7: 221–240, 1989.

[4] Walter J. Ph.D. Thesis, University of Iowa Hydraulics Laboratory, 1995.

Appendix C

Software for Air Curtains Systems

C.1 SACS: software for air-curtains design and prediction

In order to simulate the air curtains behaviour without requiring large time consuming calculations, the Software for Air Curtains Systems (SACS) was implemented [1]. This software predicts the air curtain behaviour by means of a semianalitycal approach and employs additional adjustments from tridimensional CFD calculations and experimental measurements in order to be as realistic as possible. It is worth noting that this software is continuously updated with information from CFD simulations and experimental measurements. In the Fig. C.2 it can be seen the main interface of the software.

C.1.1 Design mode

The software offer two modes: design and prediction. The design mode can be classified as an "expert system". In the design mode the user can employ his experience to chose the adjustments in order to maximize the efficiency of the air curtain. Based on a preliminar calculation, the software indicates the possible deficiencies and automatically correct them, highlighting the main cause of the problem. The more usual modifications in order to avoid the breakthrough of the jet is to increase the discharge velocity or modifying the discharge angle. The system do several iterations in order to avoid the jet breakthrough. When the air curtain shows a correct behaviour, the system pointed out the modification to the user. In this way, the user acquires additional information from the system and can improve his decisions. It should be pointed out that the SACS software do not calculate recirculating installations.

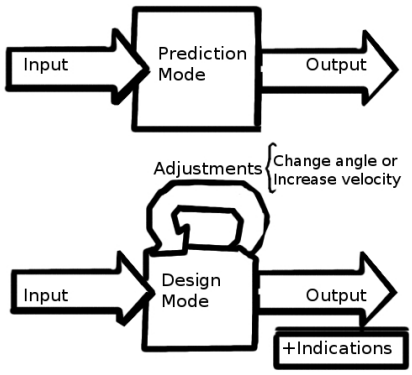

Figure C.1: Information flow of the different calculation modes in SACS.

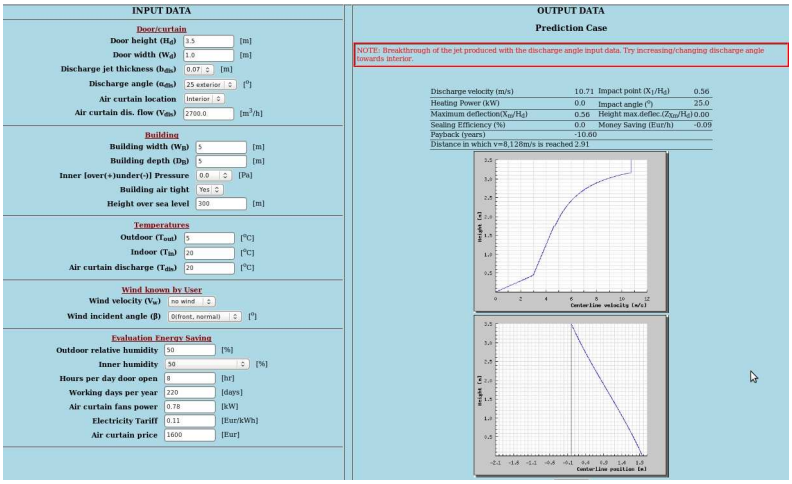

Figure C.2: SACS interface in prediction mode. Warning of breakthrough due to the discharge angle.

C.1.2 Prediction mode

In the prediction mode the user can define all the parameters. In this way, the user defines all the information and the system can not correct his decisions. The prediction mode does not give additional information, it only predicts the user defined scenario(see Fig. C.1). This mode is employed to determine the behaviour of the device even when the air jet is not working correctly.

C.1.3 Calculation examples

In the following it can be seen the results obtained with some simple configurations. The first case C.3(a) is progressively modified in order to see the effect of different parameters. In the first modification (see Fig. C.3(b)), the velocity is increased to 10 m/s, producing a larger deflection in the jet and, hence, a smaller efficiency. In the second modification (see Fig. C.4(a)), the discharge angle is modified to the exterior, producing also an excessive lateral entrainment. In the third modification (see Fig. C.4(b)) it can be seen the effect of the wind breaking the air jet. In the fourth case (see Fig. C.5), the angle is corrected in order to avoid the mentioned jet breaking by the effect of the wind. This is the usual solution employed in most of the practical cases, the air jet is directed against the external forces which produce its deflection.

References

[1] J. Jaramillo. *Suitability of Different RANS Models in the description of Turbulent Forced Convection Flows. Application to Air Curtains.* PhD thesis, Universitat Politecnica de Catalunya, 2008.

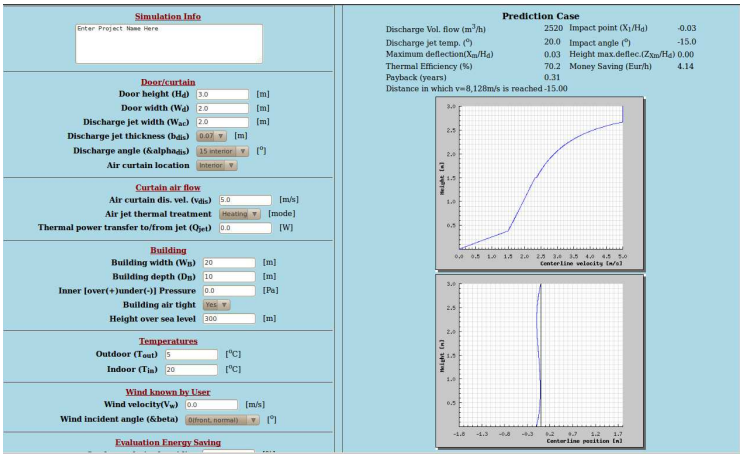

(a)

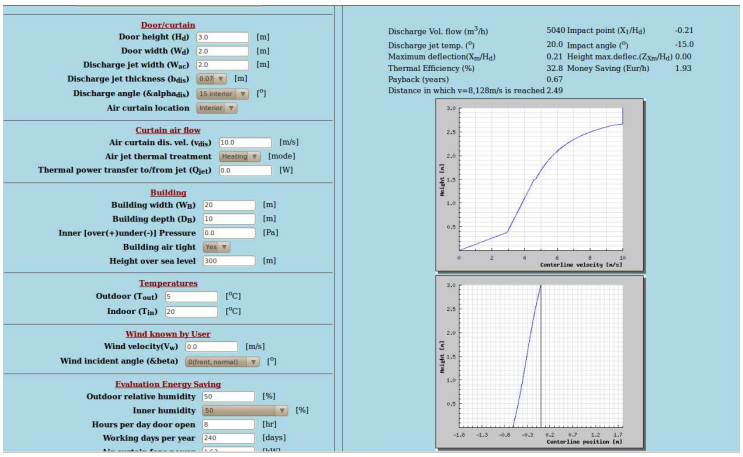

(b)

Figure C.3: (a) Base case.There is no breakthrough of the jet. (b) Modified case.The discharge velocity has been increased to 10 m/s.

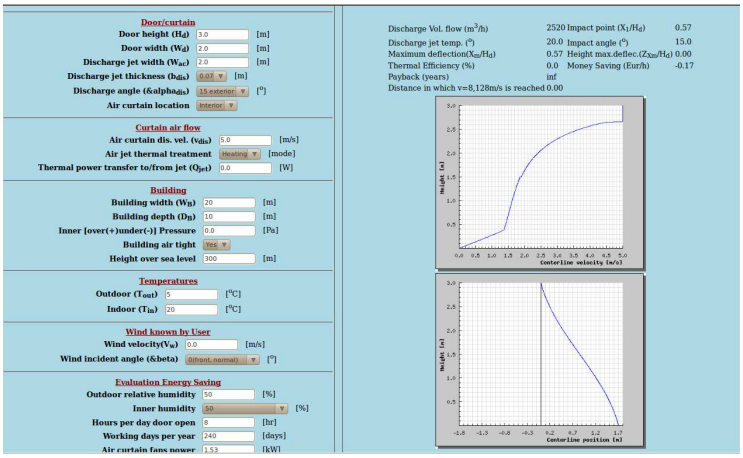

(a)

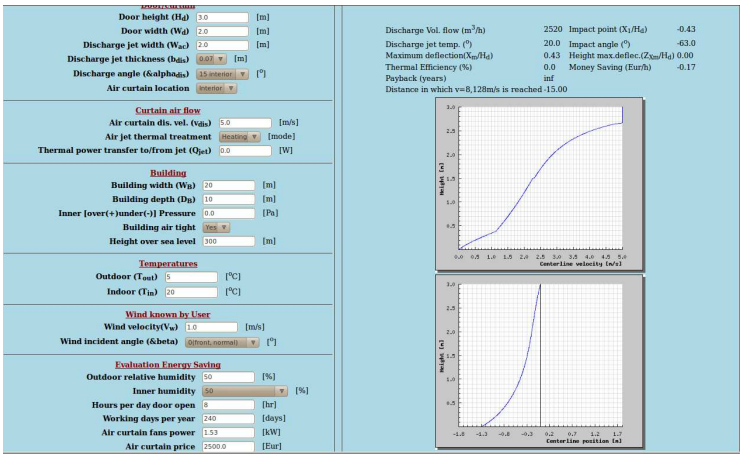

(b)

Figure C.4: (a) Modified case.The discharge angle is changed to 15 degrees to the exterior. (b) Modified case.There is the effect of the wind breaking the jet.

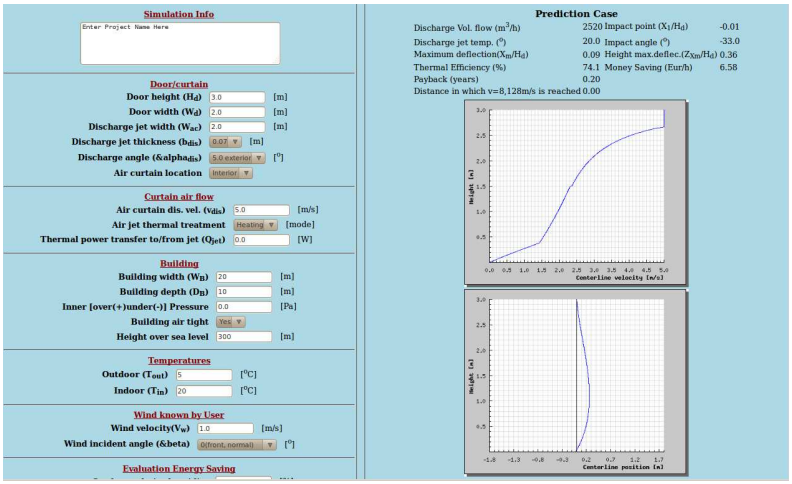

Figure C.5: Modified case.There is the effect of the wind, but the angle correction avoid the breaking.